Design, Simulation and Analysis of RF-MEMS Switches for Reconfigurable Antennas

THESIS

Submitted in partial fulfillment
of the requirements for the degree of

DOCTOR OF PHILOSOPHY

by

ASHISH KUMAR SHARMA

ID. No. 2010PHXF001P

Under the Supervision of

Dr. Navneet Gupta

BIRLA INSTITUTE OF TECHNOLOGY AND SCIENCE, PILANI

2014

BIRLA INSTITUTE OF TECHNOLOGY AND SCIENCE
PILANI (RAJASTHAN) INDIA

CERTIFICATE

This is to certify that the thesis entitled "**Design, Simulation and Analysis of RF-MEMS Switches for Reconfigurable Antennas**" and submitted by **Mr. Ashish Kumar Sharma** ID No **2010PHXF001P** for award of Ph.D. of the Institute embodies original work done by him under my supervision.

Signature of the Supervisor:

Name in capital Letters : Dr. NAVNEET GUPTA

Designation : Assistant Professor

Date:

ACKNOWLEDGEMENTS

I would like to thank my advisor, Dr. Navneet Gupta for introducing me to the applied electromagnetic and antenna design field, and for guiding my research. His high standards of research have been a blessing and I have greatly appreciated his hospitality. Many thanks to my two thesis committee members, Prof. V. K. Chaubey and Dr. Niladri Sarkar for reviewing my proposal and advising time to time during my Ph.D.

I am also grateful to Prof. Anu Gupta, Head of the Department, Prof. S. Gurunarayanan, Prof. Surekha Bhanot, Prof. Anshuman Dalvi and Prof. H. D. Mathur for their valuable guidance and motivation throughout this research.

I would also like to thank the Departmental Research Committee members (DRC), Prof. H. O. Bansal, Dr. K. K. Gupta and Dr. Abhijit R. Asati, for their constructive criticism and feedback. I greatly acknowledge the support of Dr. Praveen Kumar A. V., Dr. Rahul Singhal, Mahesh Angira and G. Meenakshi Sundaram for all kind of technical discussion which helped me a lot in my research.

I must acknowledge all my fellow research scholars, V. Balaji, Aishwarya Pandey, Yogesh B., Gaurav Purohit, Prachi Sharma, Priya Gupta, Jitendra Kumar, Satish Mohanty, Priyanka Chaudhary, Abhishek Joshi, Jyotirmoy and Fani Mani for providing me all kind of support to my research work. Working, playing, living, and arguing with my fellow research scholars in the Communication Lab has been enriching and enjoyable.

I would like to thank to Prof. N. N. Sharma, Coordinator, Nano Materials and National MEMS Design Center (NMNMDC) at BITS Pilani, and Mr. Debashis Pal, CSIR-CEERI, Pilani for their valuable support in doing simulation work reported in this thesis.

I also want to thank staff members of EEE Department: Shiv Shankar Sharma, Manoj Kumar, Amitabh, Mahesh Sani, Birdi Chand and Sanjay for their kind help in Laboratory and other official work.

Last but certainly not the least, I would also like to thank my wife Pooja Sharma, my parents, and my family members for their invaluable support and everlasting trust. Most of all, I would like to thank God for everything especially his love and grace.

Ashish Kumar Sharma
20/2F/1 Gandhi Marg,
BITS-PILANI
Rajasthan, INDIA
Pin- 333031

September 2014

To My Parents

Late Mother Asha Sharma

and Father Manohar Lal Sharma

ABSTRACT

The present work is motivated by the superior performance of RF-MEMS switches over the state-of-the-art solid-state counterpart (PIN diode and FET) and the potential applications in wireless communication such as reconfigurable antenna. Reconfigurable antennas are attractive for satellite, military and commercial applications, where it is required to have single antenna that can be adaptively reconfigurable to transmit or receive on multiple frequency band and pattern.

The performance of RF-MEMS switches depends on suitable material to be used for the switch. Ashby's approach is used to choose suitable material for RF-MEMS switch. The key material indices considered for MEMS capacitive switch are Young's modulus, electrical resistivity, Poisson's ratio, thermal expansion coefficient, and thermal conductivity. Three performance indices; actuation voltage, RF-loss and thermal residual stress, based on different material indices were optimized. Based on material selection charts, it was observed that aluminum is the best material to be used as bridge material for RF-MEMS switch.

The first-order analytical model is derived for mechanical equations of motion of a non-uniform serpentine spring constant using small displacement theory. The spring constant of non-uniform serpentine flexure with different meander sections has been equated by developing analytical expression and verified with Finite Element Method (FEM) simulations. It is observed that in comparison to the uniform serpentine flexure reported so far, the proposed design shows a considerable decrease in spring constant.

Further, the actuation voltage of RF-MEMS switches can be reduced by optimizing the spring constant of the RF-MEMS switch flexure design. Therefore the reduction in actuation voltage is achieved by introducing the concept of non-uniform serpentine flexure based suspensions. FEM analysis indicate actuation voltage as low as 5 V with single meander section for the proposed non-uniform serpentine spring design, which is reasonably low as compared to uniform serpentine spring with same span beam length.

In addition, the RF power handling capability of RF-MEMS switch is improved through low-spring constant based non-uniform flexure design. In contrast it is observed that the non-uniform flexure design shows the trade-off between spring constant and switching time, which ultimately reduces the switching speed of the RF-MEMS switch.

The electromagnetic model of RF-MEMS switch is used to accurately determine the electrical parameters (resistance, inductance and capacitance of MEMS bridge) from S-parameter measurement. It is observed that non-uniform serpentine spring based inductively tuned switch exhibit isolation of more than 30 dB for multiple resonant frequencies ranging from Ka band to Ku band. Comparison between computed and simulated results shows the close agreement which gives the validity of proposed study.

It is observed that in comparison to the uniform serpentine flexure reported so far, the proposed design shows a considerable reduced spring constant of 0.65 to 0.04 N/m and pull-in voltage of 15 to 3 V with better RF power handling capabilities of 4.29 to 0.2 W having switching time of 1-4 millisecond for span beam length varying from 100 to 280μm. Here the proposed RF-MEMS switch is designed with single meander section using a non-uniform serpentine flexure with 180 μm span beam length, offers an actuation voltage of 6.3 V, RF power handling capability of 0.6 W with adequate switching time of 3.5 millisecond. The proposed switch designs shows with better RF response in terms of return loss of << -20 dB up to 25 GHz and isolation of >>25 dB from 15 to 35 GHz.

The proposed RF-MEMS switch is integrated with antenna structure which consists of two element circular patches, to achieve reconfigurability within the band i.e. (L and S band). The proposed switch design is scaled up by a factor of 20 in order to achieve the reconfigurability in L and S band. The impedance matching between antenna and switch is provided by placing a matching network consisting of an inductor of 1.62 nH in series configuration with CPW transmission line. The analysis of reconfigurable antenna using RF-MEMS switch is done using the simulation performed on Ansys HFSS electromagnetic simulator. The analysis is done in terms of return loss, VSWR, radiation pattern and gain. It was observed that this antenna shows pattern reconfigurability at 2.3 GHz and 3.4 GHz with frequency reconfigurability at 2.3 GHz, 2.9 GHz and at 3.4 GHz.

TABLE OF CONTENTS

CHAPTERS

LIST OF TABLES

LIST OF FIGURES

LIST OF ABBREVIATIONS

2D	Two-Dimensional
3D	Three-Dimensional
CLR	Capacitor-Inductor-Resistor
CPW	Coplanar Waveguide
DC	Direct Current
FBAR	Film Bulk Acoustic Resonators
FEM	Finite Element Method
FET	Field Effect Transistors
FGCPW	Finite Ground Coplanar Waveguide
HFSS	High Frequency Structural Simulator
MAUA	Multi Attribute Utility Analysis
MEMS	Micro Electro Mechanical System
MI	Material Index
MIMO	Multi-Input Multi-Output
PCB	Printed Circuit Board
RA	Reconfigurable Antenna
RF	Radio Frequency
SOI	Silicon-on- Insulator
SPDT	Single-Pole-Double-Through
UWB	Ultra Wideband
VSWR	Voltage Standing Wave Ratio
WLAN	Wireless Local Area Network

CHAPTER 1

INTRODUCTION

1.1 BACKGROUND

In recent years, development in MEMS (Micro-Electro-Mechanical-System) technology have achieved remarkable advancement for radio frequency (RF) applications, which include switches, voltage tunable capacitors, high quality integrated inductors, film bulk acoustic resonators (FBAR), MEMS mechanical resonators and filters. Among these devices, RF-MEMS switches are the fundamental component, which can be used to develop other RF-MEMS devices [1-2]. The RF-MEMS switches have been utilized in communication application due to their miniaturized size, low weight and high performance in terms of higher isolation, low power consumption and lower insertion loss [3-4]. Moreover these RF-MEMS switches are economically and technologically competitive as compared to other microelectronic switches. The first switch was developed for microwave application by Dr. Larson and Hughes Research Labs in 1990. In 1995 Rockwell science center developed metal to metal contact switch and Texas instruments developed capacitive contact switch. These switches were suitable for DC-60 GHz and 10-120 GHz application [5].

The last one and half decade has seen an amazing growth in the research of RF-MEMS owing to its superior high frequency performance extending beyond 100 GHz [6]. This solves many problems of high frequency technology for wireless communication owing to its high Q factor. RF-MEMS demonstrated versatile application in reconfigurable antennas for defense and telecommunication systems switching networks

and satellite communication [7]. The performance of RF-MEMS switches can be analyzed on the basis of various design parameters.

1.2 FIGURE OF MERITS

The design parameters that are used to evaluate the performance of RF-MEMS switches are as follows:

(a) RF Power Handling: RF power handling is a measure of how efficiently a switch passes the RF signal at the time of signal transmission. RF power handling refers to the power at which the MEMS device fails to operate properly.

(b) Insertion Loss: The insertion loss of RF-MEMS switch refers to the RF signal power dissipated in the switch at the time of signal transmission. Insertion loss occurs at low microwave frequencies as well as at high microwave frequencies. At low frequencies it is due to the resistive loss between the finite resistances of transmission line and switch beam contact area, while at higher frequencies insertion loss occurs because of skin depth effect. For design aspect, the insertion loss should be minimized for efficient signal transmission.

(c) Isolation: The isolation of RF-MEMS switch can be defined as the RF signal power isolation between the input and output terminals in its signal blocking state. A large value (in decibels) of isolation indicates, very small coupling between input and output terminals. In RF-MEMS switches, isolation occurs due to capacitive coupling between the moving switch beam and the stationary transmission line as a result of leakage currents. One of the design objective of communication system is to achieve a very high isolation at low and high microwave frequencies.

(d) Return Loss: The return loss of the RF-MEMS switch refers to the RF signal power reflected back by the device at the input terminal of the switch in its signal transmission state. Return loss occurs due to the mismatching of the total characteristic impedance between the switch and transmission line.

(e) Actuation Voltage: Actuation voltage can be defined as the minimum voltage required to pull-down the switch beam of the RF-MEMS switch. One of the design

objective of state-of-the-art MEMS technology is to achieve the low actuation voltage, depending on the switch design and application.

The voltage that requires to pull-down the switch membrane is given by [1]:

$$V_p = \sqrt{\frac{8k}{27\varepsilon_0 Ww}\, g_0^{\,3}} \qquad \ldots (1.1)$$

Here k is spring constant, ε_0 is permittivity of free space, W, w and g_0 are the length of the pull down electrode, width of beam and gap between the electrode and beam, respectively.

(f) Resonant Frequency: The resonant frequency of the switch can be defined in terms of the effective spring constant (k) and resonating mass of the mechanical system (m). At this particular frequency, the stored potential energy and the kinetic energy of the switch tend to resonate. The natural frequency of a simple mechanical system consisting of a weight suspended by a spring can be formulated as [8]:

$$\omega_0 = \frac{1}{2\pi}\sqrt{\frac{k}{m}} \qquad \ldots (1.2)$$

The resonant frequency can also be defined for an electrical system in which the resonant frequency can be achieved by using a resonant circuit, which consists of an inductor (L) and capacitor (C) in series configuration. This LC circuit stores an oscillating electrical energy at the circuit's resonant frequency due to the collapsing magnetic field created by the inductor and capacitor. The fundamental resonant frequency of the electrical circuit can be formulated as [8]:

$$\omega_0 = \frac{1}{2\pi}\sqrt{\frac{1}{LC}} \qquad \ldots (1.3)$$

(g) Switching Speed: The switching speed can be defined as the time for toggling from one state of the switch to another. Switching speed can also be called as switching rate. Switching speed of a capacitive RF-MEMS switch can be expressed as switching time required to pull-down the switch membrane (MEMS bridge) and is given as [1]:

$$t_s = 3.67 \frac{V_p}{V_s \omega_0} \quad \ldots (1.4)$$

where ω_0 is the resonant frequency of the switch, V_p is the actuation voltage and V_s is the supply voltage.

RF-MEMS switches possess low switching speed as compared to the semiconductor switching devices.

(h) Quality Factor: The quality factor (Q-factor) is one of the most important parameter of RF-MEMS switch and can be explained as the ratio of the energy stored to the energy dissipated per cycle at the resonant frequency. Higher Q-factor indicates a lower rate of energy loss relative to the stored energy of the resonant circuit.

The RF-MEMS switch performs RF signal switching by physically blocking or opening the transmission path in a microwave devices to achieve transmit/receive operation. So these RF-MEMS switches have a broad range of application in RF and microwave based modern communication systems. RF and microwave devices can be categorized as [8]:

- **RF extrinsic:** In this type, the RF-MEMS component is situated outside the RF circuit and actuates or controls other component in the RF circuit.
- **RF intrinsic:** In this type, the RF-MEMS component is situated inside the RF circuit having actuation and RF circuit function.
- **RF reactive:** In this type, the MEMS component is located inside the RF circuit where it performs an RF function.

1.3 RF-MEMS SWITCH

RF-MEMS switches have experienced intensive use for telecommunication application in the last ten years due to their high performance compared to other microelectronic switches. Also the reduction in dimension of electromechanical systems offers advantages such as soft spring, high resonance frequency and low thermal mass, which leads to a dramatic decrease in power consumption [3].

RF-MEMS switch can be divided into two parts: *mechanical section and electrical section.*

1. **Actuation (Mechanical) section**

In RF-MEMS switches, the mechanical movement can be achieved by using different actuation techniques like electrostatic, magnetostatic, piezoelectric and thermal actuation. Electrostatic and magnetostatic actuation mechanism gives higher reliability (100 million to 60 billion cycles) as compared to other techniques for 0.1 – 100 GHz frequency operation.

2. **Electrical section**

These switches can be placed in either series or shunt configuration. Electrical section can be a metal-to-metal contact or a capacitive contact switch.

Electrostatic actuation is most prevalent technique that provides zero power consumption, small electrode size, thin layer and short switching time, 50-200 μN of achievable contact forces. Capacitive RF-MEMS switches operate on frequency beyond 4 GHz due to low dielectric constants of insulating layer [9].

Three kinds of switches that can be used in RF applications are as follows:

(i) FET Switches.

(ii) PIN diode Switches.

(iii) RF-MEMS Switches.

Detailed comparisons between these switches are given in table 1.1. Based on performance in terms of isolation, insertion loss, actuation voltage and switching speed the RF-MEMS switches provide the better performance as compared to solid-state switches.

1.4 CLASSIFICATION OF RF-MEMS SWITCHES

RF-MEMS switches are classified based on types of contact and circuit configuration. On the basis of contact type there are two types of switches: *metal-to-metal contact* and *capacitive coupled switch*. While based on circuit configuration, these are classified as series switch and shunt switch. Fig. 1.1 shows the classification of MEMS devices configuration based on actuation mechanism, movement, contact type and circuit. In this thesis switches are classified on the basis of type of contact and the mechanism for actuation is assumed to be electrostatic.

Table – 1.1 Comparison of RF-MEMS, PIN Diode and FETs switches [1, 8].

Parameters	**RF-MEMS**	**PIN**	**FET**
Voltage (V)	20-80	±3-5	3-5
Current(mA)	0	3-20	0
Power consumption (mW)	0.05-0.1	5-100	0.05-0.1
Switching time	1-300 µs	1-100 ns	1-100 ns
C_{up} (series) (fF)	1-6	40-80	70-140
Rs (series) (Ω)	0.5-2	2-4	4-6
Capacitance ratio	40-500	10	---
Cutoff frequency (THz)	20-80	1-4	0.5-2
Isolation (1–10 GHz)	Very high	High	Medium
Isolation (10–40 GHz)	Very high	Medium	Low
Isolation (60–100 GHz)	High	Medium	None
Loss (1–100 GHz) (dB)	0.05-0.2	0.3-1.2	0.4-2.5
Power handling (W)	<1	<10	<10

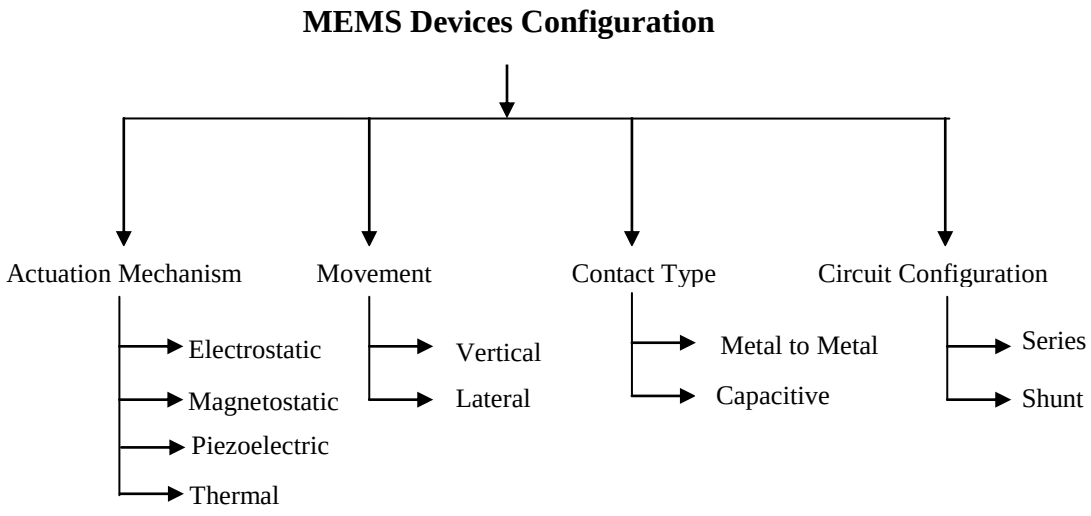

Figure 1.1 Classification of MEMS devices based on actuation mechanism, movement, contact type and circuit.

1.4.1 Metal-to-Metal contact switch

The schematic view of metal to metal contact switch is shown in figure 1.2. In this switch metal-to-metal direct contact is used to achieve an ohmic contact between the switch membrane (cantilever beam) and the pull-down electrode. These switches are capable of maintaining excellent electrical isolation in OFF state and minimal insertion loss in ON state [3]. Metal-to-metal contact switches shows excellent electrical contact while maintaining the minimum contact resistance and low parasitic capacitive coupling to provide a large dynamic range of ON-OFF state impedances. Due to this, these switches are suitable for low frequency RF application ranging from DC to 60 GHz [9]. However, one of the main disadvantages of metal-to-metal contact switch is the contact lifetime which affects the switch performance in terms of insertion loss and isolation.

1.4.2 Capacitive coupled RF-MEMS switches

The schematic view of capacitive coupled RF-MEMS switch is illustrated in figure 1.3. A capacitive coupled RF-MEMS switch uses a metal membrane (MEMS bridge) which exhibits high impedance due to an air gap between the membrane and bottom plate in unactuated state. When a DC voltage is applied between the membrane and bottom plates, the top membrane gets capacitive coupled with the bottom plate which causes the low impedance and high capacitance between the switch contacts. This low impedance path allows the RF signal to the ground and it stops the signal transmission through the MEMS switch. The capacitance ratio between down-state to the up-state capacitance is the key parameter and a high value of the capacitance ratio is always desirable for high frequency application. Capacitive coupled RF-MEMS switch uses a thin dielectric layer on the bottom plates to avoid the stiction problem between switch membrane and bottom plates of the switch [9, 10].

The switch operates as a digitally tunable capacitor with ON and OFF states of the switch. The beam over the electrode acts as a parallel plate capacitor. When the switch beam is in up-state, transmission line experiences a small capacitance and when it is in

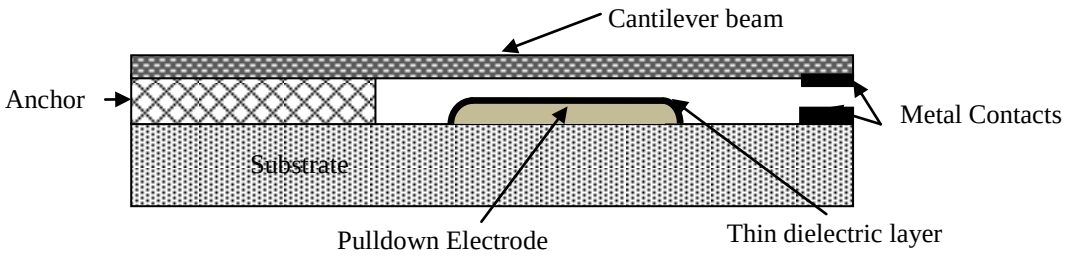

Figure 1.2 Schematic view of a typical metal-to-metal contact RF-MEMS switch.

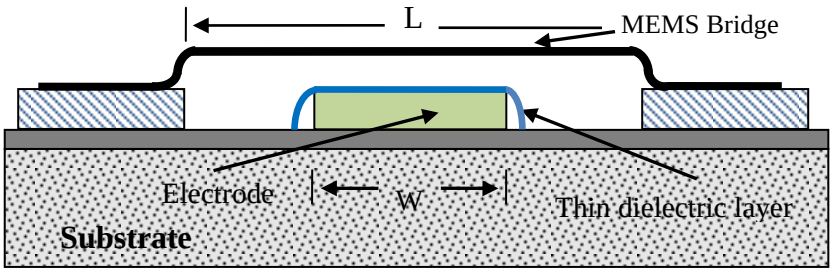

Figure 1.3 Schematic view of a typical capacitive coupled RF-MEMS switch.

Down-state the switch membrane gets touched with the transmission line therefore transmission line experiences a high capacitance with low impedance path to the ground.

Goldsmith C. et.al [9-11] developed a capacitive coupled RF-MEMS switch and this switch was used in shunt circuit configuration with coplanar waveguide (CPW) transmission line for 35 GHz frequency RF application. Tan G.L. et.al [12] also demonstrated a fixed-fixed metal-to-metal contact RF-MEMS switch in shunt configuration with transmission line by using two pull-down electrodes and a central DC-contact area.

1.5 RECONFIGURABLE ANTENNAS

RF-MEMS switches are miniature device that utilizes the mechanical movement to achieve a short circuit or an open circuit in transmission line, which are used to change the operating frequency, radiation pattern of the antenna and are usually named as "Reconfigurable Antenna" (RA). Reconfigurable RF-MEMS antennas were first introduced by E.R. Brown in 1998 [13]. RA has gained a significant interest because a

same antenna can be operated at multiple frequencies. This can be achieved by changing the resonant frequency of the antenna, whereas the resonant frequency will be varied by reconfiguring the geometrical structure of the switched beam [14].

The reconfigurable antenna concept has gained significant interest as a result of two main factors. First, a single RA can perform multiple functions by dynamically changing its properties (operating frequency, polarization and radiation pattern). This can result in a significant reduction to the overall size of multi-mode multiband wireless communication systems. Second, the properties of RA can be used as important additional degree of freedom in an adaptive system [15-16]. The main goal of an antenna is to minimize the reactance of the device by operating the antenna at resonant frequency. These switches can be used in antenna design to modify the resonant frequency by changing the shape of the switch [17].

D. E. Anagnostou et.al [18] integrated ohmic contact cantilever based RF-MEMS switches with self-similar planar antennas to provide a reconfigurable antenna system that radiates similar patterns over a wide range of frequencies. They proposed that this concept can be extended to reconfigurable linear antenna arrays or to more complex antenna structures with large improvements in antenna performance.

Reconfigurable antennas using RF-MEMS switches give several advantages for satellite, radar and mobile communication system based applications [19, 20]. Three-cactus antenna elements were integrated with RF-MEMS switches to create a diversity antenna, three MEMS switches located on CPW feed lines were employed for selection (or switched) and diversity combining, where only one particular signal branch at a given time is selected and is connected to the receiver. Selection diversity schemes with one-port antenna systems offer economical and practical advantages over multi-port diversity schemes. The spiral antenna consists of five sections that are connected with four RF-MEMS switches. One characteristic of the spiral antenna is that the maximum beam direction can be changed by physically changing its arm length thus providing tilted beam radiation with respect to its center axis [21, 22].

N. Hasan, et.al [23] proposed the design of reconfigurable microstrip antenna operating at two different frequencies bands, Y. Tawk et.al [24] has proposed a novel

frequency RA design using photoconductive Si element as optical switches. They demonstrated a new geometry for coupling the light energy onto the silicon switches, thereby facilitating conformal integration of such RA into next generation wireless devices.

H. Salti et.al [25] studied the effect of MEMS breakdowns in reconfigurable reflect arrays. It was shown that 1.5% MEMS breakdown over the array can be responsible for complete failure of the antenna. They have proposed a correction procedure that permits to increase the percentage of breakdown up to 23%. H. Rajagopalan et.al [26] described the design of reconfigurable reflectarray element using commercially available RF-MEMS switches. They performed detailed analysis of the element to obtain minimal losses and maximum phase swing. They attributed the losses mainly due to the dielectric loss tangent of the substrate and metal conductivity.

Recently some researchers [27-28] have developed reconfigurable antenna for wireless local area network (WLAN) and multiple-input-multiple-output (MIMO) communication systems using RF-MEMS switches. Besides high isolation these antenna array also shows low envelop correction, leading to good diversity gain.

1.6 MOTIVATION AND OBJECTIVES

The RF-MEMS switches can outperform its semiconductor counterparts such as transistors and diodes by having lower insertion loss, lower power consumption and higher Q, which inherently meet the antenna design requirements. However, RF-MEMS switches have their own limitations. These limitations are low actuation voltage, insertion loss during closed state, and high isolation at open state at the highest operating frequency [29]. Recently developed RF-MEMS switches for RF application need high pull-up voltage for restoring forces ranging from 20 to 80 V, which is impractical for reconfigurable circuits [30]. Out of four actuation mechanisms, electrostatic actuation mechanism provides a low actuation voltage < 50 V for RF application. Actuation voltage can also be tailored by controlling beam materials, beam thickness and meander structure. Like any other technology RF-MEMS also have some disadvantages like

inadequate RF-power handling capabilities and higher switching time in fixed - fixed beam switch design [31, 32].

RF-MEMS switches needs a low insertion loss < 0.5 dB in ON state and high isolation > 30dB in OFF state for microwave frequency ranges [18, 26]. Thus the aim of the research work was to identify the issues subjected to the design and simulation of a RF-MEMS switch with low actuation voltage, high isolation, low insertion losses, high switching speed with adequate RF power handling capabilities. By combining low-loss, high isolation RF-MEMS switches we can effectively reconfigure the antenna properties (radiation pattern and operating frequency) and their feed structures in order to provide frequency band and polarization diversity. So it is important first to design an efficient RF-MEMS switch which can fulfill the requirement of our application.

Thus, the work presented in this thesis belongs to the RF-MEMS switch design for reconfigurable antennas. This work aims to understand some of the challenges evolved in designing of RF-MEMS switch. Thus the objectives of this research were to design, simulate and analyze the RF-MEMS switches for reconfigurable antennas. In order to fulfill these objectives the work was divided into following steps:

1. To characterize various materials for RF-MEMS switches with optimized performance towards actuation voltage and RF response.
2. To design a switch beam structure for optimized performance.
3. To develop electromechanical and electromagnetic models of the proposed RF-MEMS Switch.
4. To analyze the performance of RF-MEMS switch towards the reconfigurability in antenna in terms of resonance frequency and radiation pattern.

1.7 STRUCTURE OF THE THESIS

This thesis is divided into **six** chapters. The organization of this thesis is as follows:

Chapter 1 presents an introduction and overview of RF-MEMS technology with a focus on the definitions of switch design parameters. It is followed by the classification of RF-MEMS switch technology. The next section explains the RF application of MEMS

switches particularly for reconfigurable antennas. The objectives and motivation toward this research is discussed in last section of this chapter.

Chapter 2 describes the detailed literature review of RF-MEMS switch technology. The characteristics and performance parameters such as actuation voltage, RF characterization, switch lifetime, RF signal power handling, temperature sensitivity and switching speed have been discussed in detail for various RF-MEMS switch designs. It is followed by the current research scenario of RF-MEMS switch design for reconfigurable antenna.

Chapter 3 further elaborates the material selection methodology for switch beam material of RF-MEMS switch. Ashby's material selection approach is used to select the proper switch beam material in order to achieve the better performance of switch for RF applications. This section is followed by description of the performance and material indices required for Ashby's material selection approach for RF-MEMS switches. Last section of this chapter explains how the material selection graphs are used to select the optimal candidate for MEMS bridge material on the basis of various performance and material indices.

Chapter 4 deals with electro-mechanical modeling of the RF-MEMS switch. The electromechanical aspect of the RF-MEMS switch design deals with the air-gap suspended beam mechanism. In this chapter the electro-mechanical equations of switch beam motion and spring constant were defined for proposed non-uniform serpentine flexure based meander section. An analytical model was described for low spring constant flexure design structure for RF-MEMS switch. An analytical expression of spring constant for non-uniform serpentine flexure design is derived for fixed-fixed beam RF-MEMS switch. This analytically calculated spring constant is compared with Finite Element Method (FEM) simulations. This chapter further discusses about the actuation voltage, RF power handling and switching speed for the proposed non-uniform serpentine flexure.

Chapter 5 focuses on the electro-magnetic aspect of the non-uniform serpentine flexure based RF-MEMS switch. Here the switch beam of the RF-MEMS switch is treated as lumped R-L-C model. This chapter presents the dependence of electrical

parameters (capacitance and inductance and resistance) on switch design parameters and material properties. Here the scattering parameters have been analyzed and extracted through Ansoft HFSS simulations.

Chapter 6 presents the RF-MEMS switch based reconfigurable antenna design. This chapter deals with the integration of proposed RF-MEMS switch with antenna structure to achieve the reconfigurability in terms of pattern and frequency. This chapter also discusses the impedance matching techniques and simulation results.

Chapter 7 finally concludes the implications for this research and suggests future work related to the RF-MEMS switches for reconfigurable antenna design.

CHAPTER 2

PERFORMANCE OF RF-MEMS SWITCHES: LITERATURE REVIEW

2.1 INTRODUCTION

The evolution of microfabrication techniques have helped in the development of RF-MEMS switches in diverse area of biomedical sensors, pressure sensors, accelerometers, gyroscopes, microwave and millimeter wave systems [1-4]. The RF-MEMS technology leverages existing state-of-the-art integrated circuits (IC) fabrication technology and hence also exhibits many exciting advantages indigenous to IC fabrication techniques [1]. These advantages include cost reduction through batch fabrication and device to device consistency from etching and lithography technique, which leads in significant weight and size reduction [33-34]. In addition, by using the materials like silicon (Si) and fabrication techniques compatible with IC technology, these switches can be fabricated monolithically integrated on same chip with RF front-end communication system.

The past two decades have seen a remarkable growth in the research of RF-MEMS switch design with high performance beyond 100 GHz [35-36]. This chapter describes the latest accomplishment of RF-MEMS switch design for their potential application in RF (radio-frequency) communication systems. It is seen that RF-MEMS switches offer spectacular performance at microwave frequencies but suffer from high cost packaging and reliability problems, still these switches offers tremendous advantages over the silicon and GaAs switching devices. This chapter explains the research efforts that have

done in past two decades to mature this technology in terms of actuation voltage, insertion loss, isolation, switch lifetime, RF signal power handling, temperature sensitivity and switching speed. The last section of this chapter describes the current status of the research on RF-MEMS switches based reconfigurable antennas.

2.2 ACTUATION VOLTAGE

The first MEMS switch was developed by the Petersen K.E. [37] in 1979 where cantilever based switch design was used on the silicon substrate to achieve the switching of electrical signals at actuation voltage of ~70V. Since then a large number of papers have been published in various journals and conferences with various structural designs of RF-MEMS switch to reduce the actuation voltage. Yao J. J. et.al [3] developed a surface micro-machined miniature RF-MEMS switch using a cantilever beam structure of SiO_2 and achieved an actuation voltage of 28 V. Pacheco S. et.al [38] reported two different designs of RF-MEMS capacitive switches by using serpentine and cantilever spring structure with low spring constant to achieve a low actuation voltage of 14V to 16V for DC to 40GHz frequency range application. Fig. 2.1 presents the micrographs of the serpentine and cantilever spring designs. These switches are basically identical except for the configuration of spring attached to MEMS bridge. The details about the mechanical parameters of these switches are listed in table 2.1.

Table 2.1 Mechanical parameters of spring based RF-MEMS switches as shown in fig.2.1 [38].

Parameters	**Serpentine Spring**	**Cantilever Spring**
Mass (kg)	1.48×10^{-9}	1.19×10^{-9}
Spring Constant (Nm^{-1})	0.478	0.654
Damping Coefficient($Nm^{-1}s^{-1}$)	6.76×10^{-7}	6.76×10^{-7}
Actuation Voltage (V)	4.95	5.79
Resonant Frequency (kHz)	17.97	20.95

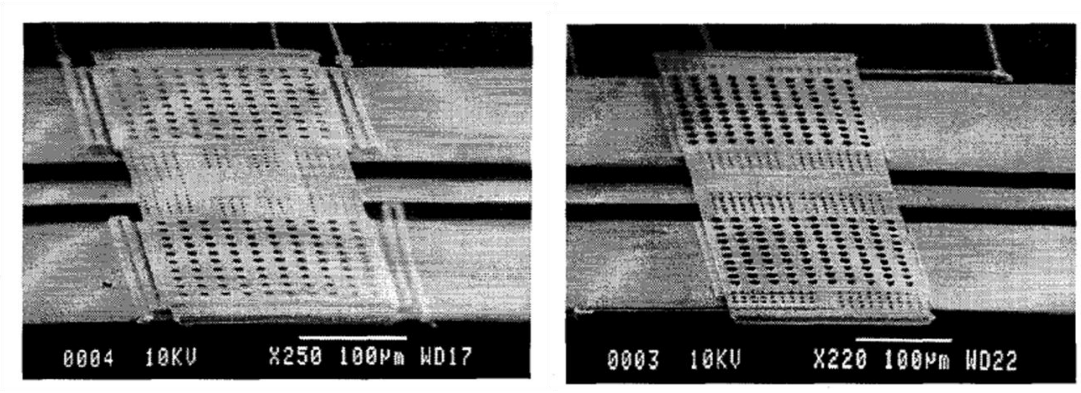

(a) (b)

Figure 2.1: Schematic photograph showing the Micromechanical switch with (a) Serpentine springs and (b) Cantilever springs [Pacheco S. P. et.al [38]].

Pacheco S. P. et.al [39] proposed a modified design of low-loss RF-MEMS switch by incorporating serpentine folded spring structure as shown in figure 2.2, to achieve low actuation voltage of 9V and minimum off-state isolation. This proposed switch was designed with a folded suspension varying from 1 to 5 meander suspension attached with a electroplate nickel membrane. The structure was attached with the actuation plates situated at center conductor of the finite ground coplanar wave guide (FGCPW), the switch membrane clamps down thereby a high capacitance at center conductor provide a short path to the RF signal. For this proposed switch design it was concluded that by increasing the number of meander structure, reduced actuation voltage can be achieved.

Balaraman D. et.al [40] also proposed a design of RF-MEMS switch with various hinge (spring) structures with high resistive silicon substrate to achieve a low actuation voltage. This switch was developed by using sputtered copper based switch membrane with four various hinge geometries. Actuation voltage and spring constant for these hinge structures has been tabulated in table 2.2.

Lee S.-D. et.al [41] developed RF-MEMS switch with a freely moving contact structure to achieve low actuation voltage in which the movement was given by electrostatic actuation. The schematic view of this switch is given in figure 2.3. This switch design was capable to reduce the sufficient amount of actuation voltage upto 4.5V, because actuation energy was not used in elastic deformation of a suspension beam.

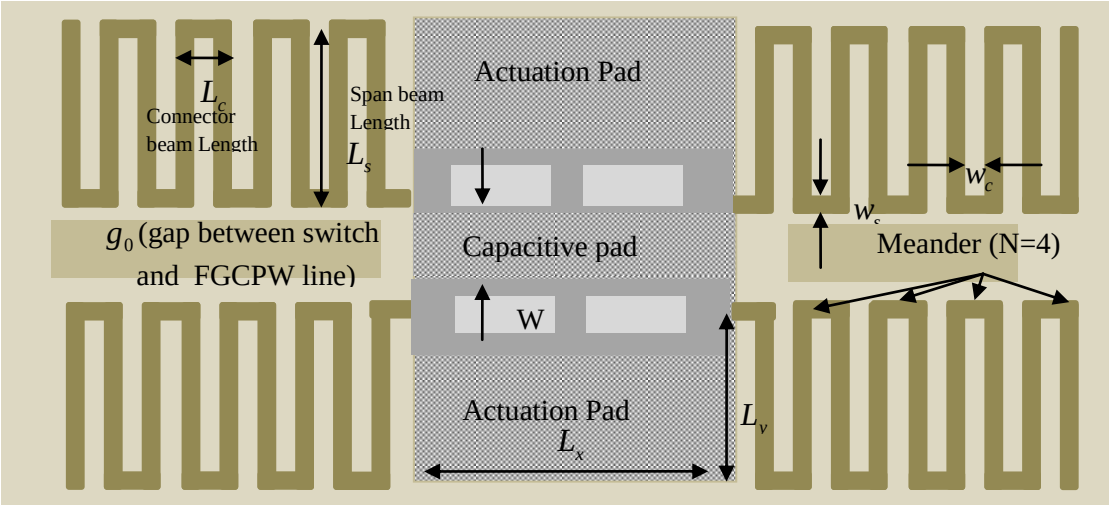

Figure 2.2: Schematic view of RF-MEMS switch with serpentine folded suspensions containing four meanders [Pacheco S. P. et.al [39]].

Table 2.2 Actuation voltages and spring constant for various hinge structures of capacitive shunt switch RF-MEMS switches. [38-40]

Hinge structures	**Actuation Voltage (V)**	**Spring constant (N/m)**	**References**
Cantilever	5.97	0.654	[38]
Serpentine spring (Each suspension contains 2 meanders)	4.95	0.478	[38]
4 suspension bridge (Each suspension contains 5 meanders)	9	---	[39]
4 suspension bridge (Each suspension contains 1 meander)	16.7	14.8	[40]
2 suspension bridge (Each suspension contains 1 meander)	5.7	1.75	[40]
Solid cantilever bridge	17.8	16.7	[40]
2 Meander cantilever bridge	11.5	7.4	[40]

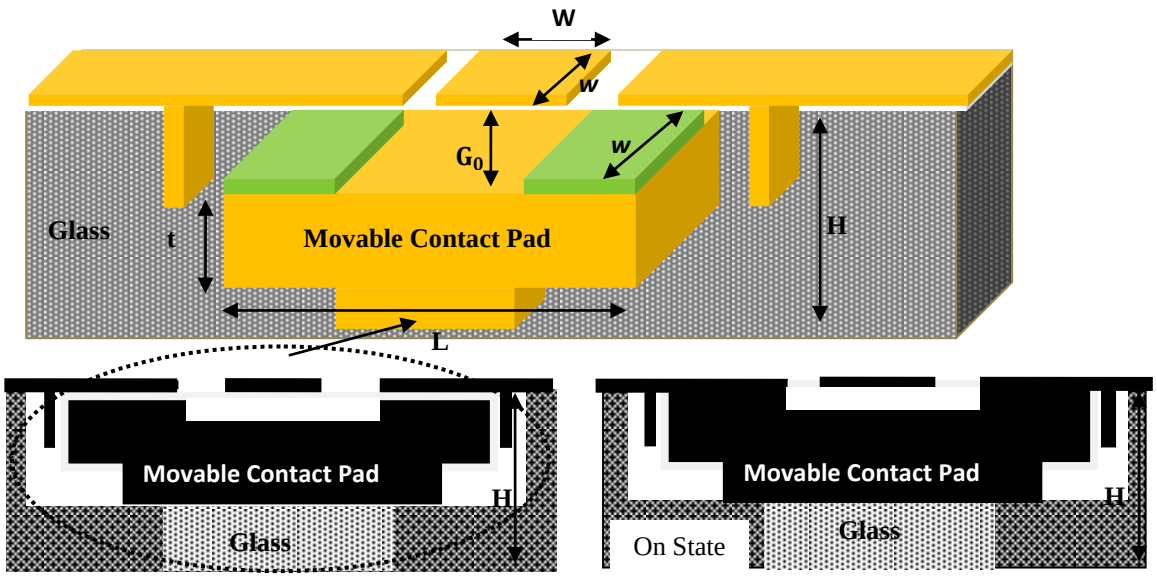

Figure 2.3 Schematic view of RF-MEMS switch with movable contact pad [Lee S.-D. et.al [41]].

Kim J. et.al [42] proposed a DC contact type RF-MEMS switch design to achieve a low actuation voltage. This switch was developed using a thick and stiff silicon membrane with a see-saw mode operation design to mitigate the effect of bending of the membrane due to an internal stress gradient. This switch was designed with uniform small gap between the electrode and the switch membrane.

Kundu A. et.al [43] presented a new design of RF-MEMS which required a very low actuation voltage with improved switching time. The actuation voltage was reduced by a sufficient amount by using a concept of moving transmission line of coplanar waveguide (CPW). This proposed switch used two movable plates where the first moving plate was switch membrane and the second moving plate was CPW transmission line. This CPW transmission line acted as a movable bottom electrode to initiate the actuation process. This switch was able to reduce the actuation voltage and switching time around 20% for optimized design parameter for the two movable plates switch.

Actuation mechanism also plays an important role to reduce the actuation voltage for fixed-fixed beam RF-MEMS switch. Electrostatic actuation is most promising actuation mechanism for RF-MEMS based reconfigurable antennas as compared to other actuation mechanism due to their low cost of implementation. Electrostatic actuation

requires 9-70 V, but does not consume any current, which results in a very low power dissipation (10-100nJ). On the other hand thermal/magnetic/piezoelectric actuation mechanism consumes more currents, which results in higher power dissipation with a probability of MEMS bridge stiction with transmission line. A comparison table of various actuation mechanisms for actuation voltage required for switching operation of MEMS bridge are listed in table 2.3.

Table 2.3 Actuation voltages for different actuation mechanism

Actuation Mechanism	Actuation voltage (V)	References
Electrostatic	9 to 70	[3, 45-49]
Piezoelectric	2 to12	[44, 73]
Electromagnetic	2	[74]
Electro-thermal	2.5-3.5	[75]

To achieve a lower actuation voltage, Polcawich R.G. et.al [44] presented a RF-MEMS series switch design using piezoelectric actuation mechanism. This actuation mechanism retains large restoring force and excellent RF performance. In this design a piezoelectric actuation mechanism was proposed as compared to the electrostatic actuation mechanism because piezoelectric actuation mechanism required extremely low currents and voltages for operation along with the ability to close the large vertical gaps. Lee H.-C. et.al [45] also developed a shunt type ohmic RF-MEMS switch with four cantilever based actuators by using piezoelectric actuation mechanism and reported that these switches can be operated at a low operating voltage of 5V with very low power consumption.

2.3 ISOLATION, INSERTION LOSS AND RETURN LOSS

The RF performance at low frequencies should be characterized by the ON resistance in signal passing state and OFF resistance in signal blocking state. At higher frequencies, RF performance can be described by its insertion and return loss in signal passing state

and isolation in signal blocking state. Till now various papers have been published to achieve a high RF performance at low as well as at high frequencies. Here the efforts done by various researchers have been described in order to achieve better RF performance of RF-MEMS switches.

Goldsmith C. et.al [9-11] developed a low-cost, low loss RF-MEMS capacitive shunt switch using electrostatic actuation mechanism. It was reported that insertion loss can be minimized by reducing the length of the transmission lines because the narrow input/output interconnects between the transmission line and switch contact area produces more insertion loss during signal passing state. High isolation can be achieved by removing the imperfection in the deposited switch membrane because these imperfections provide the improper contact between the bottom electrodes and switch membrane. Goldsmith C. et.al [11] further modified this switch for microwave and millimeter wave frequencies with significant improvement in terms of low insertion loss and high isolation. This proposed switch design used aluminum based coplanar waveguide (CPW) and switch membrane (MEMS bridge) in order to achieve low insertion loss and high isolation. Muldavin J.B. et.al [46] demonstrated a tuned cross switch incorporating four membrane shunt MEMS switches. The proposed tuned cross switch proved the advantage of the tuning approach to achieve high isolation in down-state and excellent return loss in up-state in comparison with individual RF-MEMS switch. This proposed tuned cross switch design was suitable for low-loss high-isolation communication application at 28 GHz frequency. Rizk J.B. et.al [47] reported a significant improvement in isolation and insertion loss of X-Band RF-MEMS switches by using a π-circuit network with two MEMS shunt switches.

Muldavin J.B. et.al [48] developed a RF-MEMS shunt switches to achieve a very high isolation for X-band frequency range from 7 GHz to 12 GHz. It was reported that this proposed design achieved a very high isolation by increasing the series inductance of the switch. This series inductance was maximized by adding a short section of transmission line between the MEMS bridge and ground plane thereby the resonant frequency was pushed down to the X band frequency range. The proposed switch design resulted in a lower insertion loss and much higher isolation of better than 30dB at X-band

frequencies. It was proposed that the insertion loss and isolation may be improved by using thicker metal underlying between the metal membrane and transmission line.

Tan G.-L. et.al [49] reported the effect of bias lines on the insertion loss, by using a resistive bias line attached to each of the two pull down electrodes of RF-MEMS switch. The schematic view of this developed switch design is shown in figure 2.4. They reported that resistive bias line with low value can result with improved insertion loss in DC contact MEMS shunt switches.

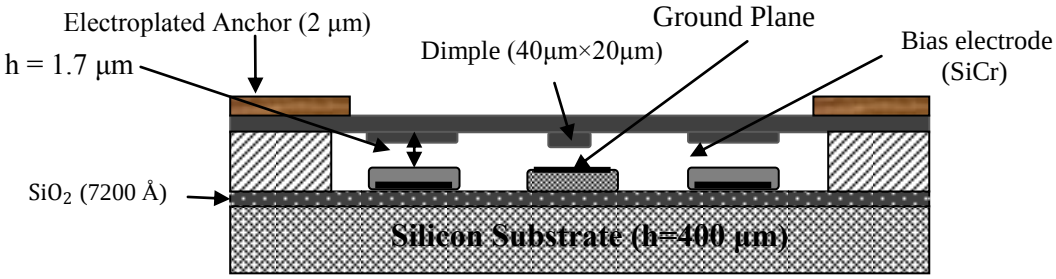

Figure 2.4: Schematic view of RF-MEMS DC-contact shunt switch [Tan G.-L. et.al [49]].

Rizk J.B. et.al [50] reported a significant improvement in isolation and insertion loss of W-Band RF-MEMS switches by using T-match and π-circuit network with two MEMS shunt switches. RF-MEMS shunt capacitive switches with W-band coplanar waveguide shows very low insertion loss (-0.2 to -0.5 dB) and better isolation (≤-30dB) over the entire wide band. Ghodsian B. et.al [51] developed a DC-contact MEMS series switch by using cantilever beam with fork tip design. Fig. 2.5 illustrates the fork tip design steps of this proposed switch. This switch design reduced the upstate capacitance by minimizing the electrode overlap area between the tip of cantilever beam and the underlying signal line. This RF-MEMS switch has also shown the high isolation at high frequencies because of up-state capacitance.

Jang Y.-H. et.al [52] proposed a RF-MEMS contact switch design to achieve the high isolation using two directional movements of the contact part: vertical and lateral by using comb and parallel-plate actuators. Yamane D. et.al [53] demonstrated a bidirectional electrostatic actuation mechanism for a dual SPDT (single-pole double-through) switch.

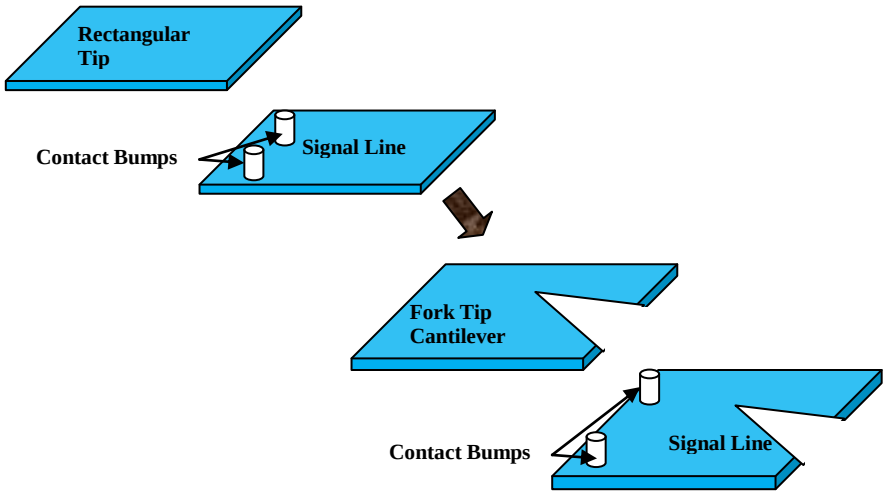

Figure 2.5: Transition from rectangular tip cantilever beam to fork tip design by cutting out the tip [Ghodsian B. et.al [51]].

This switch was designed with silicon-on-insulator (SOI) wafer to minimize the dielectric loss because suspension beam over the coplanar or microstrip line exhibited the electric field of travelling wave which prevents the condensed matter of substrate and increases the dielectric loss. In this switch design, the insertion loss is increased due to the dielectric loss in thin dielectric layer. In order to reduce the insertion loss, this switch was designed by adapting the layer-separation technique. Pacheco S.P. et.al [39] suggested that this isolation can also be reduced by decreasing the thickness of the dielectric between the switch and the conductor in such a way that dielectric break down should not happen.

2.4 SWITCH LIFETIME

Another important parameter of RF-MEMS switch is the switch lifetime. The lifetime of the switch can be measured by inspecting the degradation of the mechanical structure (switch membrane) of the switch. Switch lifetime of capacitive coupled and metal-to-metal contact switches has been intensively studied in the last few years. In metal-to-metal contact switches, the mechanism that limits lifetime is the degradation of the metal contacts with repeated actuations while in capacitive membrane switches, the limiting mechanism is the dielectric charging within the switch dielectric layer.

Switch lifetime can be further divided into two types: cold switching and hot switching life time. Cold switching lifetime is defined as zero signals passes through the switch contact area and hot switching lifetime refers to that of a switch when a specific signals level passes through the switch contact area [54, 55].

Goldsmith C. et.al [56] demonstrated a capacitive RF-MEMS switch and characterized the switch lifetime as a function of actuation voltage. It was reported that the applied electric field in RF-MEMS switch is responsible for dielectric charging which results in sticking (failure) of the switch membrane. The relation between electric field and actuation voltage is given as follows [56].

$$J = Ve^{+2a\sqrt{V}/T - q\varphi_B/kT} \quad \ldots (2.1)$$

where J is the current density, V is the applied voltage, T is the temperature in Kelvin, k is the Boltzman's constant, φ_B is the barrier height and a is a constant which depends on electron charge, insulator dynamic permittivity, and film thickness. Equation 2.1 shows that the switch lifetime (electric field) has exponential dependency on the applied actuation voltage. Czarnecki P. et.al [57] reported that the charging of the substrate can also affect the lifetime of capacitive shunt RF-MEMS switch. They had used two substrates (silicon and glass) for switch design and concluded that the substrate can also trap charges which degrade the switch lifetime. Wong W.S.H. et.al [58] proposed a novel actuation voltage technique to achieve the sufficient reduction in dielectric charging in RF-MEMS capacitive switches, leading to a longer switch lifetime. In this work, actuation voltage technique was used to analyze the dielectric charging generated by different actuation voltages. It was concluded that a suitable actuation voltage can reduce the charge buildup and thereafter extends the lifetime of the switch.

Rottenberg X. et.al [59] proposed a analytical model of RF-MEMS capacitive switch with distributed dielectric charging, demonstrating a non-uniform air-gap distribution and a non-uniform volume distribution of charges in the dielectric layer. This switch design provided a deep insight into the irreversible stiction problem in electrostatic actuation mechanism.

2.5 RF SIGNAL POWER HANDLING

RF signal power handling refers to the power at which the MEMS device fails to operate properly. RF signal power can be applied to the switch at a broad range of frequencies with different power levels to achieve high performance for microwave frequencies. RF signal power handling capability of RF-MEMS switches are mainly limited by following two factors [60]:

- **RF latching: -** RF latching can be defined as the applied RF power, which provides the enough force on the membrane to hold the switch down when DC bias is removed.
- **RF self-actuation:-** RF self-actuation is referred as a situation in which the high RF power actually creates enough potential to pull the membrane down in unactuated state without using a DC bias voltage across the switch.

Lot of research has been reported in past towards the RF signal power handling capabilities of RF-MEMS switches. To enhance the power handling capability of metal-to-metal contact type RF-MEMS switch, Jensen B.D. et.al [61] reported a electro-thermal model, to predict the current density in the metal-to-metal contact area of the switch using electromagnetic modeling. With the help of this model the accurate power handling capability can be calculated without sacrificing the switch performance. For high power application, Peroulis D. et.al [62] proposed a new RF-MEMS switch design by using DC and RF pads with a top electrode as shown in figure 2.6, This design also investigated the self actuation and stiction problem of switch membrane in high RF power handling situation. Grenier K. et.al [63] proposed a specific RF-MEMS switch with two bridge level topology to encounter the failure mechanism related to the self actuation and electromigration for high RF power handling. This topology was developed with a mobile bridge structure, which was attached with two non-movable top and bottom electrodes to achieve the capacitive contact between the switch membrane and transmission line. High RF power self actuation and electromigration phenomenon were encountered by using pull-up electrodes and large bridge dimensions respectively. Various other RF-MEMS switch designs and studies has been proposed and investigated in order to improve the power handling capability upto 6 W [64-65].

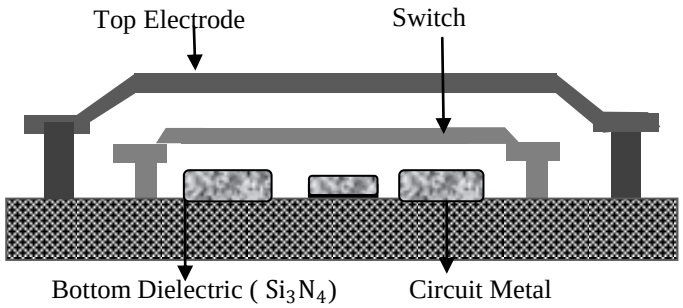

Figure 2.6: Schematic view of MEMS shunt switch with top electrode [Peroulis D. et.al [62]].

2.6 TEMPERATURE SENSITIVITY

In past few years, various RF-MEMS switch designs have been proposed to address the issue of temperature sensitivity due to fast temperature changing environment. Palego C. et.al [66] proposed RF-MEMS capacitive shunt switches with molybdenum membrane because this membrane exhibited a significantly reduced sensitivity to ambient temperature as compared to aluminum switch membrane. Mahameed R. et.al [67] presented a RF-MEMS switch which utilizes the lateral thermal buckle-beam actuator design in order to reduce the switch sensitivity to thermal stress. This switch demonstrated very low temperature sensitivity of ~-50mV/ºC at 25ºC to 125ºC. Mahameed R. et.al [68] also proposed a design by using separate and interdigitated RF and actuation electrodes which prevents dielectric charging under high actuation voltages. This design was less temperature sensitive with higher actuation voltage. Various switch design with different switch membrane structures has been developed in order to develop temperature sensitive RF-MEMS switch for wider temperature range applications [69, 70]. RF-MEMS switch designs with fixed-fixed shunt configuration are more sensitive to temperature effect, which occurs due to the air gap, thin suspended membrane and pull-down voltage. Mahameed R. et.al [70] presented a design and fabrication of capacitive switch with 0.8-μm thin Au bridge membrane using thin-film technology, which shows less than 50-mV/°C variation for pull-down voltage with 25°C to125°C temperature variation.

2.7 SWITCHING SPEED

Switching speed is another important performance parameter of RF-MEMS switches for transmit/ receive switching application. Though RF-MEMS switches exhibit excellent RF characteristics such as low insertion losses and high isolation but these switches have a very slow switching speed. Switching speed depends on mass of the switch membrane and switch construction. Switching speed can be increased by using a switch membrane with lower mass. Generally a RF-MEMS switch operates at a speed of 2 to 50ms for several million switching operations. The low mass of membrane based MEMS capacitive shunt switches make it suitable for relatively fast switching operation in comparison with cantilever-style MEMS switches [71]. Yao J.J. et.al [3] demonstrated a RF-MEMS switch on semi-insulating GaAs substrate and achieved a low switching speed. Goldsmith C. et.al [10] developed a switch whose switching speed is comparatively low with respect to semiconductor switches, and these switches are most suitable for beam steering application in phased array antennas. Goldsmith C. et.al [11] modified the RF-MEMS capacitive shunt switch design and achieved increased switching speed by using thin aluminum switch membrane. A comparison table of characteristics and performances for various RF-MEMS switches are listed in table 2.4.

2.8 RF-MEMS SWITCHES FOR RECONFIGURABLE ANTENNA: CURRENT STATUS

Anagnostou D. E. et.al [76] has demonstrated reconfigurable ultra wideband (UWB) antenna with series ohmic-contact RF-MEMS switches. These switches are used as relays to activate or deactivate the stubs with 30 V actuation voltage. It was concluded that RF-MEMS switches are the better choice as switching element because they do not require extra bias line to activate or deactivate the MEMS bridge. Taye J. et.al [77] has described a novel design of RF-MEMS shunt capacitive switch for actuation voltage and high capacitance ratio. This design was demonstrated with meander based switch beam, which needs a low actuation voltage of 2-6 V with down-state to up-state capacitance ratio of 117.

Table 2.4 Characteristics and performances of different RF-MEMS switches.

Switch Design	Contact Type	Substrate used	Actuation voltage (V)	Insertion loss (dB)	Isolation (dB)	Switching speed	Frequency range	Ref
Cantilever based Series switch	Metal to metal	GaAs	~28	0.1 at 4 GHz	-50 at 4 GHz	30 µs	DC to RF frequency	[3]
Cantilever based Series switch	Metal to metal	silicon	2	1 upto 40 GHz	20 upto 60 GHz	40-60 ms	---	[44]
Fixed-fixed beam shunt switch	Capacitive	silicon	30-50	<0.25 at 35 GHz	35 at 35 GHz	<5 µs	Up to 40 GHz	[11]
Fixed-fixed beam shunt switch	Capacitive	--	14-16	<0.2 at 20 GHz	-30 at 40 GHz	--	--	[38]
Fixed-fixed beam shunt switch	Capacitive	silicon	15-20	0.6 at 22-38 GHz	50	--	DC to 40 GHz	[46]
Fixed-fixed beam shunt switch	Capacitive	silicon	--	<0.2	35 at 10 GHz	--	7-12 GHz	[48]
Fixed-fixed beam shunt switch	Metal to metal	silicon	65	-0.1 to -0.15 upto 30GHz	-34 at 0.1 to 2 GHz-20 at 18 GHz	--	0.1 to 20 GHz	[49]
Fixed-fixed beam shunt switch	Capacitive	quartz	--	-0.2 to -0.5 at W band	≤ -30 at W band	--	75 to 110 GHz	[50]
Fixed-fixed beam shunt switch	Capacitive	silicon	25	0.29 at 24 GHz	30.1 at 24 GHz	8 ms	24 GHz	[72]

The main advantage of this switch design was to attain higher isolation of 40 dB, insertion loss of 0.75 dB from 10-20 GHz frequency range.

Fathi M. B. et.al [78] explained the design and simulation of a new electrostatically actuated RF-MEMS switch for reconfigurable antenna application. This RF-MEMS switch structure was designed with two-step electrostatic actuation mechanism which requires 3.5 V actuation voltage with promising RF performance in terms of isolation of -12 dB and insertion loss of -20 dB at 30 GHz. Bansal D. et.al [79] reported a novel design of RF-MEMS switch with anti stiction and low insertion loss

properties for RF application. A new mechanism of floating metal was utilized to increase the capacitance ratio from 97.5 to 1755 with improved return loss of -38 dB at 9.5 GHz. The reliability of the switch was also improved by reducing stiction failure. Vu T. M. et.al [80] explained a RF-MEMS switch design for V band reconfigurable antenna application. In this study it was concluded that pull-down electrode should be placed correctly in order to ensure a lower actuation voltage requirements for higher frequency applications. They simulated the switch on COVENTOR and obtained the actuation voltage of 32 V for contact between MEMS bridge and transmission line.

Pourziad A. et.al [81] presented a novel multistate RF-MEMS switch for reconfigurable microstrip antenna application. The proposed switch design exhibits better RF characteristics with simple DC biasing mechanism. The proposed design requires three switch beams to achieve the switching operation, which increases the space complexity of actuation electrode with higher actuation voltage requirements. Meng X. et.al [82] reported RF-MEMS switch based frequency reconfigurable antenna design for eight band operations covering the operating bands of 700-787 MHz, 824-960 MHz, and 1710-2690 MHz. In this design it was concluded that DC-bias circuit of capacitive RF-MEMS switch has little effect on radiation pattern and antenna efficiency.

Armenta C. J. A. et.al [83] demonstrated a reconfigurable phased array antenna at 12.5-12.34 GHz, which was fabricated with RF-MEMS switches on same PCB board. It was reported that RF-MEMS switch shows a good behavior with a return loss of -25 dB and insertion loss of better than -0.6dB, whereas the whole antenna shows return loss below to the -15dB at 12.5 GHz. However this switch design required higher actuation voltage requirements, which results in terms of stiction issues of switch beam due to the dielectric charging.

Lucyszyn S. et.al [84] described that RF-MEMS based antenna offers enhanced performance over the conventional solid state devices. It was reported that RF-MEMS switches behaves as non radiating element, although these switches provide some form of frequency tuning for reconfigurable antennas.

CHAPTER 3

MATERIAL SELECTION METHODOLOGY

3.1 INTRODUCTION

The demand of RF-MEMS switches is on the rise because of the ever increasing demand for low power wireless systems. Their miniaturization, improvement in performance, reliability and low power consumption made RF-MEMS devices a rapidly growing sector of microelectronic industry [85, 17]. There is a significant impact of MEMS technology in communication applications and RF-MEMS are emerging as a promising alternative to their solid-state counterparts. However MEMS switches possesses slow switching speed and high actuation voltage [86-87] as mentioned in previous two chapters.

RF-MEMS switches are being used widely for reconfigurable antennas. C.C. Cheng et.al [87] described a reconfigurable millimeter-wave lens-array antenna based on DC contact MEMS switches with cantilever design and concluded that MEMS bridge resistance and up-state capacitance have the largest impact on the frequency response of the antenna. C.W. Jung et.al [88] achieved RF switching for a reconfigurable rectangular spiral antenna with a set of capacitive MEMS switches having low power consumption, higher Q and low RF loss, to provide scan-beam capability. These RF-MEMS switches are used to change spiral overall arm length for different beam direction radiation with low RF loss. So this shows that the performance of an antenna depends vastly on RF-MEMS switches which in turn depend on suitable material to be used for switch. So to

select the best possible material for RF-MEMS switch is a challenge as every material is having it advantages and limitations.

Though, several material selection strategies have been developed in the past. But the methodology of material selection for bridge material used in RF-MEMS switches particularly for reconfigurable antenna has never been proposed. Material selection strategies should have the functional requirement for MEMS bridge and various important factors need to be considered [89]. R. V. Rao [90] suggested a material selection methodology based on graph theory and matrix approach. However, this approach does not provide the provision of checking the consistency of results for relative comparison between the attributes. One of the major drawbacks of Rao's material selection approach is more computational complexity. R. Roth et.al [91] presented a multi-attribute utility analysis (MAUA) for material selection but this approach takes longer time to complete the analysis, as this strategy demands more computations and needs an exact knowledge of the attribute levels with accuracy to prepare questionnaires. G. Guisbiers et.al [92] also presented a material selection methodology for RF-MEMS switches but they have taken only two material indices into consideration. Ashby provides a comprehensive material selection strategy with less computation [93]. So the Ashby approach is widely accepted for MEMS based design.

Through literature review [66, 94-96] it has been observed that the possible materials used for bridge material for fixed-fixed beam capacitive shunt switch are gold, aluminum, platinum, molybdenum, copper, nickel, alumina and silicon nitride. In this study the key material indices considered for MEMS capacitive switch are Young's modulus, electrical resistivity, Poisson's ratio, thermal expansion coefficient and thermal conductivity.

So this chapter presents the results of the study on material selection issue of RF-MEMS switch. First, in section 3.2, a detailed description of Ashby's material selection approach is presented. Section 3.3 discusses about the RF-MEMS switch bridge design and performance. Section 3.4 explains about the performance indices required in Ashby's approach. Section 3.5 discusses the results and analysis of the study and finally section 3.6 provide the conclusion drawn in this chapter.

3.2 ASHBY'S METHODOLOGY

The Ashby's material selection strategy tells how to characterize the appropriate material for desired performance depending upon their attributes (mechanical, electrical and thermal properties of the material). A design demands a certain profile of these attributes. The identification and short listing of these attribute profile are done by screening and ranking [93].

Ashby's material selection approach involves five steps, as illustrated in fig. 3.1. In the first step, the design requirements for the structural component are derived based on function, objectives and constraints. The next step of Ashby methodology shows that the immense wide choice is narrowed, first by applying property limits which screen out the material which cannot meet the design requirements. Further narrowing is achieved by applying the material indices and ranking the candidate based on their ability to provide best performance. Then the detailed supporting information for each shortlisted candidate called as prime candidates, provide the final choice of material. A material index is a combination of material properties which maximize the performance of a component for a given requirement. These material indices are derived from the design requirement for a component through an analysis of function, objectives and constraints. A performance index is group of material properties which governs some aspect of the performance of a component. A material selection using performance indices is best achieved by plotting one material property on each axis of material selection chart [97]. The design of a component is specified by three parameters: functional requirements, geometrical properties and material properties. The performance of element is described by

$$P = f\,[(F\ G\ M)] \qquad \ldots (3.1)$$

Here P describes the performance of element and f describes the function of the functional requirement (F), geometrical properties (G) and material properties (M) respectively. Eq. (3.1) can also be written as:

$$P = f_1(F)\, f_2(G)\, f_3(M) \qquad \ldots (3.2)$$

Here element performance is described by individual functions of F, G and M. So the optimum subset of material can be identified by single functional requirement. For all F and G the performance can be optimized by optimizing the appropriate material indices.

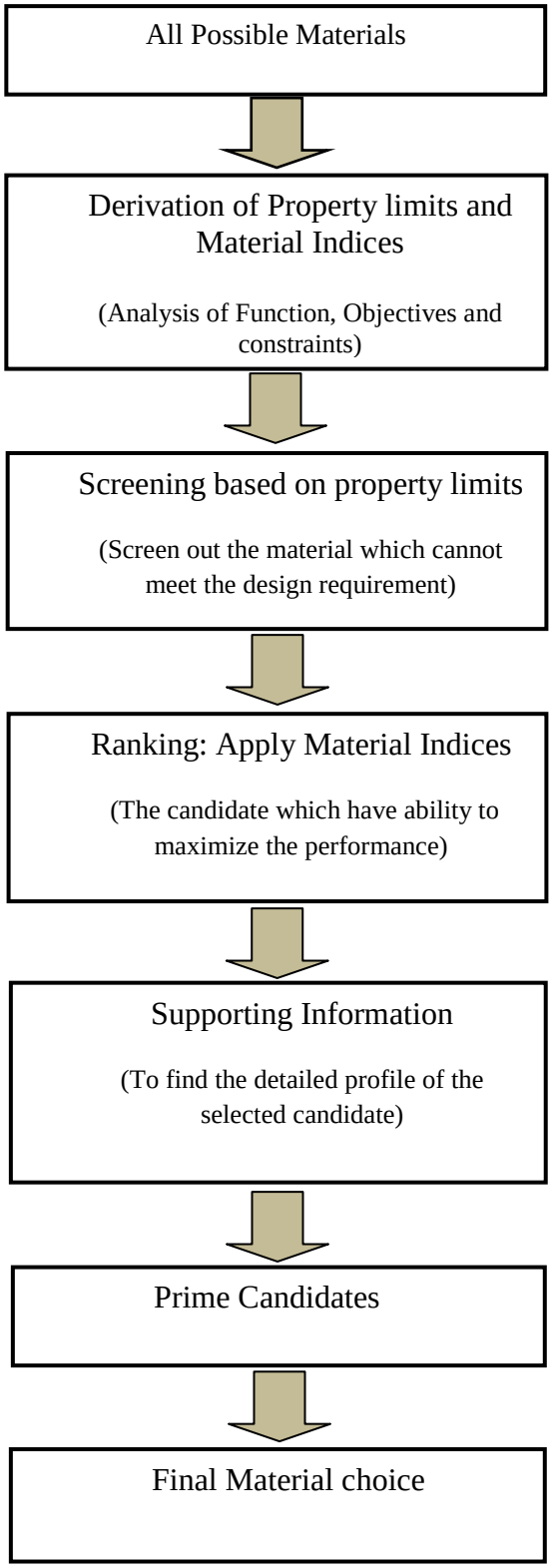

Figure 3.1: Material Selection chart for Ashby's Methodology.

This optimization conventionally performed using graphs with axes corresponding to different material indices or material properties [97].

3.3 RF-MEMS SWITCH BRIDGE DESIGN

The most common design of switch is the fixed-fixed beam capacitive shunt switch. This switch beam is suspended at a height of *g* above the dielectric layer on the transmission line. A suspended micro-machined bridge structure with a length *L*, width *w* and thickness *t* and an actuation electrode of a length *W*, as shown in Fig. 3.2a, can be approximately modeled as a fixed-fixed beam with these parameters as illustrated in Fig. 3.2 b.

The switch operates as a digitally tunable capacitor with two states. When a voltage is applied between a switch beam and the pull-down electrode, an electrostatic force is induced on the beam. The beam over the electrode acts as a parallel-plate capacitor. When the switch beam is in upstate, the transmission line experiences a small capacitance and when it is in down state, transmission line experiences a high capacitance [95].

But these switches have their own limitations. These limitations are low actuation voltage, RF loss during closed state and thermal residual stress of the switch beam. Various design aspects and governing equations concerning with performance of RF-MEMS switch should be able to optimize the device performance using Ashby's material selection approach.

3.4 PERFORMANCE AND MATERIAL INDICIES

Various material properties of RF-MEMS bridge materials such as Young's modulus (*E*), Poisson's ratio (ν), thermal expansion coefficient (α), thermal conductivity (K) and electrical resistivity (ρ) are taken into consideration, which affect the performance of the device and hence form performance indices. Table 3.1 shows the material properties of various possible materials, used as bridge material for RF-MEMS switches.

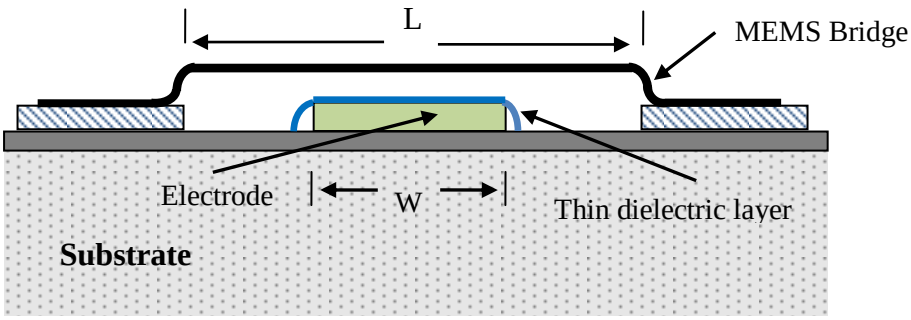

Figure 3.2a: Sketch of a fixed-fixed beam RF-MEMS switch structure.

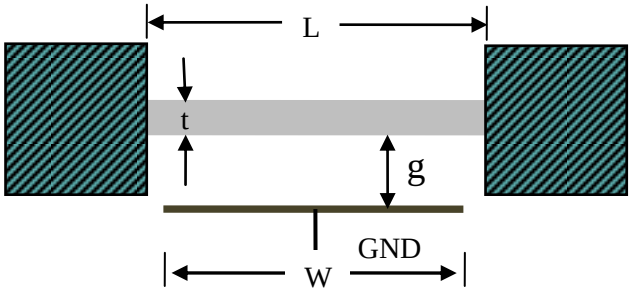

Figure 3.2b: Model of a fixed-fixed beam structure shown in figure 3.2a.

3.4.1 Actuation voltage

At the time actuation, sufficient actuation voltage is the important parameter for RF-MEMS switches and hence it forms the first performance index of the RF-MEMS switch bridge material. At the time of actuation, sufficient actuation voltage is applied between the electrode and MEMS bridge, which is given by [1].

$$V_p = \sqrt{\frac{8k}{27\varepsilon_0 Ww}\, g^3} \qquad \ldots (3.3)$$

where k is spring constant, ε_0 is permittivity of free space, W, w and g are the length of the pull down electrode, width of beam and gap between the electrode and beam, respectively.

From eq. 3.3, it is clear that the actuation voltage can be reduced in three different ways: first by decreasing the height between the bridge and the electrode, secondly by increasing the area of the bridge and lastly by diminishing the bridge structure with low spring constant. Out of these possibilities, third possibility depends on bridge material parameter, so this is an appropriate way to minimize the actuation voltage.

Table 3.1 Material Properties of the considered materials [98].

Material	**Young's Modulus E (GPa)**	**Poisson's Ratio (ν)**	**Electrical Resistivity ρ (Ω-m)**	**Thermal Conductivity k (W/m-K)**	**Thermal Expansion Coefficient α $(10^{-6}(^{\circ}C)^{-1})$**
Aluminum	69	0.33	2.90×10^{-8}	222	23.6
Gold	77	0.42	2.35×10^{-8}	388	14.2
Copper	115	0.33	1.72×10^{-8}	315	17
Platinum	171	0.39	10.60×10^{-8}	71	9.1
Nickel	204	0.31	9.50×10^{-8}	70	13.3
Silicon Nitride	304	0.3	$> 10^{12}$	29	2.7
Molybdenum	320	0.32	5.20×10^{-8}	142	4.9
Aluminum oxide	380	0.22	$> 10^{13}$	39	7.4

(i) ***Spring constant component due to Young's modulus***

The spring constant for fixed-fixed beam structure can be given by [1].

$$k = 4Ew\left(\frac{t}{L}\right)^3 \quad \ldots (3.4)$$

where E is the Young's modulus and w, t and L are, width, thickness and length of the beam, respectively. So from eq (3.3) and (3.4) it is clear that actuation voltage is directly proportional to the square root of the Young's modulus. So, the first material index (MI) related to the actuation voltage is

$$\mathrm{MI}_1 = \sqrt{E} \quad \ldots (3.5)$$

(ii) ***Spring constant component due to thermal residual stress and Poisson's ratio***

Spring constant also depends on the thermal residual stress and Poisson's ratio of the beam material which is given by [66].

$$k = \frac{8\gamma\ (1-\nu)(\sigma_0 - \Delta\sigma)tw}{L} \quad \ldots (3.6)$$

where γ is geometric factor, σ_0 is thermal residual stress at reference temperature, ν is Poisson's ratio, $\Delta\sigma$ is the change in thermal residual stress. So from eq (3.3) and (3.6) it is clear that the second material index related to the actuation voltage is

$$\mathrm{MI}_2 = \nu \quad \ldots (3.7)$$

Now temperature variation results in the change in thermal residual stress of the beam which is given by [66].

$$\Delta\sigma = E\ \Delta\alpha\,\Delta\mathrm{T} \quad \ldots (3.8)$$

where $\Delta\alpha$ is the difference in thermal expansion coefficient between the beam and substrate and $\Delta\mathrm{T}$ is the temperature change of the beam. Eq. 3.8 shows that thermal residual stress is directly proportional to the thermal expansion coefficient. From eq. (3.6) and (3.8) it can be analyzed that higher value of thermal expansion coefficient provides the lower spring constant. So the third material indices related to the actuation voltage is

$$\mathrm{MI}_3 = \alpha \quad \ldots (3.9)$$

Therefore, the first performance index related to the actuation voltage is;

$$\mathrm{PI}_1 = \mathrm{f}\,(E, \nu, \alpha) \quad \ldots (3.10)$$

3.4.2 RF Loss

Second performance index of the bridge material is related to the RF loss which can be reduced significantly by choosing suitable bridge material having good conductivity. RF power dissipated in the beam is given by [1].

$$\mathrm{P}_{\mathrm{loss}} = \mathrm{I}^2.\mathrm{R} \quad \ldots (3.11)$$

where I is the current in the switch beam and R is the beam resistance which is given by [66]

$$R = \frac{\beta \rho L}{4 t w} \quad \text{... (3.12)}$$

where β is a constant and is related to the current crowding into the membrane, and ρ is electrical resistivity of the beam. From the eq. (3.11) and (3.12) it can be concluded that power loss in beam structure is directly proportional to the electrical resistivity of the bridge material. Therefore the fourth material index related to the power loss is

$$MI_4 = \rho \quad \text{… (3.13)}$$

Therefore, second performance index related to the RF loss in beam structure is;

$$PI_2 = f(\rho) \quad \text{… (3.14)}$$

3.4.3 Thermal residual stress

For large RF signals, the MEMS bridge experiences the temperature change due to the self heating which further causes the change in thermal residual stress which is given by [66].

$$\Delta\sigma = E\ \Delta\alpha P_{loss} R_{TH} \quad \text{… (3.15)}$$

where P_{loss} is RF power loss and R_{TH} is thermal resistance which is given as [66].

$$R_{TH} = \frac{\varepsilon L}{4 K t w} \quad \text{… (3.16)}$$

where K is thermal conductivity and ε is non-uniform temperature distribution. The product of electrical and thermal resistances of the bridge material (R. R_{TH}) produces the self heating in the MEMS bridge. Therefore from eq. (3.16) and eq.(3.12) it is concluded that, the fifth material index is;

$$MI_5 = R_{TH} R = \frac{1}{K}.\rho \quad \text{… (3.17)}$$

Therefore, third performance index related to the thermal residual stress in beam structure is;

$$PI_3 = f\left(\frac{1}{K}.\rho\right) \quad \text{… (3.18)}$$

3.5 RESULTS AND ANALYSIS

The optimal performance of MEMS bridge material varies with different performance indices. The material selection graphs are used to select the optimal candidate for MEMS bridge material and also used to identify the trade-offs between the conflicting material indices.

Fig. 3.3 shows the variation between thermal expansion coefficient (α) and Poisson's ratio (ν) for all possible bridge materials. It is considered that a material with high values of Poisson's ratio (ν) and thermal expansion coefficient (α) is suitable to minimize the actuation voltage. From the plot, it is observed that there is a trade-off between gold and aluminum. Because gold shows the higher value of ν with a lower value of α, but aluminum shows higher value of α with lower value of ν.

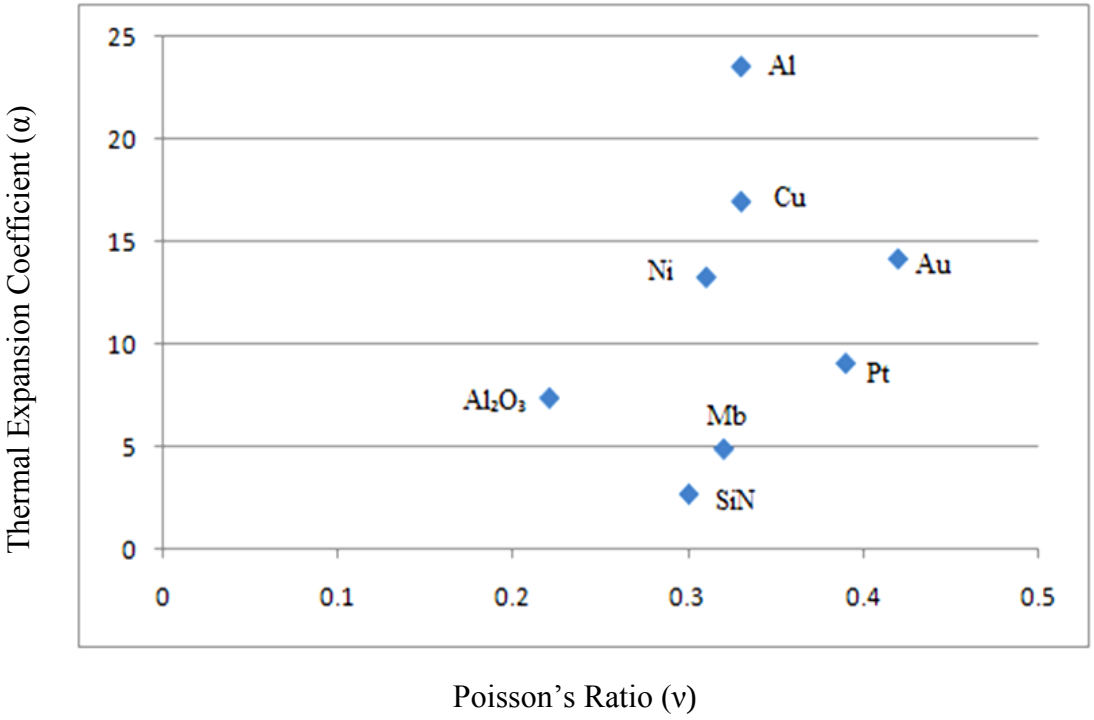

Figure 3.3: Thermal expansion coefficient (α) versus poisson's ratio (ν) for considered materials.

Fig. 3.4 shows the plot of Poisson's ratio (ν) versus Young's modulus (*E*). From the eq. (3.5) and (3.7) it can suggested that a material with low value of Young's modulus (*E*) and high value of Poisson's ratio (ν) diminish the actuation voltage. From the plot it can be concluded that gold and aluminum are the best material to reduce the actuation voltage.

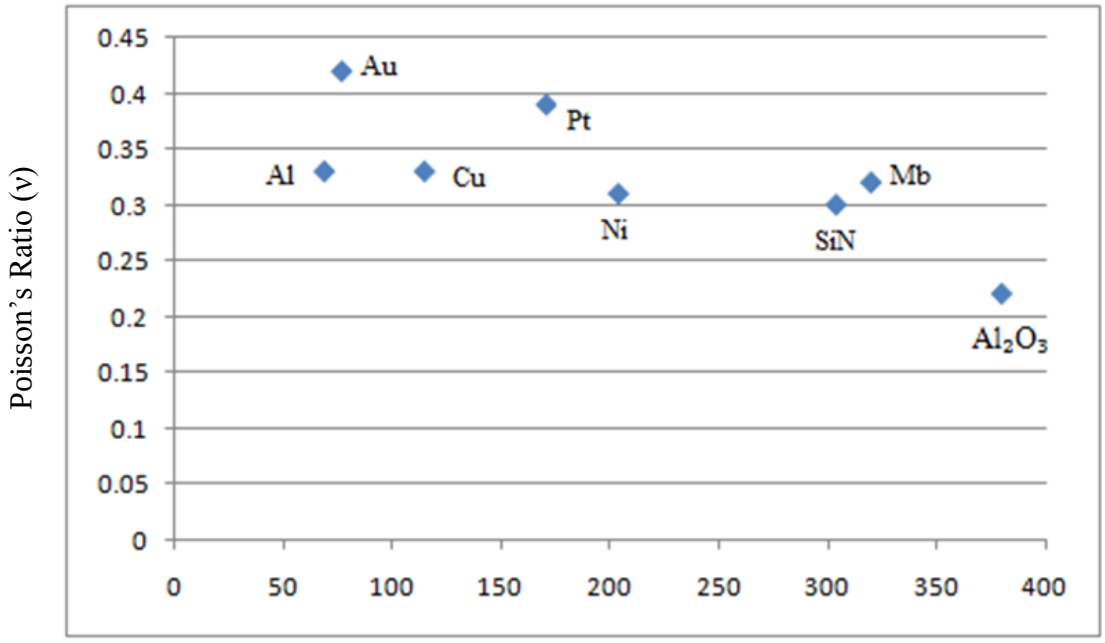

Figure 3.4: Poisson's ratio (ν) versus Young's modulus (E) for considered materials.

Fig. 3.5 shows the plot of electrical resistivity (ρ) versus Young's modulus (*E*) to reduce the RF loss for considered materials. Here we found that aluminum and gold shows the minimum value of Young's modulus (*E*) and electrical resistivity (ρ) to provide the minimum RF loss.

Fig. 3.6 shows the plot of electrical resistivity (ρ) versus thermal conductivity (K). From the plot it can suggested that gold and copper followed by aluminum provide the minimum thermal residual stress for a low value of electrical resistivity (ρ) and a high value of thermal conductivity (K) of the bridge material.

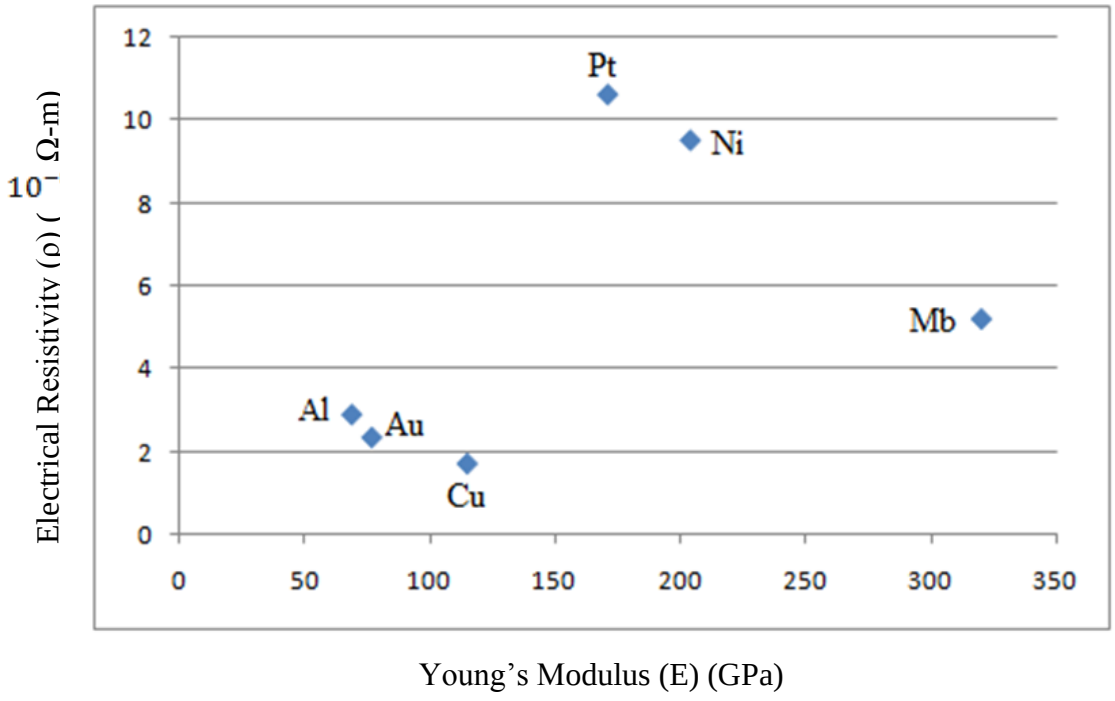

Figure 3.5: Electrical resistivity (ρ) versus Young's modulus (E) for considered materials.

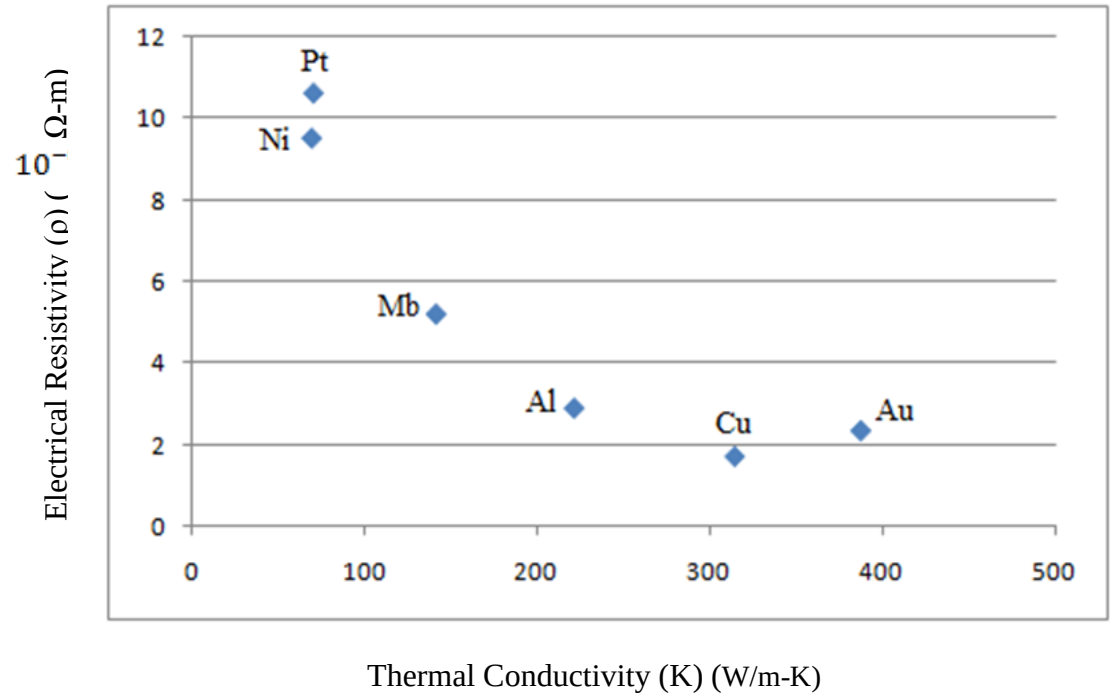

Figure 3.6: Electrical resistivity (ρ) versus Thermal conductivity (K) for considered materials.

So in order to fulfill the desirable criteria of bridge material for RF-MEMS switches, the results show that aluminum (Al) is the best possible material out of all the materials taken into consideration. Gold also shows the desired property but is a very expensive material. In order to validate the outcome of this paper, the results were compared with experimental results of various researchers [99-101] and found the confirmation of this study.

3.6 CONCLUSION

Material selection for RF-MEMS capacitive shunt switch with the help of Ashby approach has been discussed in this chapter. Three performance indices based on different material indices to enhance the performance of the MEMS Bridge were optimized. Based on material selection charts it was observed that gold and aluminum are the appropriate material to be used as bridge material in RF-MEMS switch to obtain the desire properties to give the best performance of the switch in reconfigurable antenna. As gold is very expensive material as compared to aluminum, so if we have to go for mass production of switch, we propose aluminum as the best material to be used as bridge material for RF-MEMS switch. Al is considered as beam material for the calculations in the rest of the thesis. The values taken for bridge material in rest of the thesis are of Al.

CHAPTER 4

ELECTROMECHANICAL MODELING OF RF-MEMS SWITCH

4.1 INTRODUCTION

RF-MEMS switches with fixed-fixed beam configuration use electrostatic actuation mechanism, which results the switch beam to get deflected towards the electrode. This electrostatic deflection is in perpendicular direction to the switch beam plane and is used to realize the electro-mechanical behavior of RF-MEMS switch [3, 9, 40]. Various researchers have made continuous efforts to improve the performance of the RF-MEMS switches in terms of actuation voltage, insertion loss, isolation, switch lifetime, RF signal power handling, temperature sensitivity and switching speed [38, 47-48, 56, 58, 61]. However, in these proposed switch design structures, trade-off between various design parameters exists [10, 58, 61, 63-64]. Hence mechanical design aspect of capacitive RF-MEMS switch need further investigations to improve electromechanical characteristics, such as spring constant, actuation voltage, RF power handling and switching speed.

Pacheco S.P. et.al [39] has shown that serpentine springs folded suspensions can be used to attain low spring constant in compact area. They suggested that this spring constant can be further reduced by adding more meander sections. Consequently, increasing the meander sections lead to structure complexity. This indicates that further improvements in serpentine suspension are needed to decrease the spring constant with

minimum number of meander sections. Kundu A. et.al [43] proposed a concept of movable transmission line of coplanar waveguide (CPW) to reduce the actuation voltage, but this switch design increases the possibility of RF self actuation with low RF power handling capabilities.

Lee S. - D. et.al [41] also developed a capacitive RF-MEMS switch by using a freely moving contact structure, which provides a serious limitation of operating angle range, which increases the actuation voltage requirement. RF power handling capabilities have been improved with various switch designs, these switch designs incorporate pull-up electrodes with non-uniform air gap. However these pull-up electrodes results in undesired movement of the switch membrane without applying any actuation voltage [59, 62-63]. So these designs are inappropriate to reduce the actuation voltage requirements and to attain better RF handling capabilities.

So the aim of this study is to investigate the improvement in electromechanical design parameters, which can significantly enhance the RF-MEMS switch performance. These electromechanical design parameters can be derived by using static analysis of RF-MEMS switch. This static analysis of RF-MEMS switch is subjected to the serpentine spring suspensions, which describe the external loads acting on serpentine spring. The free body diagram of serpentine flexure is used to calculate the spring constant. RF-MEMS switch design with serpentine spring suspensions are able to reduce the spring constant by a sufficient amount, and this modified spring constant is used for actuation voltage, switching speed and RF power handling calculations.

This chapter deals with the electromechanical modeling of capacitive RF-MEMS switch. First, in section 4.2 RF-MEMS switch motion is discussed by using mechanical equations. Section 4.3 provides the details of polysilion flexures for micromechanical structures. Section 4.4 describes the design of proposed non-uniform serpentine flexure and analytical calculation for spring constant. Section 4.5 provides the spring constant comparison between analytical and Finite Element Method (FEM) simulations. Section 4.6 describes the calculation of actuation voltage for designed non-uniform serpentine flexure. Section 4.7 and 4.8 discusses the RF power handling and switching speed for the proposed switch structure, respectively. Finally section 4.9 concludes study for

electromechanical modeling of the proposed non-uniform serpentine flexure based RF-MEMS switch.

4.2 MECHANICAL EQUATIONS FOR MEMS SWITCH MOTION

RF-MEMS switches can be modeled simply as rigid body mass elements by using rigid-body dynamics. These RF-MEMS switch (micromechanical system) models include the effects of bending, torsion, axial and shear stress. A micromechanical system having *n* degrees of freedom, can be modeled in terms of *n* generalized coordinates, $q_1, q_2, q_3, \ldots\ldots q_n$. A mechanical equation for MEMS switch motion can be derived by using Lagrange's equation as [102]:

$$\frac{d}{dt}\left(\frac{\partial L}{\partial \dot{q}_i}\right) - \frac{\partial L}{\partial q_i} = Q_{nc,i} \quad : \quad i = 1, 2, 3, \ldots\ldots, n \qquad \ldots (4.1)$$

where dots indicate differentiations with respect to time, $\partial \dot{q}_i$ is the partial derivative of $\dot{q}_i$ coordinate and $Q_{nc,i}$ is the force associated with coordinate q_i. Lagrangian operator (L) is defined as difference between kinetic energy (T) and potential energy (V) of the system. i.e.

$$L = T - V \qquad \ldots (4.2)$$

Non-conservative forces, such as dissipative forces, are lumped in the terms of $Q_{nc,i}$. Lagrange's equation can be denoted in terms of viscous damping as:

$$\frac{d}{dt}\left(\frac{\partial L}{\partial \dot{q}_i}\right) - \frac{\partial L}{\partial q_i} + \frac{\partial F}{\partial q_i} = Q_{ext,i} \qquad : i = 1, 2, 3, \ldots\ldots, n \qquad \ldots (4.3)$$

where F is the Rayleigh dissipation function and $Q_{ext,i}$ is the generalized external force associated with coordinate q_i. Kinetic energy, potential energy and dissipation factor for a RF-MEMS switch can be written as follows

$$T = \frac{1}{2}\sum_{i=1}^{n}\sum_{j=1}^{n} m_{ij}\dot{q}_i\dot{q}_j \qquad \ldots (4.4)$$

$$V = \frac{1}{2}\sum_{i=1}^{n}\sum_{j=1}^{n} k_{ij}\dot{q}_i\dot{q}_j \qquad \ldots (4.5)$$

$$F = \frac{1}{2}\sum_{i=1}^{n}\sum_{j=1}^{n} B_{ij}\dot{q}_i\dot{q}_j \qquad \ldots (4.6)$$

where m_{ij} is the inertia coefficient, k_{ij} is the stiffness coefficient and B_{ij} is the damping coefficient for a rigid system. Now these equations can be applied on rectangular plate suspended by four springs, connected with plate's corner as shown in fig. 4.1. Here cartesian coordinates *x*, *y* and *z* axis have been chosen with angles of rotation, θ, ϕ, and ψ. Here stored potential energy in plate's spring can be calculated as follows.

$$V = 2\left(k_x x^2 + k_y y^2 + k_z z^2 + k_z L_{ky}^2\theta^2 + k_z L_{kx}^2\phi^2 + k_y L_{kx}^2\psi^2\right) \qquad \ldots (4.7)$$

where k_x, k_y and k_z are the spring constant in *x*, *y* and *z* directions respectively, while L_{kx} and L_{ky} are the distances along the *x* and *y* axis from the centroid of the rectangular plate to the each spring. Here spring's potential energy is approximated by the contribution of each spring. As per our assumption, spring force varies linearly with the plate displacement in *z* direction. So the kinetic energy of these non-linear massless springs can be modeled as follows.

$$T = \frac{1}{2}\left(m\dot{x}^2 + m\dot{y}^2 + m\dot{z}^2 + I_\theta\dot{\theta}^2 + I_\phi\dot{\phi}^2 + I_\psi\dot{\psi}^2\right) \qquad \ldots (4.8)$$

where *m* is the mass of rectangular plate. The moment of inertia of this rectangular plate with respect to rotational angles, can be written as:

$$I_\theta = \frac{m}{12}L_y^2 \qquad \ldots (4.9)$$

$$I_\phi = \frac{m}{12}L_x^2 \qquad \ldots (4.10)$$

$$I_\psi = \frac{m}{12}\left(L_x^2 + L_y^2\right) \qquad \ldots (4.11)$$

Viscous damping of this rectangular plate can be represented by using dissipation function given by:

$$F = \frac{1}{2}\left(B_x\dot{x}^2 + B_y\dot{y}^2 + B_z\dot{z}^2 + B_\theta\dot{\theta}^2 + B_\phi\dot{\phi}^2 + B_\psi\dot{\psi}^2\right) \qquad \ldots (4.12)$$

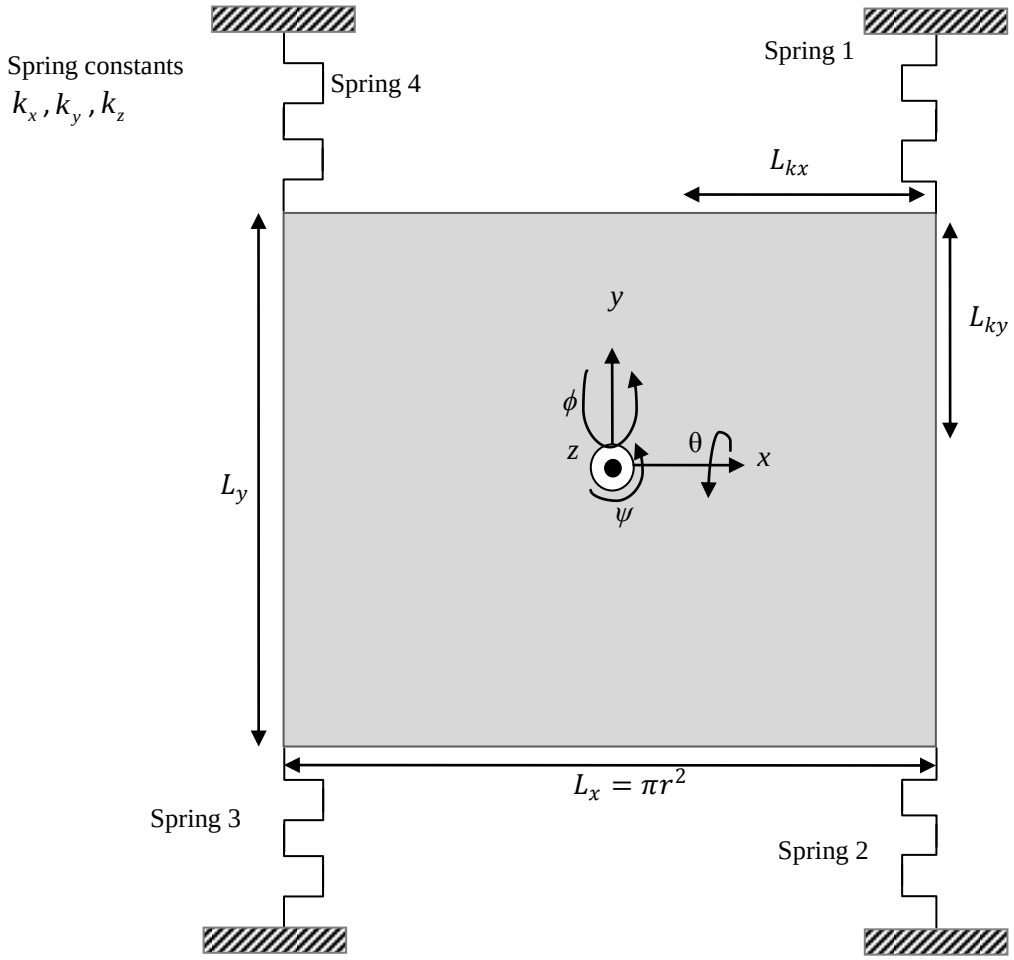

Figure 4.1: Schematic view of a rigid rectangular plate with dimensions of L_x, L_y connected with four springs at distance L_{ky}, L_{kx} along *y* and *x* axis.

where B_x , B_y , B_z , B_θ , B_ϕ , B_ψ are the damping modes of six directional modes. The expressions of potential energy, kinetic energy and dissipation function of rectangular plate are substituted in eq. 4.3. Now mechanical motion equations for vertical motion can be written for *z, θ, ϕ* coordinates as:

$$F_z = m\ddot{z} + B_z\dot{z} + k_z z \qquad \ldots (4.13)$$

$$\tau_\theta = I_\theta \ddot{\theta} + B_\theta \dot{\theta} + k_z L_{ky}^2 \theta \quad \ldots (4.14)$$

$$\tau_\phi = I_\phi \ddot{\phi} + B_\phi \dot{\phi} + k_z L_{kx}^2 \phi \quad \ldots (4.15)$$

where F_z , τ_θ and τ_ϕ are external forces and torque acting on the plate in the direction of *z,* θ and ϕ. Now considering only vertical motion of the plate, F_z, τ_θ and τ_ϕ can be written in following form:

$$F_z = m\left(\ddot{z} + 2\varsigma_z \omega_z \dot{z} + \omega_z^2 z\right) \quad \ldots (4.16)$$

$$\tau_\theta = I_\theta \left(\ddot{\theta} + 2\varsigma_\theta \omega_\theta \dot{\theta} + \omega_\theta^2 \theta\right) \quad \ldots (4.17)$$

$$\tau_\phi = I_\phi \left(\ddot{\phi} + 2\varsigma_\phi \omega_\phi \dot{\phi} + \omega_\phi^2 \phi\right) \quad \ldots (4.18)$$

where ω_z , ω_θ , ω_ϕ are resonant frequencies and ζ_z , ζ_θ and ζ_ϕ are damping coefficients of *z,* θ*,* and ϕ directional modes. The resonant frequency and damping coefficients of i^{th} rotational mode can be given as:

$$\omega_i = \sqrt{\frac{k_i}{m_i}} \quad \ldots (4.19)$$

$$\xi_i = \frac{B_i}{2\ k_i m_i} \quad \ldots (4.20)$$

where k_i is the stiffness coefficient and m_i is the inertia coefficient for i^{th} rotational mode. In order to change the resonant frequency, effective spring mass plays an important role.

4.3 POLYSILION FLEXURES FOR MICROMECHANICAL STRUCTURES

Recent development shows that the surface micromachining techniques have proven their ability to use polycrystalline silicon (polysilicon) as a structural layer in micro structure devices. So several researchers have used polysilicon for micromechanical flexures designs to develop various microstructures [103, 104]. Kim C.-J. et.al [105] developed flexure based surface micromachined polysilicon microgripper to avoid the frictional

effects of micro joints. Yun W. et.al [106] reported about micro accelerometer in which they used polysilicon based suspension to reduce the temperature sensitivity and residual stress in the spring. Tang W.C. et.al [107] demonstrated polysilicon based resonant microstructure with frequency ranging from 18 kHz to 80 kHz. In general these polysilicon based suspension are used to have a very compliant suspension in one direction while very stiff in other directions. Most of the microstructures are designed to move in the direction normal to the substrate. Polysilicon based micromechanical structures provide bending in rectilinear direction which gives limitation on mechanical design for rotatable and sliding mechanical elements. Fan L. S. [108] has discussed about the design issues in movable, rotatable and sliding microstructures for large displacements. Fedder G.K. [103] has done the thorough study of polysilicon based fixed–fixed flexure, crab leg flexure, folded flexure and serpentine flexure, as shown in fig. 4.2. His study concluded that polysilicon based micromechanical structures need long, thick and narrow beams for lateral motion in one direction. The fabrication process and distributed forces affect the beam weight and fixed charge in substrate, which impose limitation on polysilicon beam dimensions.

Pisano A. P. et.al [109] derived the expression for spring constant for fixed-fixed flexures and concluded that residual stress increases the stiffness in polysilicon flexure. Cho Y.-H. et.al [110] presented a modified design of fixed-fixed flexure, where thigh section was added to make the crab leg flexure. This design was able to reduce the peak stress at a cost of reduced stiffness in the undesired direction. The folded flexure and serpentine flexures were also designed to reduce the axial stress in the beam. These two flexure design proved their ability to give desired residual stress, stiffness ratio by adjustment of meander width [111].

However it is desirable to have a very compliant flexure in one direction, while stiff in other directions. Motion in other directions increases sensitivity to cross-acceleration. So the following discussion will focus on small rectilinear displacements in one direction.

4.4 PROPOSED SWITCH DESIGN AND MODELING

Linear spring constant for micromechanical structures can be calculated by energy methods as proposed by Fedder G.K. et. al [103, 112]. In this method the displacement (δ) is calculated by applying force (F_z) in *z* direction and is given as:

$$k_z = \frac{F_z}{\delta_z} \qquad \ldots (4.21)$$

In developing the analytical model, only bending and torsion displacements are considered, while the deformation from shear, beam elongation and beam shortening have been neglected. Each flexure is designed by four springs with two fold symmetry, so we need to analyze only one spring, hence the resulting spring constant will be the one fourth of flexure's spring constant. Flexure symmetry is important for the translation of boundary condition, so the guided end boundary condition have been defined at spring ends as shown in fig. 4.2. Displacement and rotation of the spring ends are assumed to be zero except from the direction of applied force. The boundary condition at each beam segment can be determined in terms of torsion, moments and reaction force as:

$$\sum T = 0, \quad \sum M = 0, \quad \sum F = 0 \qquad \ldots (4.22)$$

The moment and torsion of each beam segment will be calculated as a function of position along the beam's *z* axis. According to the Castigliano's second theorem, the beam segment's displacement (δ_z) at the point of applied force (F_z) in the *z* direction, can be determined as:

$$\delta_z = \frac{\partial U}{\partial F_z} \qquad \ldots (4.23)$$

where ∂U is the partial derivative of the strain energy of beam and ∂F_z is the partial derivative of applied force on the beam segment.

Angular displacement (θ_z) can be given as a function of applied moment.

$$\theta_z = \frac{\partial U}{\partial M_z} \qquad \ldots (4.24)$$

where ∂M_z is the partial derivative of applied moment on the beam segments.

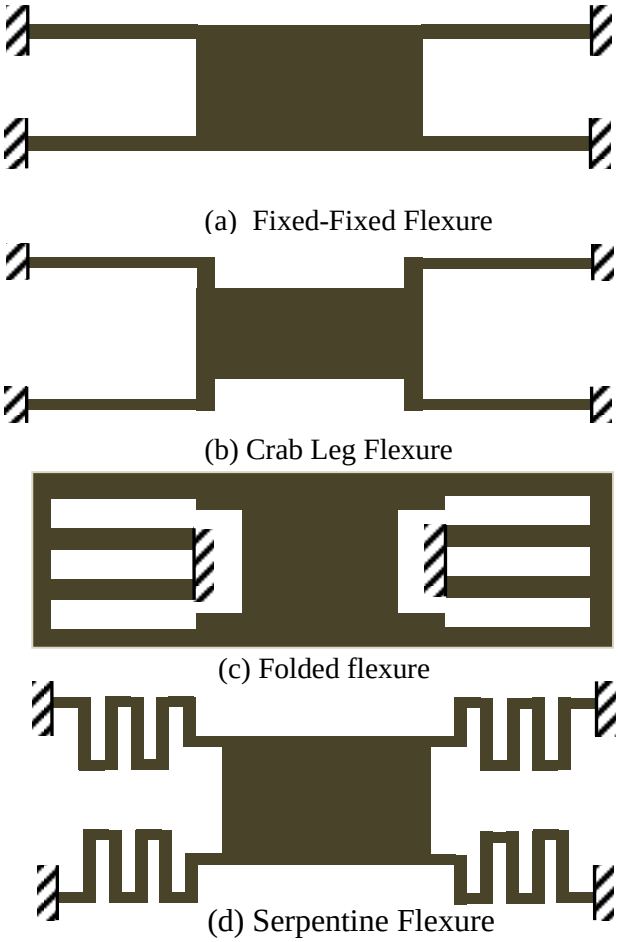

Figure 4.2 Schematic view of various flexure designs (a) Fixed-Fixed flexure (b) Crab leg flexure (c) Folded flexure (d) Serpentine flexure [103].

Now last step is to calculate the spring constant which is equal to the applied force (F_z) divided by the displacement (δ_z). Now the next section will describe the non-uniform serpentine flexure design and the spring constant calculation for this flexure design.

4.4.1 Non-uniform Serpentine Flexure Design

A schematic view of non-uniform serpentine spring with two meander sections is shown in fig. 4.3. Each meander is made up of four beam segments, called as connector beams and span beams. These connector beams and span beams are denoted as meander length and meander width with the length of *a* and *b* respectively, having a thickness of *t* and

width of *w'*. For non-uniform serpentine flexure design, the meander width (*b*) increases in multiples of varying span beam segments. In this design the meander widths are represented as *b*, *2b*, *3b* and *4b* for two meander based serpentine spring. Non-uniform serpentine spring get their name due their non-uniform meander width. The meander width can be adjusted to provide the appropriate stiffness ratio with reduced spring constant [113]. Most of the uniform serpentine springs are designed with constant meander width [39, 114]. These developed micromechanical serpentine springs designs exhibit low spring constant, which increase the sensitivity to frictional effects of the beam joints [114]. So in the proposed model, a varying meander width concept is used to reduce the spring constant of RF-MEMS switch.

4.4.2 Spring constant calculation for non-uniform serpentine flexure

This section explains the spring constant calculation for non-uniform serpentine flexure with one, two and three meander sections. Because of two fold flexure symmetry of non-uniform serpentine spring, the spring end is used as a guided end boundary condition. In this analysis only *z* direction motion is taken into consideration. A free-body diagram of non-uniform serpentine structure is shown in fig. 4.4. A perpendicular force F_z is applied in *z* direction at the end of the beam resulting in a displacement of δ_z. The guided end has separate ε and δ coordinate system where ε is the coordinate along the beam axis and δ is the coordinate normal to the ε axis. Here rotational angle of θ_0 and ϕ_0 are considered from guided end boundary conditions. Residual stress and extensional stress are neglected in the following analysis. This non-uniform serpentine flexure contains three meander sections (N=3) with 6 connector beam (i=1 to 2N) and 6 span beams (j=1 to 2N). At the fixed point "F" all six degrees of freedom are assumed to be fixed. The free end of the flexure is connected with the beam of main switch, where the bending moment and torsion of each beam segment is derived from the free-body diagram.

Bending moment and torsion for connector beam segment (i=1) are;

$$M_{a,1} = M_o - F_z \varepsilon \quad \ldots (4.25)$$

$$T_{a,1} = T_o \quad \ldots (4.26)$$

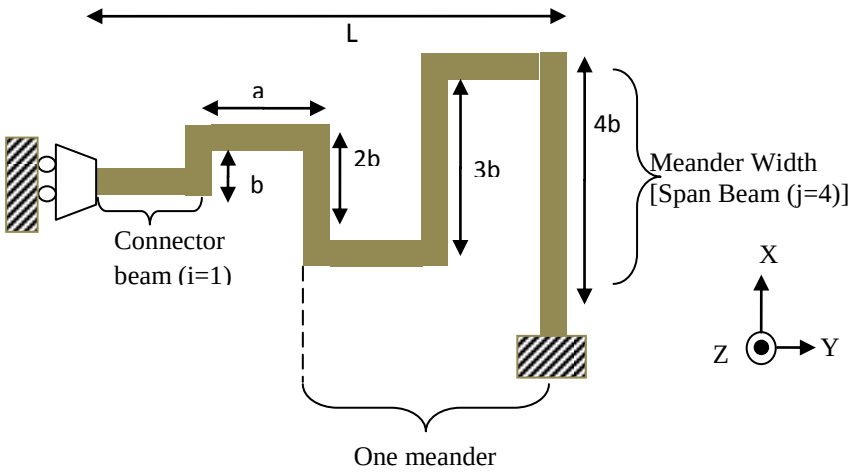

Figure 4.3 Non-uniform serpentine flexure with two meander sections.

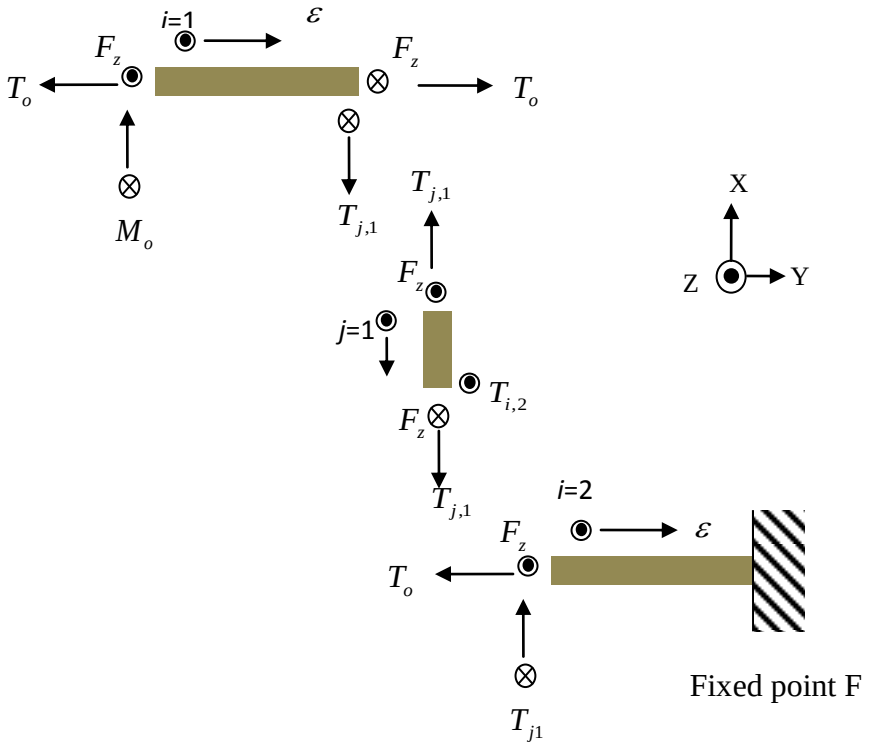

Figure 4.4: Free body diagram of non-uniform serpentine spring

Bending moment and torsion for span beam segment (j=1) are;

$$M_{b,1} = -T_o - F_z\varepsilon \quad \ldots (4.27)$$

$$T_{b,1} = M_o - F_z\varepsilon \quad \ldots (4.28)$$

Bending moment and torsion for connector beam segment (i=2) are;

$$M_{a,2} = M_o - F_z\varepsilon - F_z a \quad \ldots (4.29)$$

$$T_{a,2} = -(-T_o - F_z b) = T_o + F_z b \quad \ldots (4.30)$$

Bending moment and torsion for span beam segment (j=2) are;

$$M_{b,2} = T_o + F_z b - F_z\varepsilon \quad \ldots (4.31)$$

$$T_{b,2} = -(M_o - F_z a - F_z a) = -M_o + 2F_z a \quad \ldots (4.32)$$

Bending moment and torsion for connector beam segment (i=3) are;

$$M_{a,3} = -(-M_o + 2F_z a) - F_z\varepsilon = M_o - 2F_z a - F_z\varepsilon \quad \ldots (4.33)$$

$$T_{a,3} = T_o + F_z b - F_z 2b = T_o - F_z b \quad \ldots (4.34)$$

Bending moment and torsion for span beam segment (j=3) are;

$$M_{b,3} = -(T_o - F_z b) - F_z\varepsilon = -T_o + F_z b - F_z\varepsilon \quad \ldots (4.35)$$

$$T_{b,3} = M_o - 2F_z a - F_z a) = M_o - 3F_z a \quad \ldots (4.36)$$

Bending moment and torsion for connector beam segment (i=4) are;

$$M_{a,4} = M_o - 3F_z a - F_z\varepsilon \quad \ldots (4.37)$$

$$T_{a,4} = -(-T_o + F_z b - F_z 3b) = T_o + 2F_z b \quad \ldots (4.38)$$

Bending moment and torsion for span beam segment (j=4) are;

$$M_{b,4} = (T_{a,4}) - F_z\varepsilon = T_o + 2F_z b - F_z\varepsilon \quad \ldots (4.39)$$

$$T_{b,3} = -(M_o - 3F_z a - F_z a) = -M_o + 4F_z a \quad \ldots (4.40)$$

Bending moment and torsion for connector beam segment (i=5) are;

$$M_{a,5} = -(T_{b,4}) - F_z\varepsilon = M_o - 4F_z a - F_z\varepsilon \quad \ldots (4.41)$$

$$T_{a,5} = M_{b,4} = T_o + 2F_z b - F_z 4b = T_o - 2F_z b \quad \ldots (4.42)$$

Bending moment and torsion for span beam segment (j=5) are;

$$M_{b,5} = -(T_{a,5}) - F_z\varepsilon = -T_o + 2F_z b - F_z\varepsilon \quad \ldots (4.43)$$

$$T_{b,5} = M_o - 4F_z a - 4F_z a = M_o - 5F_z a \quad \ldots (4.44)$$

Bending moment and torsion for connector beam segment (i=6) are;

$$M_{a,6} = M_{a,5} - F_z \varepsilon = M_o - 5F_z a - F_z \varepsilon \quad \ldots (4.45)$$

$$T_{a,6} = -(M_{b,5}) = T_o - 2F_z b + F_z 5b = T_o + 3F_z b \quad \ldots (4.46)$$

The total energy for non-uniform serpentine spring can be given as:

$$U = \sum_{i=1}^{2N} \int_0^a \left(\frac{M_{a,i}^2}{2EI_{x,a}} + \frac{T_{a,i}^2}{2GJ_a} \right) d\varepsilon + \sum_{j=1}^{2N} \int_0^{jb} \left(\frac{M_{b,j}^2}{2EI_{x,b}} + \frac{T_{b,j}^2}{2GJ_b} \right) d\varepsilon \quad \ldots (4.47)$$

where N is the number of meander sections, E is the Young's Modulus of elasticity, G is the torsion (or shear) modulus of the elasticity, J is the torsion constant, $I_{x,a}$ and $I_{x,b}$ are the bending moment of inertia about x axis for connector and span beam segments respectively. These bending moment of inertia for rectangular beam about x axis can be given as.

$$I_x = I_{x,a} = I_{x,b} = \int_{-w/2}^{w/2} \int_{-t/2}^{t/2} x^2 dxdz = \frac{wt^3}{12} \quad \ldots (4.48)$$

Moment of inertia about z axis can be given as follows:

$$I_z = \int_{-t/2}^{t/2} \int_{-w/2}^{w/2} x^2 dxdz = \frac{tw^3}{12} \quad \ldots (4.49)$$

Torsion modulus of the elasticity can be given by:

$$G = \frac{E}{2(1+\nu)} \quad \ldots (4.50)$$

Torsion constant for rectangular beam is given by [115]:

$$J = \frac{1}{3} t^3 w \left(1 - \frac{192t}{\pi^5 w} \sum_{i=1,i\,odd}^{\infty} \frac{1}{i^5} \tanh\left(\frac{i\pi w}{2t} \right) \right) \quad \ldots (4.51)$$

$$J = 0.413(I_x + I_z) \quad \ldots (4.52)$$

where $t<w$, t is the thickness and w is the width of the beam segments.

The guided end constraints tilt $_c$and rotation ϕ_0 at the end of connector beam segment can be given as:

$$\theta_0 = \frac{\partial U}{\partial M_0} = \sum_{i=1}^{2N} \int_0^a \left(\frac{M_{a,i}}{EI_{x,a}} \frac{\partial M_{a,i}}{\partial M_0} + \frac{T_{a,i}}{GJ_a} \frac{\partial T_{a,i}}{\partial M_0} \right) d\varepsilon + \ldots$$
$$\sum_{j=1}^{2N} \int_0^{jb} \left(\frac{M_{b,j}}{EI_{x,b}} \frac{\partial M_{b,j}}{\partial M_0} + \frac{T_{b,j}}{GJ_b} \frac{\partial T_{b,j}}{\partial M_0} \right) d\varepsilon = 0 \quad \ldots (4.53)$$

$$\phi_0 = \frac{\partial U}{\partial T_0} = \sum_{i=1}^{2N} \int_0^a \left(\frac{M_{a,i}}{EI_{x,a}} \frac{\partial M_{a,i}}{\partial T_0} + \frac{T_{a,i}}{GJ_a} \frac{\partial T_{a,i}}{\partial T_0} \right) d\varepsilon + \ldots.$$
$$\sum_{j=1}^{2N} \int_0^{jb} \left(\frac{M_{b,j}}{EI_{x,b}} \frac{\partial M_{b,j}}{\partial T_0} + \frac{T_{b,j}}{GJ_b} \frac{\partial T_{b,j}}{\partial T_0} \right) d\varepsilon = 0 \quad \ldots (4.54)$$

The moment and torsion of each beam segment will be calculated as function of position along the beam z axis. We can calculate the resulting moment and torsion for unit load at beam segments.

$$M_0 = F_z \left(\frac{G.Ja^2 + EI_x 55ab}{G.J6a + EI_x 15b} \right) \quad \ldots (4.55)$$

$$T_0 = F_z \left(\frac{G.J3ab + EI_x a\left(\frac{b^2}{2}\right)}{G.J6a + EI_x 15b} \right) \quad \ldots (4.56)$$

We substitute these values in equation of bending and torsion moment and thereafter Castligliano's unit load theorem will be applied to get the z direction spring constant for the non-uniform flexure is given by

$$\delta_z = \frac{\partial U}{\partial F_z} = \sum_{i=1}^{2N} \int_0^a \left(\frac{M_{a,i}}{EI_{x,a}} \frac{\partial M_{a,i}}{\partial F_z} + \frac{T_{a,i}}{GJ_a} \frac{\partial T_{a,i}}{\partial F_z} \right) d\varepsilon + \ldots$$
$$\sum_{j=1}^{2N} \int_0^{jb} \left(\frac{M_{b,j}}{EI_{x,b}} \frac{\partial M_{b,j}}{\partial F_z} + \frac{T_{b,j}}{GJ_b} \frac{\partial T_{b,j}}{\partial F_z} \right) d\varepsilon = 0 \quad \ldots (4.57)$$

Now the spring constant for non-uniform serpentine flexure can be calculated using:

$$k_z = \frac{F_z}{\delta_z} \quad \ldots (4.58)$$

Here the spring constant analysis is done for three different meander sections for non-uniform flexure design.

4.4.3 Non-uniform flexure design with 1, 2 and 3 meander sections

Non-uniform flexure design with 1 meander section is shown in fig. 4.5. After solving the bending moments and torsion using eq. (4.25-4.32) for 4 beam segments (2- span beam and 2-connector beam), the resulting moment and torsion can be calculated for applied unit load at beam segments.

$$M_0 = F_z\left(\frac{G.J\,2a^2 + EI_x\,5ab}{G.J\,2a + EI_x\,3b}\right) \quad \ldots (4.59)$$

$$C_1 = \frac{G.J\,2a^2 + EI_x\,5ab}{G.J\,2a + EI_x\,3b} \quad \ldots (4.60)$$

where C_1 is a constant and is used to simplify the mathematical operations. Hence,

$$M_0 = F_z C_1 \quad \ldots (4.61)$$

$$T_0 = -F_z\left(\frac{G.J\left(\frac{b^2}{2}\right) + EI_x ab}{G.J\,3b + EI_x\,2a}\right) \quad \ldots (4.62)$$

$$C_2 = \frac{G.J\left(\frac{b^2}{2}\right) + EI_x ab}{G.J\,3b + EI_x\,2a} \quad \ldots (4.63)$$

where C_2 is a constant and is also used to simplify the mathematical operations. Hence,

$$T_0 = -F_z C_2 \quad \ldots (4.64)$$

Now M_0 and T_0 are substituted in the equations of bending moment and torsion of connector and span beam segments. Now these new equations of bending moment and torsion will be used in eq. (4.57) to obtain the vertical displacement of the serpentine flexure in z direction. The unit load method (Castligliano's second theorem) is employed to determine the deflection of the beam [115]. Hence eq. (4.57) becomes;

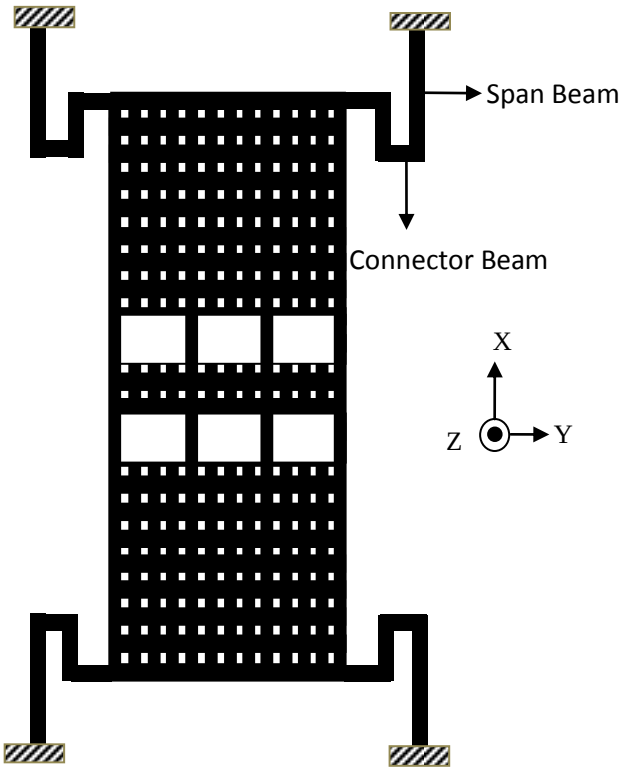

Figure 4.5: Non-uniform serpentine spring design with 1 meander section.

$$\delta_z = \frac{\partial U}{\partial F_z} = \sum_{i=1}^{2} \int_0^a \left(\frac{M_{a,i}}{EI_{x,a}} \frac{\partial M_{a,i}}{\partial F_z} + \frac{T_{a,i}}{GJ_a} \frac{\partial T_{a,i}}{\partial F_z} \right) d\varepsilon + \sum_{j=1}^{2} \int_0^{jb} \left(\frac{M_{b,j}}{EI_{x,b}} \frac{\partial M_{b,i}}{\partial F_z} + \frac{T_{b,j}}{GJ_b} \frac{\partial T_{b,i}}{\partial F_z} \right) d\varepsilon \quad \ldots (4.65)$$

Now this equation can be simplified for beam displacement in *z* direction as follows

$$\delta_z = \delta_{z1} + \delta_{z2} + \delta_{z3} + \delta_{z4} \quad \ldots (4.66)$$

where $\delta_{z1}, \delta_{z2}, \delta_{z3}, \delta_{z4}$ are the displacements for connector and span beam segments because of the bending moment and torsion. Now

$$\delta_{z1} = \sum_{i=1}^{2} \int_0^a \left(\frac{M_{a,i}}{EI_{x,a}} \frac{\partial M_{a,i}}{\partial F_z} \right) d\varepsilon = \frac{F_z}{EI_{x,a}} \left(2C_1^2 a + \frac{8}{3} a^3 - 4C_1 a^2 \right) \quad \ldots (4.67)$$

$$\delta_{z2} = \sum_{i=1}^{2} \int_0^a \left(\frac{T_{a,i}}{GJ_a} \frac{\partial T_{a,i}}{\partial F_z} \right) d\varepsilon = \frac{F_z}{GJ_a} \left(2C_2{}^2 a + b^2 a - 2C_2 ba \right) \quad \ldots (4.68)$$

$$\delta_{z3} = \sum_{j=1}^{2} \int_0^{jb} \left(\frac{M_{b,j}}{EI_{x,b}} \frac{\partial M_{b,i}}{\partial F_z} \right) d\varepsilon = \frac{F_z}{EI_{x,a}} \left(3C_2{}^2 b + b^3 - 4C_2 b^2 \right) \quad \ldots (4.69)$$

$$\delta_{z3} = \sum_{j=1}^{2} \int_0^{jb} \left(\frac{T_{b,j}}{GJ_b} \frac{\partial T_{b,i}}{\partial F_z} \right) d\varepsilon = \frac{F_z}{GJ_b} \left(3C_1{}^2 b + 9a^2 - 10C_1 ab \right) \quad \ldots (4.70)$$

The *z* direction spring constant for one meander non-uniform flexure is given as:

$$k_z = \frac{F_z}{\delta_{z1} + \delta_{z2} + \delta_{z3} + \delta_{z3}} \quad \ldots (4.71)$$

$$k_z = \begin{bmatrix} \frac{1}{EI_{x,a}} \left(2C_1{}^2 a + \frac{8}{3} a^3 - 4C_1 a^2 + 3C_2{}^2 b + b^3 - 4C_2 b^2 \right) + ... \\ \frac{1}{GJ_a} \left(2C_2{}^2 a + b^2 a - 2C_2 ba + 3C_1{}^2 b + 9a^2 - 10C_1 ab \right) \end{bmatrix}^{-1} \quad \ldots (4.72)$$

Eq. (4.72) shows the spring constant for single meander based non-uniform serpentine flexure.

Now this spring constant analysis can also be used to determine the spring constant for 2 meander (4- span beam and 4-connector beam) and 3 meander (6- span beam and 6-connector beam) based non-uniform serpentine flexures. These non-uniform serpentine flexure designs are shown in fig. 4.6 and 4.7. The spring constant for 2 meander non-uniform serpentine flexure is given as:

$$k_z = \begin{bmatrix} \frac{1}{EI_{x,a}} \left(4C_1{}^2 a + \frac{64}{3} a^3 - 16C_1 a^2 + 10C_2{}^2 b - 24b^3 + \frac{100}{3} b^3 \right) + ... \\ \frac{1}{GJ_a} \left(4C_2{}^2 a + 6b^2 a - 4C_2 ba + 10C_1{}^2 b + 100a^2 - 60C_1 ab \right) \end{bmatrix}^{-1} \quad \ldots (4.73)$$

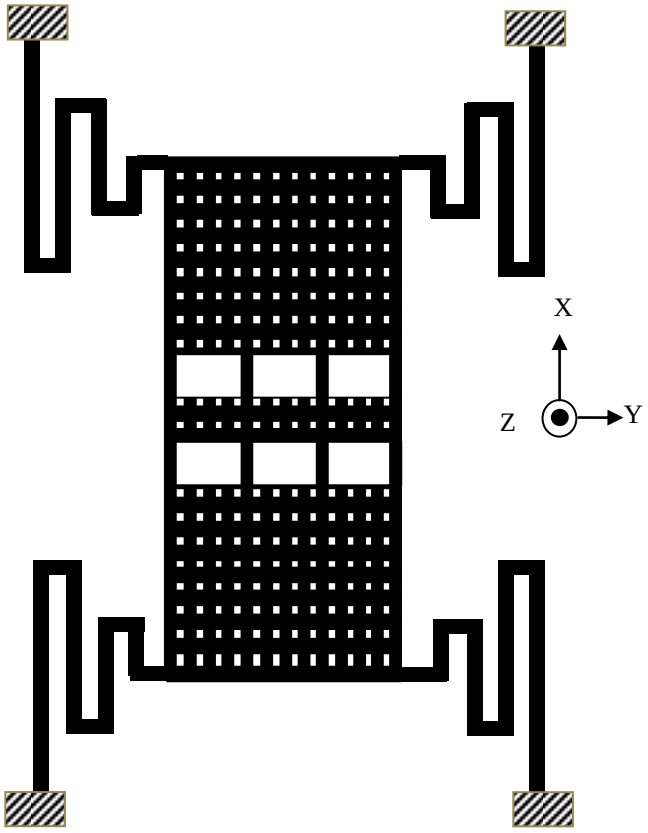

Figure 4.6: Non-uniform serpentine spring schematic with 2 meander sections.

Similarly the spring constant for 3 meander based non-uniform serpentine flexure can also be given as:

$$k_z = \begin{bmatrix} \frac{1}{EI_{x,a}}\left(6C_1{}^2a + \frac{216}{3}a^3 - 36C_1a^2 + 21C_2{}^2b + \frac{441}{3}b^3 - 30C_2b^2\right) + \ldots \\ \frac{1}{GJ_a}\left(6C_2{}^2a + 19b^2a - 6C_2ba + 16C_1{}^2b + 441a^2 - 182C_1ab\right) \end{bmatrix}^{-1}$$

… (4.74)

In the eq. (4.72-4.74), it is observed that the spring constant occurs due to bending moment and torsion of beam segments. These terms only depend on the beam dimensions and beam material.

Table 4.1 Non-uniform serpentine spring design parameters.

Parameter Name	**Parameter values**
Span Beam Length (*b*)	100 to 280 μm
Connector Beam Length (*c*)	25 μm
Width (for all Beams) *w*	10 μm
Thickness (for all Beams) (*t*)	1.5 μm
Poisson's Ratio (υ)	0.31

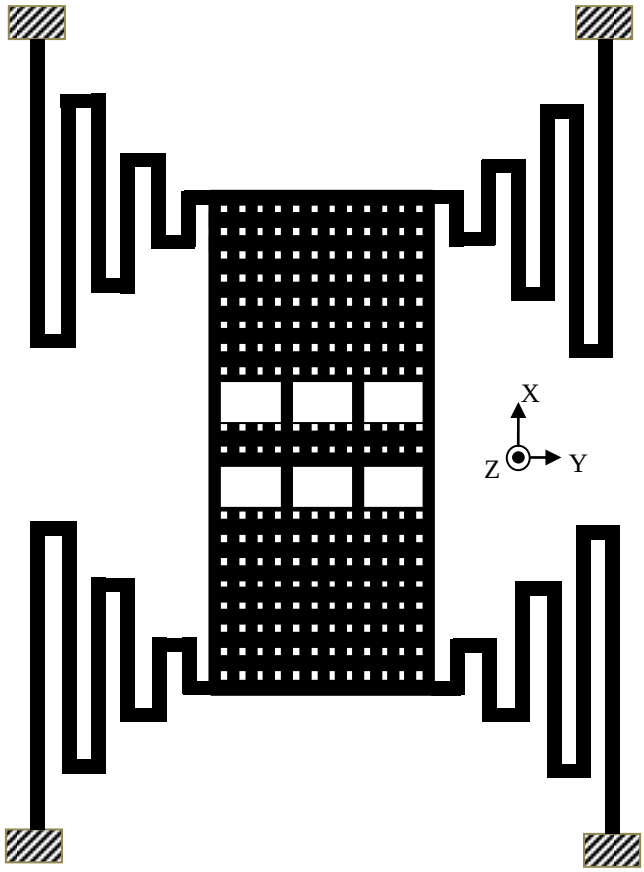

Figure 4.7: Non-uniform serpentine spring schematic with 3 meander sections.

4.5 COMPARISON BETWEEN ANALYTICAL AND SIMULATED RESULTS

This section explains the spring constant comparison between the values calculated from the spring constant expression and with Finite Element Method (FEM) analysis. This spring constant analysis is done for 1, 2 and 3 meander based non-uniform serpentine flexures. A sufficiently large set of physical dimensions has been considered for this analysis. The design parameters of non-uniform serpentine meander considered for analysis are given in table 4.1. Spring constant equations of different meanders flexures (eq. 4.72, 4.73, 4.74) were verified by Finite element method (FEM). The physical dimensions for designed spring structure were applied to the FEM simulation tool (COMSOL Multiphysics 4.2) [116] and these simulation results are compared with analytically calculated values. For FEM simulations, a concentrated *z* direction force (F_z =1μN) was applied at the free end of the spring with adequate guided end boundary conditions. The FEM simulations were performed for three different meander sections with varying span beam length (100μm to 280μm).

Fig. 4.8 shows the comparison between analytical model and FEM simulation for non-uniform serpentine structure for single meander section for different span beam length ranging from 100μm to 280μm. It is observed that the spring constant decreases with increase in span beam length. Comparison between the calculated and simulated values of spring constant shows the close agreement with each other. However, it is observed that analytically calculated spring constant is 10% to 30% higher than the simulated values.

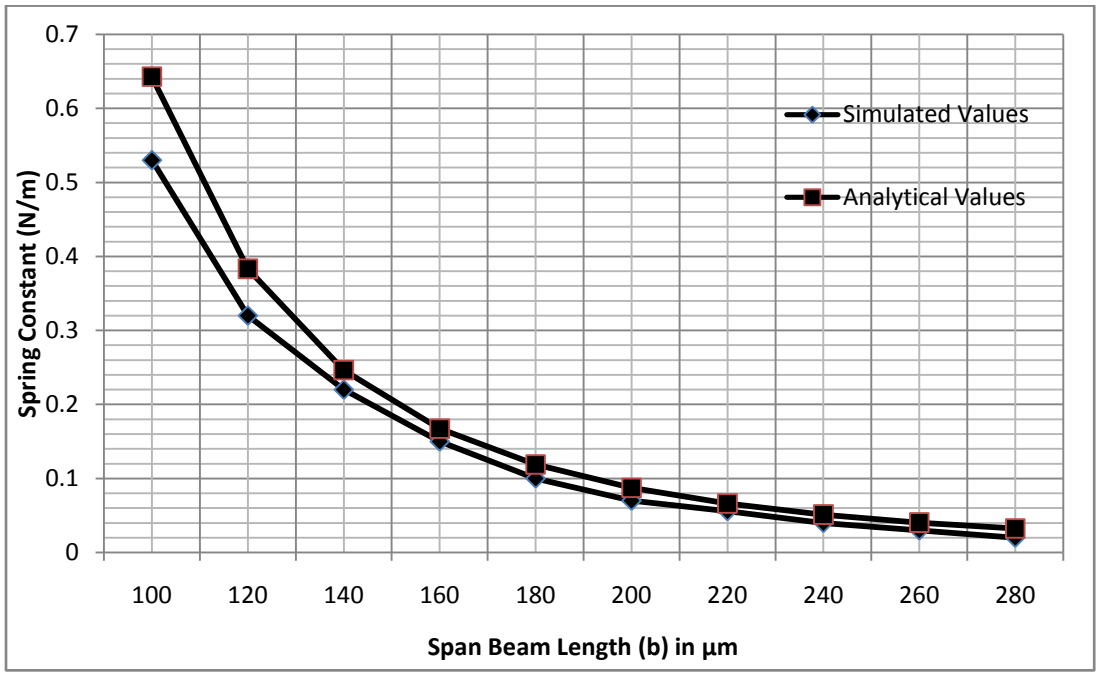

Figure 4.8: Comparison of analytically calculated spring constant with FEM simulated values for non-uniform serpentine spring with different span beam lengths (b) ranging from 100µm to 280µm, with 1 meander section.

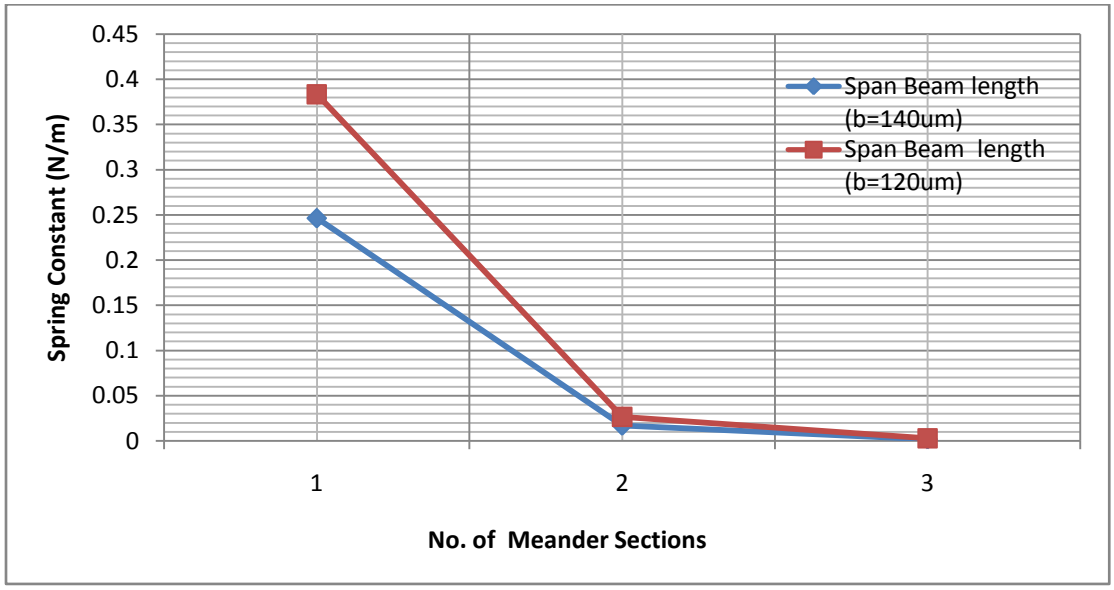

Figure 4.9: Spring constant of non-uniform serpentine flexure design for 1, 2 and 3 meander sections with span beam length of 120µm and 140µm.

Fig 4.9 shows the variation of spring constant of non-uniform serpentine flexure design for 1, 2 and 3 meander sections with span beam length of 120 μm and 140 μm. It is observed that the value of spring constant decreases drastically from 1 meander section to 2 meander sections but using more meander sections may increase the structure complexity and require more space. This overpowers the advantage of low value of spring constant with more number of meander sections. A spring constant comparison between uniform and non-uniform meander structure with different span beam length has been shown in table 4.2.

Table 4.2 Spring Constant comparison between non-uniform and uniform meander structure with different span beam length (*b*).

Span beam length (*b*) μm	**Spring constant for non-uniform meander structure**			**Spring constant for uniform meander structure [120]**		
	1 meander	**2 meanders**	**3 meanders**	**1 meander**	**2 meanders**	**3 meanders**
100	0.642559	0.044883	0.004822	2.462025	0.941959	0.451341
120	0.383188	0.026418	0.002793	1.555122	0.634546	0.323777
140	0.246287	0.016821	0.001760	1.042127	0.444525	0.238068
160	0.167451	0.011356	0.001180	0.731317	0.321977	0.179011
180	0.118930	0.008021	0.000829	0.532454	0.239935	0.137350
200	0.087464	0.005873	0.000605	0.399476	0.183193	0.107313
220	0.066179	0.004427	0.000455	0.307264	0.142820	0.085218
240	0.051272	0.003420	0.000350	0.241344	0.113375	0.068664
260	0.040523	0.002696	0.000276	0.192988	0.091431	0.056052
280	0.032580	0.002162	0.000221	0.156722	0.074761	0.046296

4.6 ACTUATION VOLTAGE CALCULATION FOR PROPOSED RF-MEMS SWITCH

Actuation voltage is an important parameter for electrostatically actuated capacitive RF-MEMS switch. From design point of the view actuation voltage should be low for capacitive RF-MEMS switch for wireless communication devices. Various researchers have proposed switch designs for an actuation voltage in the range 20-50V [3, 9, 38, 47-48]. Therefore this section describes the proposed non-uniform serpentine flexure to reduce the actuation voltage requirements for RF-MEMS switches.

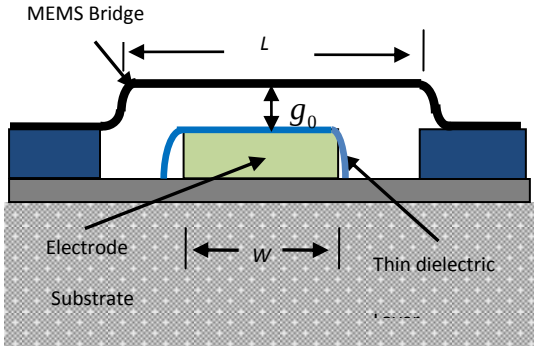

Figure 4.10a: Sketch of a typical RF-MEMS bridge structure.

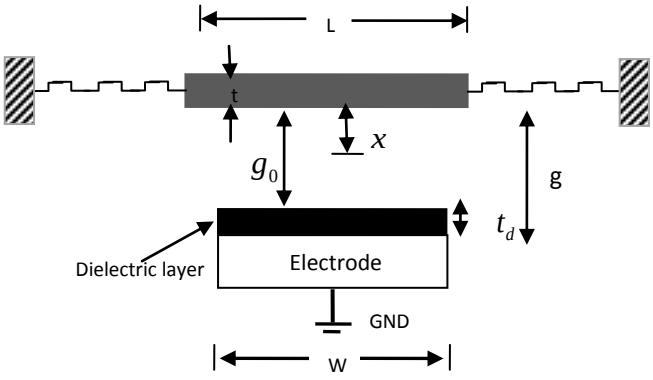

Figure 4.10b: Sketch of a fixed-fixed beam model used to model the structure shown in fig. 4.10a.

A capacitive contact RF-MEMS switch with metal membrane exhibits high impedance due to an air gap between the switch beam and bottom plate in off-state. This switch beam is suspended at a height of g_0 above the dielectric layer on the transmission line as shown in fig. 4.10a and b [117].

When a voltage is applied between a switch beam and the pull-down electrode, an electrostatic force is induced on the beam. The beam over the electrode acts as a parallel plate capacitor and the capacitance of which is given as:

$$C = \frac{\varepsilon_0 W w}{g} \qquad \ldots (4.75)$$

where g is the height of the MEMS bridge above pull-down electrode, W is the width of the actuation electrode and w is the width of bridge structure. The electrode force applied between MEMS bridge and pull-down electrode can be calculated as [1].

$$F_e = \frac{1}{2}V^2 \frac{dC(g)}{dg} = \frac{1}{2}\frac{\varepsilon_0 WwV^2}{g} \quad \ldots (4.76)$$

where V is the applied voltage on pull down electrode. Spring constant will be used to determine the distance covered by the beam after applying potential V. MEMS bridge has its own stiffness so the applied electrostatic force and restoring force can be equated as follows.

$$F_e = K_z(g - g_0) \quad \ldots (4.77)$$

where K_z is total spring constant for RF-MEMS switch and g_0 is the initial gap between the electrode and MEMS bridge with zero potential. So this spring constant will be the sum of all four suspensions attached to the flexure. Hence the total spring constant is

$$K_z = \frac{4k_z}{N} \quad \ldots (4.78)$$

where k_z is the spring constant for single spring and N is the number of meander sections. So eq. (4.76) and (4.77), we have

$$\frac{1}{2}\frac{\varepsilon_0 WwV^2}{g} = K_z(g - g_0) \quad \ldots (4.79)$$

$$V = \sqrt{\frac{2K_z g^2(g - g_0)}{\varepsilon_0 Ww}} \quad \ldots (4.80)$$

Now the electrostatic force in terms of electric field applied to the beam can be given as.

$$F_e = \frac{QE}{2} \quad \ldots (4.81)$$

where Q is the charge on the beam and E is the electric field due to the applied voltage. When a constant voltage is increased, the electrostatic force will also get increased due to an increase in the charge. Due to this excessive charge, MEMS bridge height gets decreased, simultaneously it increases the capacitance. At $\frac{2}{3}g_0$, electrostatic force is

greater than beam restoring force which results in beam collision with pull down electrode [118-119]. Now the pull down electrode can be given as.

$$V_p = V\left(\frac{2g_0}{3}\right) \quad \text{... (4.82a)}$$

$$= \sqrt{\frac{8K_z}{27\varepsilon_0 Ww}\, g_0^{\,3}} \quad \text{… (4.82b)}$$

From eq. 4.82b, it is clear that the actuation voltage can be reduced in three different ways: First by decreasing the height between the bridge and the electrode, secondly by increasing the area of the bridge and lastly diminishing the bridge structure with low spring constant. Out of these possibilities, the third possibility depends on spring constant K_z. So actuation voltage can be minimized by using a serpentine spring with less K_z. Here k_z is used from eq. (4.72-4.74) for single spring with different meander based serpentine springs to reduce the actuation voltage. Switch design parameters for RF-MEMS switch are listed in table 4.3.

The optimal performance of RF-MEMS switch varies with actuation voltage which can be minimized by using a non-uniform serpentine flexure spring. Fig. 4.11 shows the actuation voltage for uniform and non-uniform serpentine flexure based RF-MEMS switch.

Table 4.3 RF-MEMS switch design parameters.

Parameter Name	**Parameter values**
Beam Width (w)	104 μm
Beam length (L)	640 μm
Gap height (g_o)	3 μm
Beam thickness (t)	1.5 μm
Electrode Width (W)	100 μm

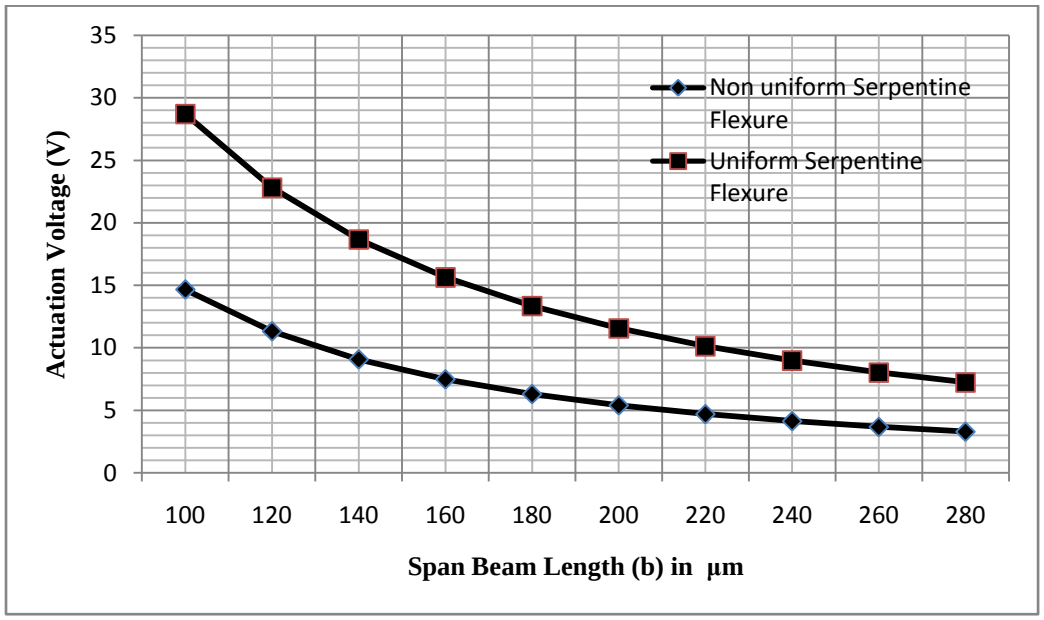

Figure 4.11: Actuation voltage comparison between uniform and non-uniform serpentine flexure based RF-MEMS switch, with different span beam lengths (b) ranging from 100µm to 280µm, with 1 meander section.

Table 4.4 Actuation Voltage comparison between non-uniform and uniform meander structure with different span beam length (*b*).

Span beam length (*b*) in µm	**Actuation Voltage for non-uniform meander structure**			**Actuation Voltage for uniform meander structure [120]**		
	1 meander	**2 meanders**	**3 meanders**	**1 meander**	**2 meanders**	**3 meanders**
100	14.656371	2.739023	0.733047	28.689057	12.5479	7.091886
120	11.318161	2.101363	0.557877	22.800913	10.298796	6.006655
140	9.073834	1.676794	0.44288	18.665098	8.619921	5.150624
160	7.481924	1.377743	0.362619	15.635901	7.33614	4.466309
180	6.305449	1.157903	0.303988	13.341698	6.332892	3.912221
200	5.407363	0.990781	0.259621	11.556214	5.533617	3.458082
220	4.703605	0.860261	0.22509	10.135042	4.885953	3.081587
240	4.140092	0.756042	0.19759	8.982311	4.353254	2.766131
260	3.680641	0.671267	0.175269	8.032213	3.909317	2.499215
280	3.300229	0.601216	0.156857	7.238268	3.535024	2.271331

This plot illustrate that non-uniform serpentine flexure provides actuation voltage of 15V to 3V for span beam length from 100 to 280 μm. But uniform serpentine flexure provides actuation voltage of 28V to 8V for same span beam lengths. It is also observed that actuation voltage is not significantly reduced after span beam length of 200 μm for both the types. From this plot it can be concluded that non-uniform serpentine flexure based RF-MEMS switch needs 30-40% less actuation voltage as compared to uniform serpentine flexure based switches [120]. Actuation voltage given between non-uniform and uniform meander structure with different span beam length are compared and is tabulated in table 4.4.

4.7 RF SIGNAL POWER HANDLING

RF power handling refers the power at which the MEMS device fails to operate properly. RF signal power can be applied to the capacitive MEMS switch at a broad range of frequencies with different power levels to achieve high performance for microwave frequencies, which is described as the RF power required for self actuation of the MEMS switch beam. RF power handling capability is mainly affected by the self actuation of the switch beam due to the current density of RF power applied to the switch [60]. Self actuation of capacitive MEMS switch can be controlled by current density on the transmission line by using low spring constant and low actuation voltage MEMS switch beam. RF signal power handling capability of RF-MEMS switches are mainly limited by the two factors [60, 71].

(i)- **RF latching: -** RF latching can be defined as the applied RF power that provides the enough force on the membrane to hold the switch down when DC bias is removed.

(ii)-**RF self-actuation:-** RF self-actuation is referred as a situation in which the high RF power actually creates enough potential to pull the membrane down in unactuated state without using a DC bias voltage across the switch.

RF power handling capability of RF-MEMS switch can be controlled by current density on the transmission line. The voltage on transmission line can be calculated by using characteristic impedance (Z_0) and power (*P)* which is given by

$$P = \frac{V_P^{\,2}}{Z_0} \quad \ldots (4.83)$$

$$\text{or} \quad V_P = \sqrt{PZ_0} \quad \ldots (4.84)$$

where V_P is the actuation voltage applied to the transmission line of characteristic impedance (Z_0 = 50Ω). So the power (P) required for self actuation is directly proportional to the applied actuation voltage. Therefore low-spring constant based RF-MEMS switches require low actuation voltage, which controls the current density on the transmission line and avoid self actuation of the switch beam.

Fig. 4.12 shows variation of RF power handling capability with actuation voltage for RF-MEMS switch using a transmission line with characteristic impedance of 50Ω. From this figure it is observed that RF-MEMS switch using non-uniform serpentine flexure provide the RF power of 0.2-4.29 W for self actuation (RF power handling capability) with actuation voltage of 3-14.6 V. However the uniform serpentine flexure based RF-MEMS switch require higher actuation voltage due to their higher spring constant, which increases the current density on transmission line and decreases the probability of self actuation of switch beam.

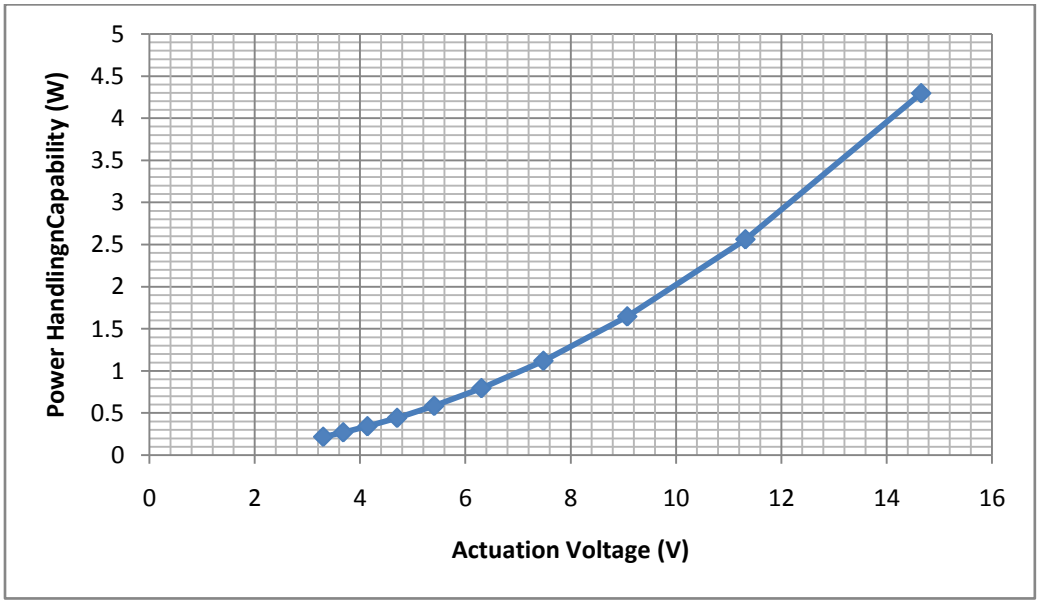

Figure 4.12: Variation of RF power handling capability with actuation voltage for non-uniform serpentine flexure based RF-MEMS switch having a transmission line of 50Ω characteristic impedance.

4.8 SWITCHING SPEED

Switching speed is another important performance parameter of RF-MEMS switches. Though RF-MEMS switches exhibit excellent RF characteristics such as low insertion losses and high isolation but these switches have a very slow switching speed. This switching speed depends on mass of the switch membrane and switch construction. This switching speed can be increased by using a switch membrane with lower mass. Generally a RF-MEMS switch operates at a speed of 2 to 50ms for several million switching operations [3, 10]. The low mass of membrane based MEMS capacitive shunt switches make it suitable for relatively fast switching operation in comparison with cantilever-style MEMS switches [11]. Now let us discuss how low spring constant affects the switching speed of RF-MEMS switch in terms of actuation voltage. The equation that governs the 1-D non linear model of the fixed-fixed beam switch as shown in fig. 4.10b is given as [1]:

$$m\frac{d^2x}{dt^2} + b\frac{dx}{dt} + kx + k_s x^3 = F_e + F_c \quad \ldots (4.85)$$

$$k = k' + k'' \quad \ldots (4.86)$$

where k' and k'' are the bending and residual-stress spring constants, k_s is the stress-stiffening spring constant (stretching effect), F_e is the electrostatic force and F_c represent the attractive and repulsive force between beam and dielectric layer.

Switching time can be calculated from closed loop solution for inertia limited systems. So for small damping coefficient and $Q \geq 2$, equation of motion can be given as:

$$m\frac{d^2x}{dt^2} + kx = -\frac{1}{2}\frac{\varepsilon_0 W w V^2}{g_0^{\,2}} \quad \ldots (4.87)$$

Switching time can be given for constant applied force as [36]:

$$t_s \approx 3.67 \frac{V_p}{V_s \omega_0} \quad \ldots (4.88)$$

where ω_0 is the resonant frequency of the switch, V_p is the actuation voltage and V_s is the supply voltage which is 1.4 times the actuation voltage (V_p) [121]. Eq. (4.88) can also be written in terms of resonant frequency as:

$$t_s = 2.62 \sqrt{\frac{m_e}{K_z}} \quad \ldots (4.89)$$

where K_z is the spring constant of the switch beam and m_e is the effective mass of the switch beam which is given by [1]:

$$m_e = 0.35(ltw)\rho = 311 \times 10^{-9} \text{ gram} \quad \ldots (4.90)$$

where *l*, *t*, and *w* are the length, thickness, and width of the switch beam as shown in fig. 4.10b, respectively and ρ is the density of the switch beam material.

From eq. (4.89) it is clear that switching time is inversely proportional to the square root of spring constant. However switch beam with lower spring constant provide higher switching time, which decrease the switching speed. So RF-MEMS switch beam with low spring constant shows a trade-off with higher switching speed.

Fig. 4.13 shows the variation of spring constant with switching time for the proposed non-uniform serpentine flexure based RF-MEMS switch with 1 meander section. It is observed that spring constant decreases with increase in switching time. But the optimal performance of the RF-MEMS switch needs a low switching time to achieve higher switching speed for transmit/receive switching applications. Hence, serpentine flexure with higher span beam length would be a good compromise between low spring constant and switching speed. For our design the switching time ranges from 1 - 4ms with varying span beam length of 100-280μm.

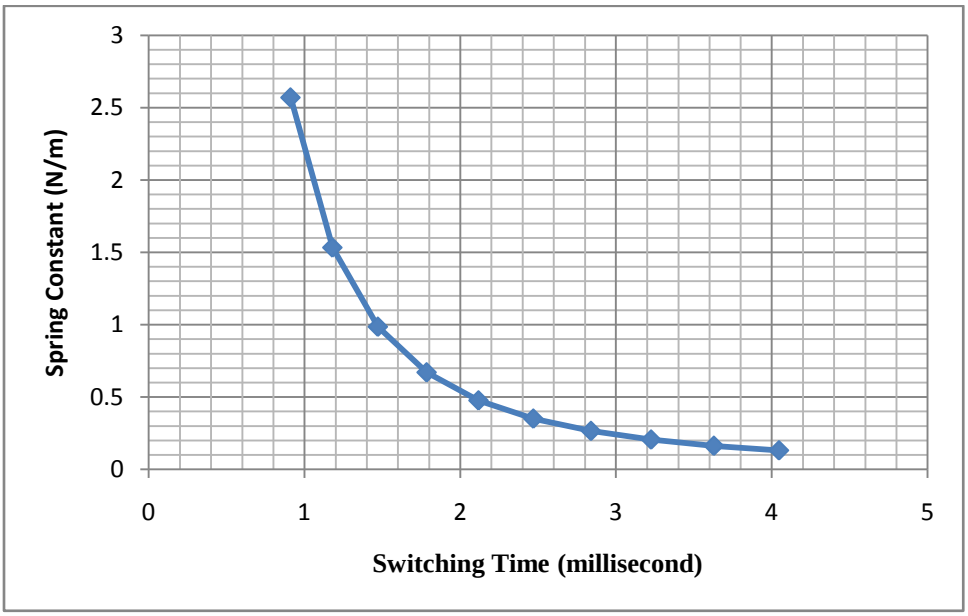

Figure 4.13: Variation of switching time with spring constant for non-uniform serpentine flexure based RF-MEMS switch with 1 meander section.

4.9 CONCLUSION

Electromechanical modeling of RF-MEMS switch has been explained in this chapter. A non-uniform serpentine flexure design for RF-MEMS switch has been described to achieve low spring constant. By using this flexure design we achieved a spring constant of 0.04-0.6 N/m for single meander based flexure design. These analytical results were confirmed with FEM analysis and we received considerable match between these two techniques. The proposed design shows an actuation voltage of 15 to 3 V with better RF power handling capabilities of 4.29 to 0.2 W having switching time of 1-4 millisecond for span beam length varying from 100 to 280μm. Here it is observed that increase in actuation voltage gives a trade-off between RF-power handling capability and switching speed. So it can be concluded that RF-MEMS switch using a single meander section with span beam length 100 to 180 μm provide a reasonable balance for switching speed and RF-power handling with adequate actuation voltage.

CHAPTER 5

ELECTROMAGNETIC MODELING OF RF-MEMS SWITCH

5.1 INTRODUCTION

RF-MEMS metal-to-metal and capacitive contact switches have been successfully demonstrated for microwave and millimeter wave RF applications [3, 9, and 40]. For metal-to-metal contact series RF-MEMS switches, an up-state (off-state) capacitance lies in the range of 2–10 fF, which shows high isolation for 20–40 GHz frequency range. However in case of capacitive contact fixed–fixed beam RF-MEMS switches, the down-state (off-state) capacitance lies between 1.4 and 3.5 pF with excellent isolation at resonant frequencies [13, 109]. When a dc bias is applied through central conductor of coplanar waveguide (CPW), the metallic MEMS bridge comes in contact with central conductor, passing the RF signal through ground plane of CPW [71]. This has been demonstrated in chapter 4. Muldavin et.al [122-123] have demonstrated that capacitive RF-MEMS switch can be electrically characterize using CLR model and discussed that this CLR model can be used to determine the RF performance using S-parameters. A similar approach has been applied to find the electromagnetic model parameters for proposed non-uniform serpentine spring based RF-MEMS switch.

The capacitive RF-MEMS switch is used with coplanar waveguide (CPW) configuration and subsequently this switch is represented by three lumped (active and passive) elements. These lumped elements; are bridge resistance (R_b), bridge capacitance

(C_b) and bridge inductance (L_b). These parameters are extracted from simulation results to characterize the RF performance [124].

So, this chapter deals with the electromagnetic modeling of the non-uniform serpentine flexure based RF-MEMS switch. In this an inductively tuned RF-MEMS switch is considered for which, the electrical model parameters are extracted using S-parameter measurements. The inductive tuning is obtained by inserting a recess between the ground plane and central conductor of CPW (called as inductive section) to attain higher isolation bandwidth at multiple resonant frequencies [125]. Section 5.2 describes the RF-MEMS switch in CPW configuration. Section 5.3 details the electromagnetic (CLR) model of RF-MEMS switch. Section 5.4 describes about the S-parameter measurements for design parameters of RF-MEMS switch such as capacitance, inductance and resistance. Section 5.5 explains the extraction of circuit model parameters of RF-MEMS switch. Section 5.6 discusses the result and analysis of the electromagnetic modeling of RF-MEMS switch. Finally section 5.7 describes the conclusion of this chapter.

5.2 RF-MEMS SWITCH IN CPW CONFIGURATION

The most common design of RF-MEMS switch is the fixed-fixed beam capacitive shunt switch. Microstrip and coplanar waveguide (CPW) are the most popular transmission lines for RF-MEMS devices. CPW transmission line shows the integration capability of lumped component in series and shunt configuration which offers a easier access to the ground plane and monolithic integration with RF-MEMS devices whereas microstrip lines gives a limited integration capability with MEMS switches [13, 71]. CPW transmission lines have also proven better performance as compared to microstrip transmission line in terms of dispersion, guide wavelength and loss. So the CPW is the most commonly used transmission line in RF-MEMS devices [124-125]. The schematic view of capacitive RF-MEMS switch in CPW configuration with non-uniform serpentine springs is illustrated in fig. 5.1.

Since the uniform serpentine spring based RF-MEMS switches are designed with constant span beam length, it require more number of meander sections to reduce the

spring constant and actuation voltage, while a non-uniform serpentine spring uses varying span beam segments whose length increases in consecutive multiples of first span beam length. It was proposed that a varying span beam length concept can reduce the spring constant of the serpentine spring which requires less actuation voltage without increasing the meander section as discussed in chapter 4. A non-uniform serpentine spring design with single meander section is proposed to provide longer bridge length and higher inductive section dimensions, which produces better isolation characteristics at multiple resonance frequencies.

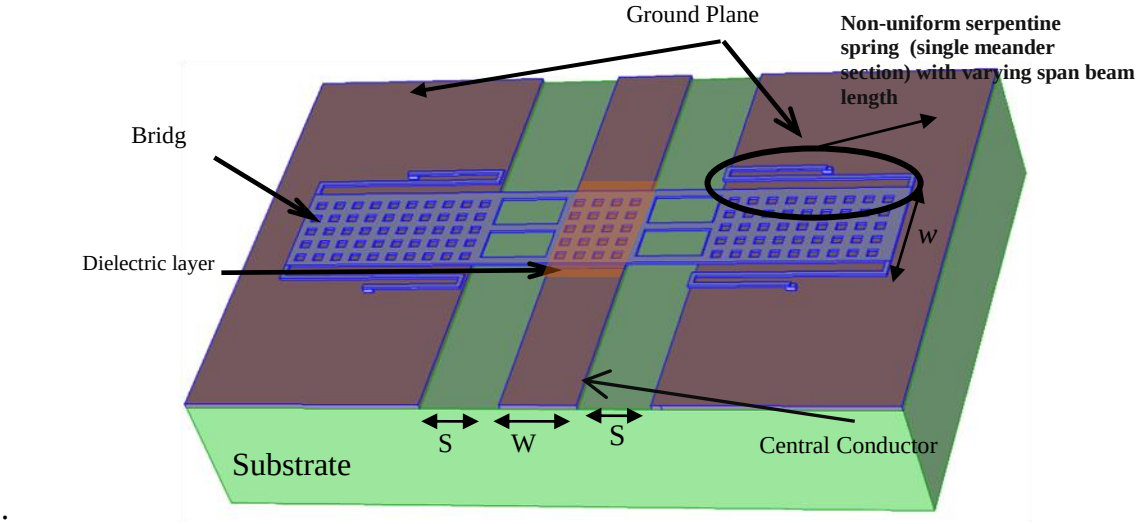

.

Figure 5.1: Schematic view of non-uniform serpentine flexure based RF-MEMS switch in CPW configuration**.**

5.3 ELECTROMAGNETIC MODELING OF RF-MEMS SWITCH

The RF-MEMS bridge is represented by three parameters, bridge resistance R_b, bridge capacitance C_b, and bridge inductance L_b. This RF-MEMS switch is modeled as transmission line with impedance Z_b and lumped series model of RF-MEMS bridge (RLC). In unactuated state, the RF-MEMS switch passes the RF signal through the CPW with up-state capacitance C_u ranging from 20-50 fF. However in actuated state, RF-MEMS switches stops the RF signal due to higher down-state capacitance.

This RF-MEMS switch is modeled as transmission line with impedance Z_b and lumped series model of RF-MEMS bridge (RLC) as shown in fig.5.2. The bridge impedance can be given as [11]

$$Z_b = R_b + j\left(\omega L_b - \frac{1}{\omega C_b}\right) \quad \ldots (5.1)$$

where the bridge capacitance C_b depends on the up-state and down-state capacitance of MEMS bridge. The resonant frequency of the MEMS switch can be obtained by:

$$\omega L_b - \frac{1}{\omega C_b} = 0 \quad \ldots (5.2)$$

$$\omega = \frac{1}{\sqrt{L_b C_b}} \Rightarrow f_0 = \frac{1}{2\pi\sqrt{L_b C_b}} \quad \ldots (5.3)$$

The RF-MEMS switch bridge impedance can be given as [47]

$$Z_b = \begin{cases} \dfrac{1}{\omega C_b} & f \le f_0 \\ R_b & f = f_0 \\ j\omega L_b & f \ge f_0 \end{cases} \quad \ldots (5.4)$$

Eq. 5.4 shows that the lumped capacitor-inductor-resistor (CLR) model of the MEMS bridge behaves as capacitor below the resonant frequency. At resonant frequency, this model behaves as bridge resistance R_b and as an inductor L_b above the resonant frequency. The bridge inductance is mainly dominated by the portion of the bridge over the CPW gaps.

The portions of MEMS bridge over the CPW conductor and ground plane provide insufficient bridge inductance, because the current is mainly carried on the edges of ground plane and CPW central conductor as shown in fig. 5.2a. This large series inductance occurred due to current carrying edges, can be easily achieved by adding a short high impedance section with length L_{tune} and width W_{tune}, between ground plane and MEMS bridge as shown in fig. 5.2b. The resonant frequency can be varied by choosing proper high impedance section length L_{tune} .

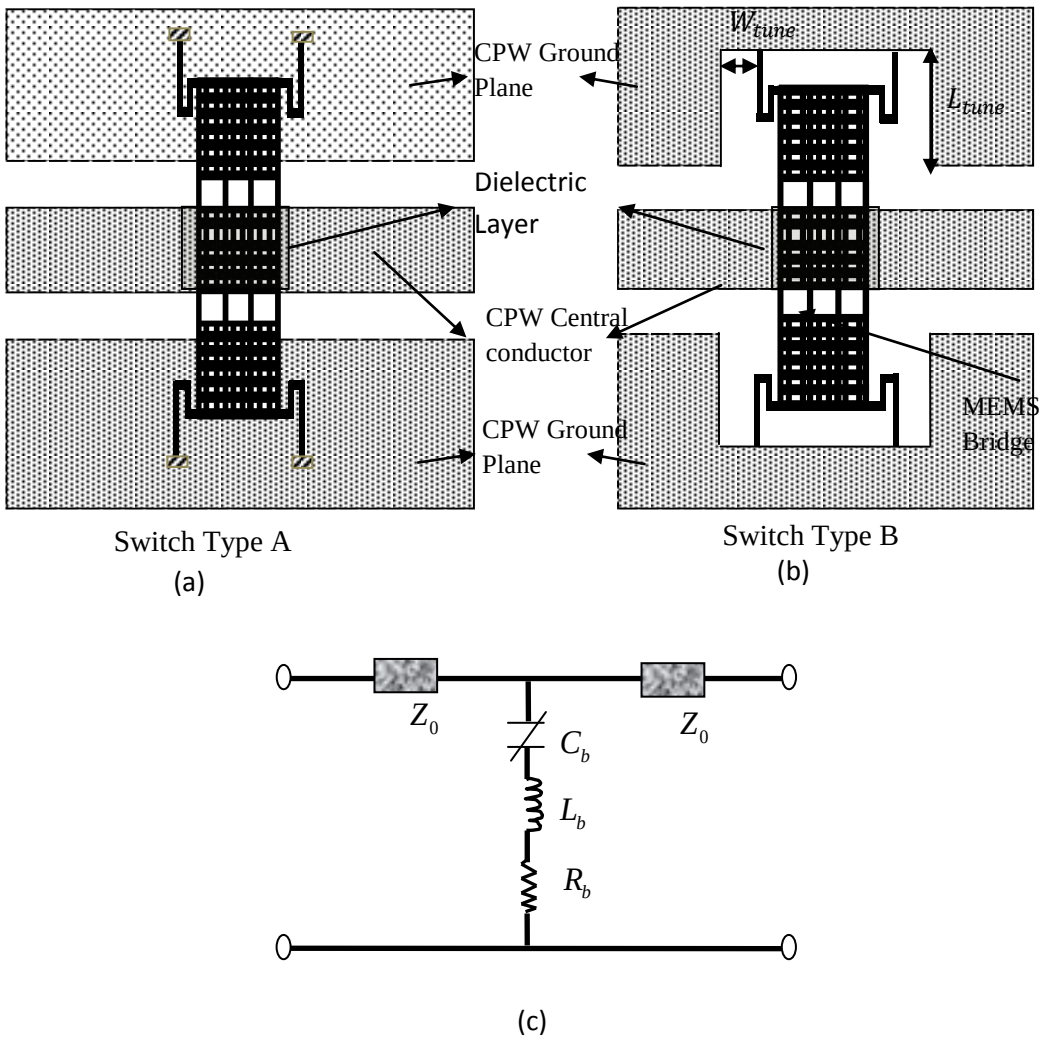

Figure 5.2: Schematic view of RF-MEMS switch in CPW configuration (a) RF-MEMS switch type A (b) RF-MEMS switch type B with inductive tuning (c) CLR Model for RF-MEMS switch.

5.4 SCATTERING-PARAMETER OF SWITCH

RF-MEMS switch electrical performance has been characterized by S-parameter in up and down-state of the MEMS bridge. This RF-MEMS switch can be modeled as two port network with a shunt connection. The general S-parameter for RF-MEMS switch can be given as [47]:

$$S_{11} = -20\log\left|\frac{-Z_b}{2Z_b + Z_0}\right| \quad \ldots (5.5)$$

$$S_{21} = -20\log\left|\frac{2Z_b}{2Z_b + Z_0}\right| \quad \ldots (5.6)$$

where Z_b is the MEMS bridge impedance and Z_0 is the CPW characteristic impedance. The S-parameters S_{11} & S_{21} have been estimated in up-state position of the MEMS bridge, which represents the return loss and insertion loss respectively. In down-state position S_{21} represents the isolation and S_{11} represents the return loss of RF-MEMS switch. The design parameters of the RF-MEMS switch such as capacitance, inductance and resistance plays an important role to calculate the return loss, insertion loss and isolation in actuated and unactuated states [49].

5.4.1 Capacitance

The total capacitance of the RF-MEMS switch in actuated and unactuated state determines the isolation and insertion losses over the range of frequencies.

(i) Up-state capacitance- In up-state position of MEMS bridge, the bridge capacitance C_b appears due to the air capacitance C_a and dielectric capacitance C_{di}. Therefore the up-state-capacitance can be given as [49]:

$$C_u = \frac{(Ww - A')\varepsilon_0}{g_0 + \frac{t_d}{\varepsilon_r}} \quad \ldots (5.7)$$

where *w* is the MEMS bridge width, *W* is the dielectric layer width, A' is the area of square cuts (2500 μm^2) in overlapped beam, g_0 is the air gap between MEMS bridge and dielectric layer, t_d is the dielectric layer thickness and ε_r is the relative permittivity of the dielectric layer. The fringing field capacitance C_f, is present in RF-MEMS shunt switches. It usually forms a sufficient amount of the up-state capacitance C_u.

Table 5.1 shows the calculated up-state capacitance C_u^c for bridge width of 120 μm and gap varying between 1 μm to 5.5 μm. Here fringing field capacitance is not considered for up-state capacitance calculation. Table 5.2 shows the Up-state and down-state capacitance calculation for gap height of 3 μm and bridge width varying between 60 μm to 180 μm. From table 5.1 it is also observed that higher bridge height provide the smaller up-state capacitance which leads to better return loss and insertion loss in unactuated state. From table 5.2 it is illustrated that smaller cross-section area between bridge width and electrode width shows low up-state capacitance which leads to low insertion and better return loss.

Table 5.1 Up-state capacitance calculation for bridge width of 120 μm for different gap heights

Gap (μm)	Up-State Capacitance (fF)
1	103.947273
2	52.313333
2.5	41.905445
3	34.951703
3.5	29.977303
4	23.335102

Table 5.2 Up-state and down-state capacitance calculation for different bridge widths with gap height of 3 μm

MEMS Bridge Width (w-μm)	Up-State Capacitance (fF)	Down-State Capacitance (μF)
60	13.80445	3.16122
80	20.85353	4.77546
100	27.90262	6.38907
140	42.00078	9.61818
180	56.09895	12.84666
220	70.19711	16.07514
250	80.77074	18.49165
280	91.34436	20.91786

The up-state capacitance C_u affects the insertion loss and return loss in unactuated state of the RF-MEMS switch. These losses have been calculated for different up-state capacitance values ranging from 23fF to 103 fF with bridge resistance R_b , bridge inductance L_b , CPW transmission line impedance Z_0 , of 0.1Ω, 7 pH, 50Ω respectively. The resulting plot, calculated by using eq. (5.5) and (5.7), shows the insertion loss and return loss of different Up-state capacitance C_u over a frequency range from 0 to 50 GHz. Fig. 5.3 shows the insertion loss in unactuated state for different up-state capacitance. This figure illustrate that insertion loss is slightly similar upto 10 GHz thereafter it diverges slowly for lower up-state capacitance. Here it is observed that above 10 GHz, higher up-state capacitance shows higher insertion loss as compared to lower up-state capacitance.

Fig. 5.4 shows the return loss in unactuated state, which illustrate that smaller up-state capacitance, leads to better return loss as compared to higher up-state capacitance. At 10 GHz up-state capacitance with 103 fF shows the return loss of -15 dB, whereas up-state capacitance with 23 fF shows the return loss of -30 dB. This shows that better return loss can be achieved with lower up-state capacitance.

(ii) Down-state capacitance

When the RF-MEMS switch is in down-state position it disconnects the two ports of the network. This down-state capacitance occurs due to the dielectric layer between the MEMS bridge and pull-down electrode. This down-state capacitance can be given as [49]:

$$C_d = \frac{(Ww - A')\varepsilon_0 \varepsilon_r}{t_d} \quad \ldots (5.9)$$

where ε_0 is the relative permittivity of free space and ε_r is the relative permittivity of dielectric material. From table 5.2, it is clear that larger bridge width (w) shows the higher down-state capacitance which leads to higher down-state to up-state capacitance ratio. This higher capacitance ratio improves the isolation with increase in frequency. For example at 10 GHz, when down-state capacitance is 21 pF, its isolation is 35 dB which is much better than 15 dB when down-state capacitance is 3 pF, as shown in fig. 5.5.

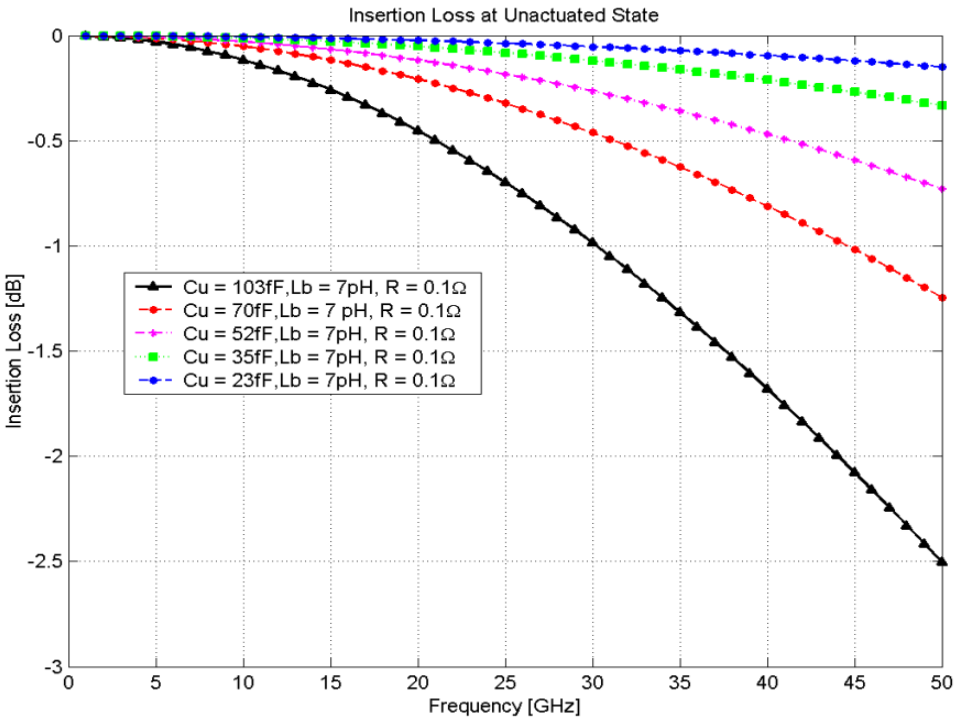

Figure 5.3: Insertion loss of RF-MEMS switch in unactuated state.

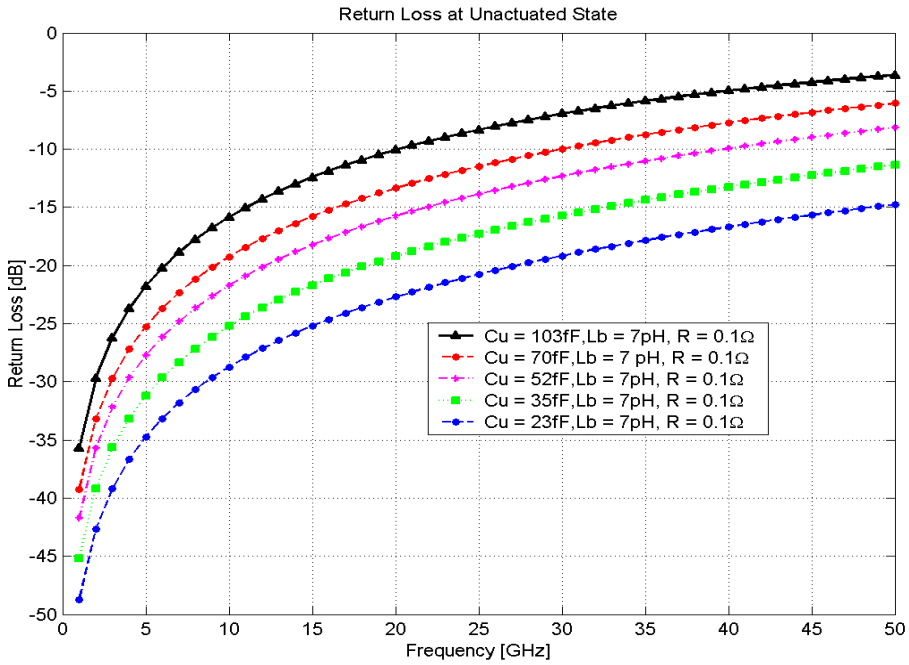

Figure 5.4: Return loss in unactuated state for different up-state capacitance.

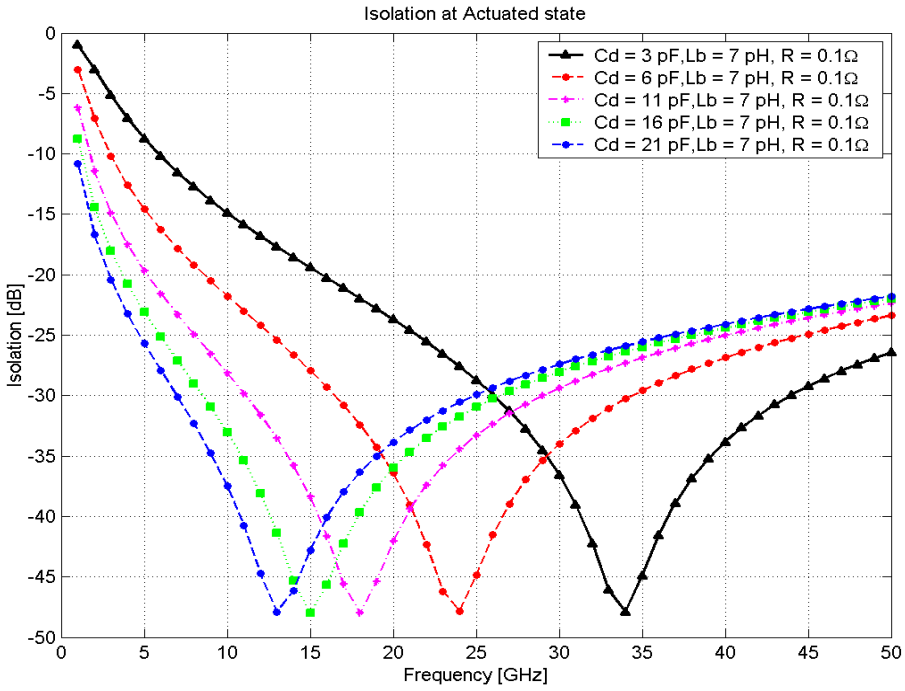

Figure 5.5: Isolation in actuated state with different down-state capacitances.

From these graphs it can be concluded that low insertion loss and good return loss can be achieved with low up-state capacitance in unactuated state. This low up-state capacitance can be attained by using small bridge width. In order to achieve higher isolation in actuated state, the down-state capacitance should be high. To achieve high isolation at low frequency, large bridge width is needed. So the bridge width shows a trade-off between higher isolation and lower insertion loss in actuated and unactuated state respectively.

5.4.2 Bridge resistance

In down-state position the current will pass the MEMS bridge through the CPW central conductor. Hence the equivalent resistance of RF-MEMS switch can be given as:

$$R_b = R_{bridge} + R_{CPW} \quad \ldots (5.10)$$

where R_{bridge} and R_{CPW} are the resistance due to the MEMS bridge and CPW central conductor respectively. The MEMS bridge resistance R_{bridge} can be given as:

$$R_{bridge} = \frac{\rho_b L}{4A} \quad \ldots (5.11)$$

where ρ_b is the resistivity of the MEMS bridge, *L* is the MEMS bridge length and *A* is the cross sectional area of MEMS bridge. At high frequencies, the skin effects take place due to the skin depth (δ_b). So the area in eq. (5.11) is

$$A = 2\delta_b (w + t) \quad \ldots (5.12)$$

where *t* and *w* represents the thickness and width of the MEMS bridge respectively and δ_b is the skin depth which is given by:

$$\delta_b = \sqrt{\frac{2}{\omega \mu_0 \sigma_b}} = \sqrt{\frac{1}{\pi f_0 \mu_0 \sigma_b}} \quad \ldots (5.13)$$

where μ_0 denotes permeability of the free space, σ_b represents the conductivity of the bridge and f_0 shows the operational frequency of the RF-MEMS switch. Fig. 5.6 & 5.7 show the insertion loss and return loss in unactuated state for different bridge resistances. Here it is observed that lower bridge resistance provide lower insertion and return loss in frequency range 20-50 GHz.

From fig. 5.8 and 5.9 it is observed that, the actuated RF-MEMS switch shows the sharper and deeper resonance for smaller bridge resistances. So the smaller bridge resistance of 0.01 Ω gives the higher isolation of 68 dB at resonant frequency of 15 GHz, where as a bridge resistance of 10 Ω gives an isolation of 10 dB at same resonant frequency. Similarly the smaller bridge resistances shows better return loss in actuated state as shown in fig. 5.9. Here it is observed that smaller bridge resistance shows higher isolation and better return loss in actuated state.

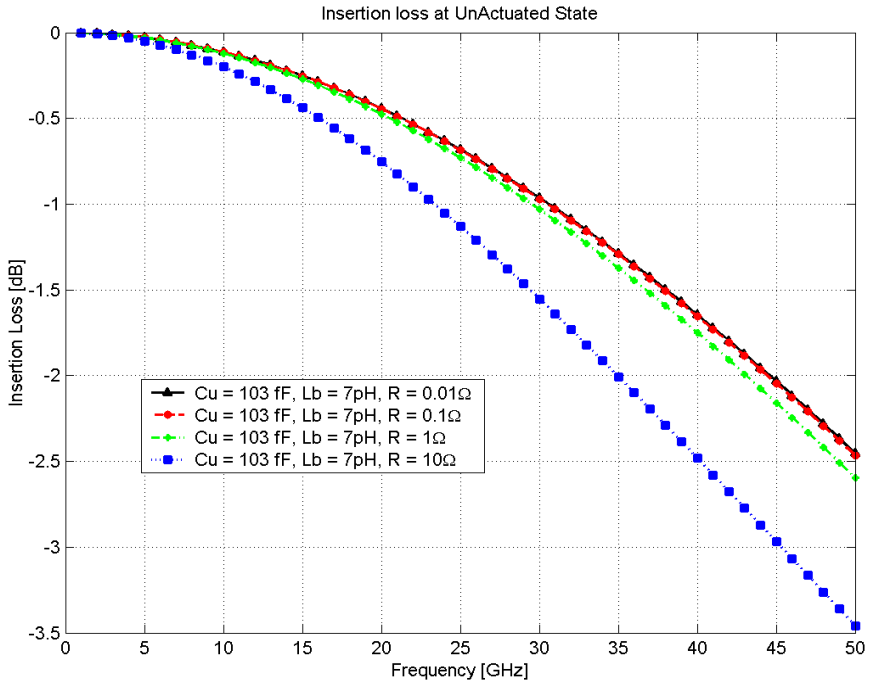

Figure 5.6: Insertion loss of proposed RF-MEMS switch for different bridge resistances in unactuated state.

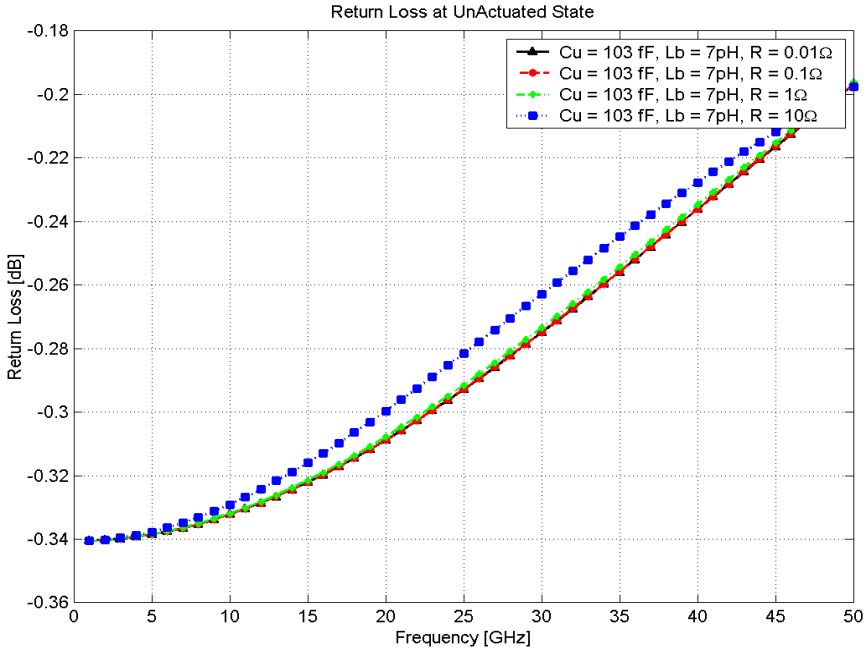

Figure 5.7: Return loss of proposed RF-MEMS switch for different bridge resistances in unactuated state.

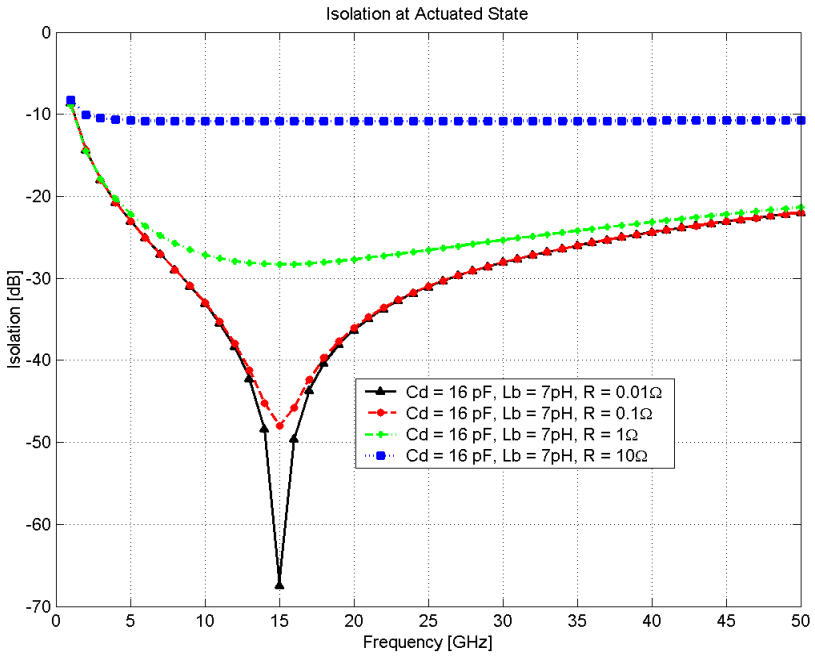

Figure 5.8: Isolation of proposed RF-MEMS switch for different bridge resistances in actuated state.

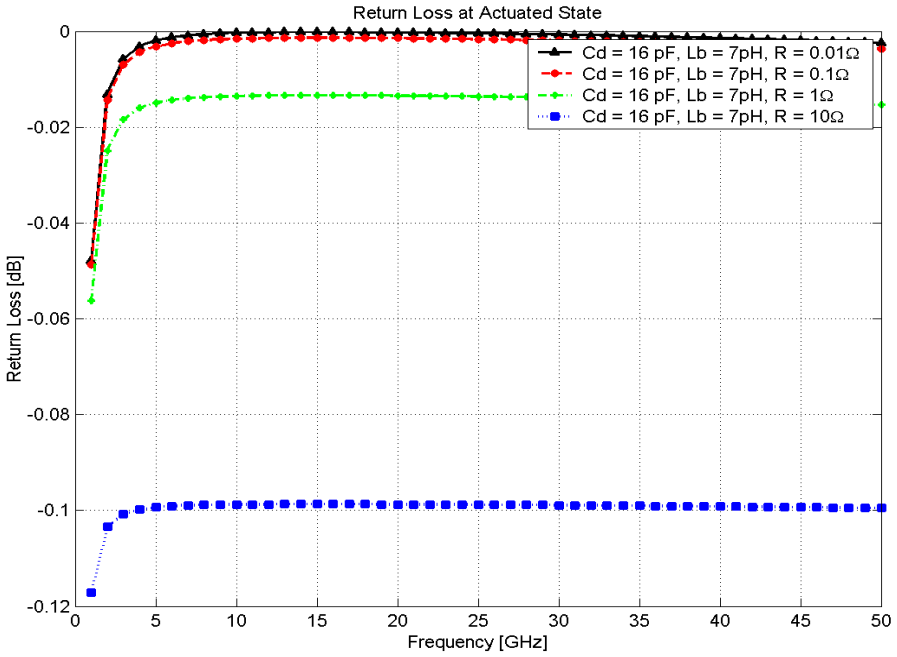

Figure 5.9: Return loss of proposed RF-MEMS switch for different bridge resistances in actuated state.

5.4.3 Bridge inductance

The bridge inductance plays an important role when the switch is in actuated state whereas it has little effect in an unactuated state. RF-MEMS switch bridge shows a small inductance in series with bridge capacitance (C_b) and bridge resistance (R_b). This bridge inductance shows a small effects on S-parameter in unactuated state whereas a significant effect in actuated state. Here different values of bridge inductance 4, 8, 12 and 16 pH are used to understand the effects of bridge inductance on isolation and return loss in actuated state. From fig. 5.10 it is observed that for higher values of inductance, resonance occurs at lower frequency whereas for lower values of inductance resonance occurs at higher frequencies. Hence if better isolation is required at lower frequencies, high value of bridge inductance is required. Fig. 5.11 shows return loss of proposed RF-MEMS switch in actuated state with different bridge inductances. It is observed that the effect of bridge inductance is very nominal in the considered frequency range.

5.5 EXTRACTION OF CIRCUIT MODEL PARAMETERS

This section describes the extraction of circuit model parameters for non-uniform serpentine spring based RF-MEMS switches of both types. The dimensions of the switch considered here, are: bridge width is 100 μm, gap height between bridge and dielectric layer is 3 μm, capacitive area is 7500 μm^2 and dielectric layer thickness is 0.2 μm. For both type of switches, the number of non-uniform meander section is assumed as 1 and dielectric layer constant is taken as 7.6. The characteristic impedance of CPW central conductor is taken as 50 Ω. For switch type B the inductive section length and width are taken as 280 and 60 μm, respectively.

5.5.1 Up-state bridge capacitance

The effect of up-state capacitance (C_u) on return loss in unactuated state of RF-MEMS switch is studied using Ansys HFSS™ electromagnetic simulation tool for the frequency range of 0–50 GHz. In unactuated state the RF-MEMS switch behaves as a capacitor, so the total return loss S_{11} can be express in terms total up-state capacitance [125].

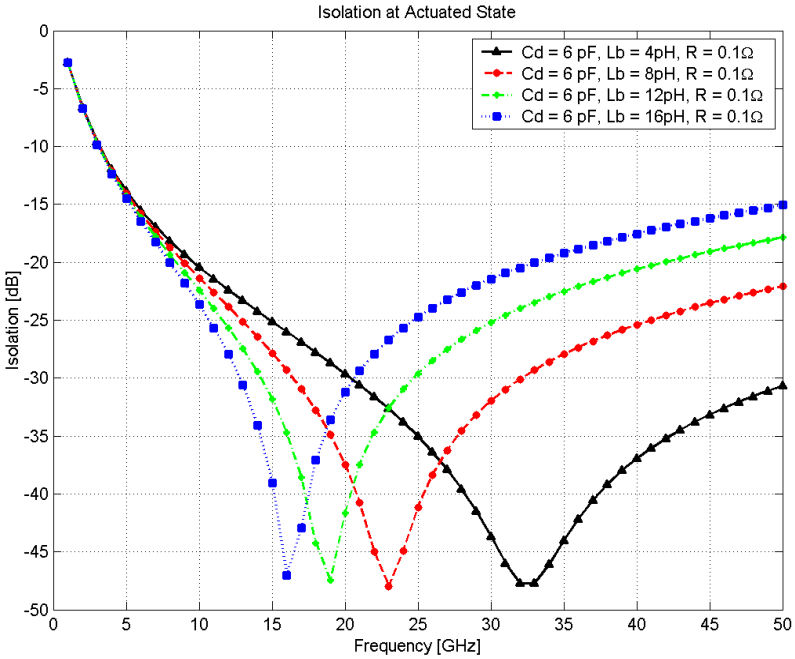

Figure 5.10: Isolation of proposed RF-MEMS switch in actuated state with different bridge inductances.

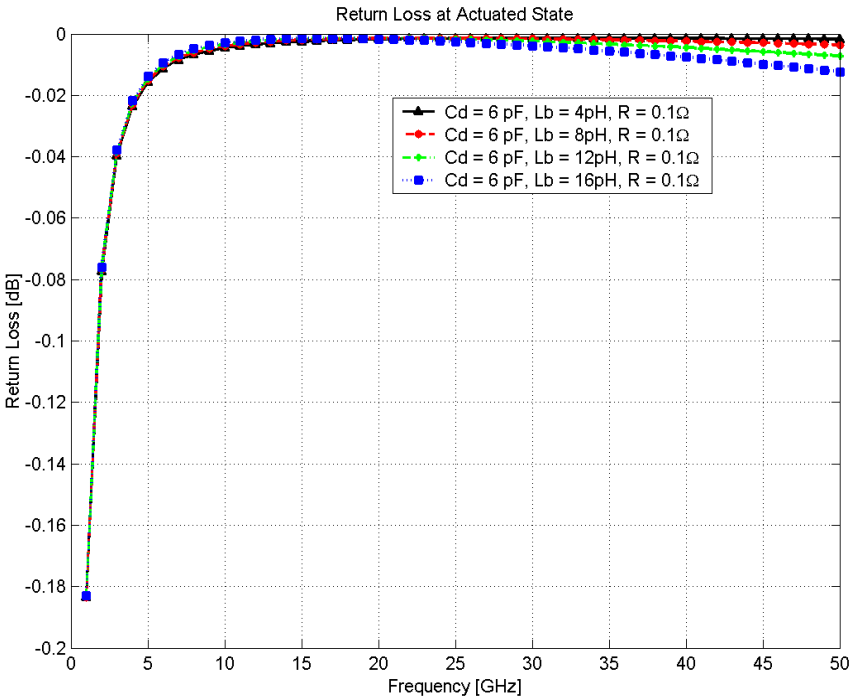

Figure 5.11: Return loss of proposed RF-MEMS switch in actuated state with different bridge inductances.

$$S_{11} = -20\log\left|\frac{-j\omega C_u Z_0}{2+j\omega C_u Z_0}\right| \quad \ldots (5.14)$$

It is observed that the simulated and computed return loss are in close agreement with each other in the given frequency range as depicted in fig. 5.12.

In order to extract the up-state capacitance from the simulated return loss, frequency of 5 GHz is chosen because the RF-MEMS switch behaves as capacitor below the LC resonant frequency. It is observed that the resonant frequency (f_0) of RF-MEMS switch is 27 GHz and at 5 GHz the simulation shows that the return loss is -33 dB. This value of return loss provides the extracted up-state capacitance of 27 fF, which is quite similar to the calculated up-state capacitance of 24 fF. The slight difference in the values is attributed due to the fringing effects present at the bridge edges, which are not considered during mathematical calculation.

5.5.2 Down-state bridge capacitance

In down-state, the RF-MEMS switch behaves as a LC resonance circuit, so the isolation S_{21} can be expressed in terms of down-state capacitance as [125] using:

$$S_{21} = -20\log\left|\frac{2}{2+j\omega C_D Z_0}\right| \quad \ldots (5.15)$$

From fig. 5.13 it is observed that the theoretical calculated isolation plot and simulated plots coincide with each other below 5 GHz ($f < f_0/5$). Hence we have chosen a frequency of 3 GHz below $f_0/5$ to extract down-state capacitance which correspond the isolation of 8 dB, as shown in Fig. 5.13. This value of isolation gives the down-state capacitance (C_d) of 3.2 pF which is considerably close to the calculated down-state capacitance of 2.63 pF.

5.5.3 Bridge resistance and bridge inductance

In order to extract the bridge resistance (R_b) and bridge inductance (L_b) from simulated isolation plots, the resonant frequency is chosen because at LC resonant frequency the

RF-MEMS switch behaves as bridge resistance. So the isolation S_{21} can be expressed in terms of bridge resistance and bridge inductance as follows [125]:

$$S_{21} = -20\log\left|\frac{2R_b}{2R_b + Z_0}\right| \quad \ldots (5.16)$$

$$S_{21} = -20\log\left|\frac{2\omega L_b}{2j\omega L_b + Z_0}\right| \quad \ldots (5.17)$$

Using Fig. 5.13 it is observed that the resonance frequency is 27 GHz and the resulting isolation is about 47 dB. This value of isolation will yield an extracted bridge resistance of 0.1Ω.

To extract the bridge inductance from simulated isolation plot, the frequency of 50 GHz is chosen because the RF-MEMS switch behaves as bridge inductance above the resonant frequency. From fig. 5.13 it is observed that at 50 GHz, the resulting isolation of 24 dB yields an extracted bridge inductance of 4.7 pH. The large discrepancy between the calculated and simulated isolation plots in Fig 5.13 is attributed due the values of L_b & R_b which are taken as zero for the calculation of isolation plots.

Similar process is used to extract the CLR parameter for type B switch shown in fig. 5.2(b). Type B switch with inductive tuning possess the down-state capacitance of 1.4 pF, bridge resistance of 0.25Ω and bridge inductance of 52 pH. It is observed that the inductive tuning section shifts the resonant frequency to a lower frequency. This inductive tuning enables to tune isolation bandwidth for multiple frequency bands from Ka band to Ku band.

5.6 RESULTS AND ANALYSIS

The comparison of the circuit model parameters between inductive tuned and non-inductive RF-MEMS switch is given in table 5.3. This result shows that type A switch gives 50% higher capacitance ratio as compared to type B switch. This higher capacitance ratio exhibit higher isolation at higher resonant frequencies whereas the lower capacitance ratio gives lower isolation at lower resonant frequencies. Here the bridge width is restricted up to 100 μm and air gap up to 3 μm because the higher bridge width shows trade-off between higher isolation and lower insertion loss as discussed in section 5.4.

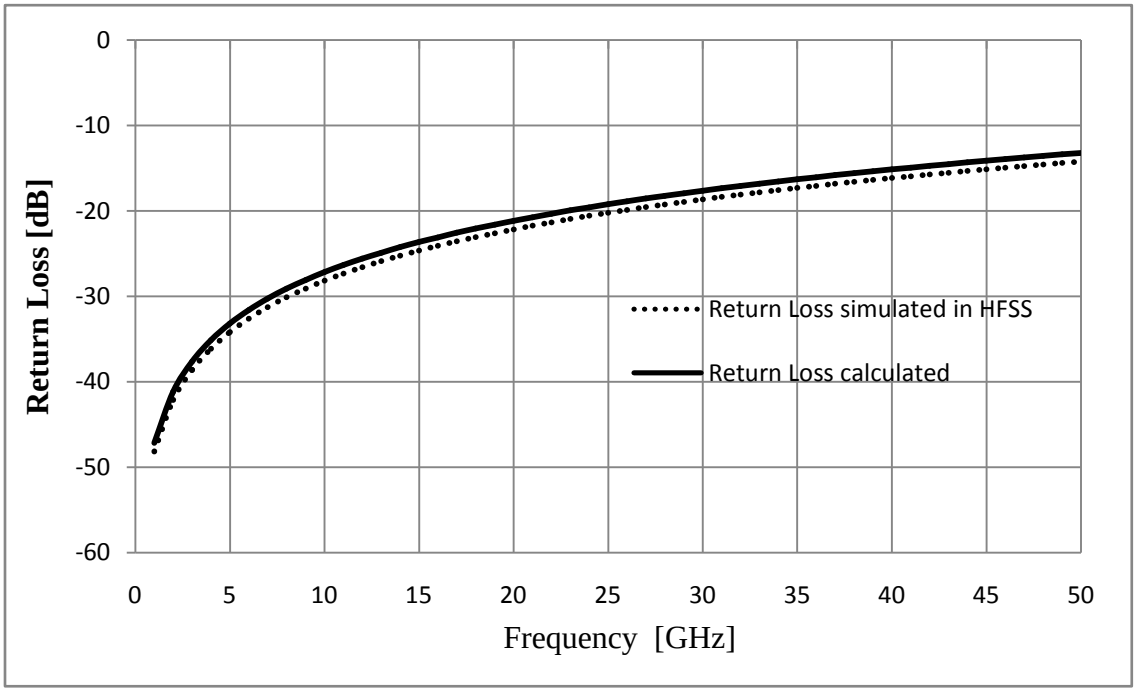

Figure 5.12: Simulated and calculated return loss for the proposed RF-MEMS switch.

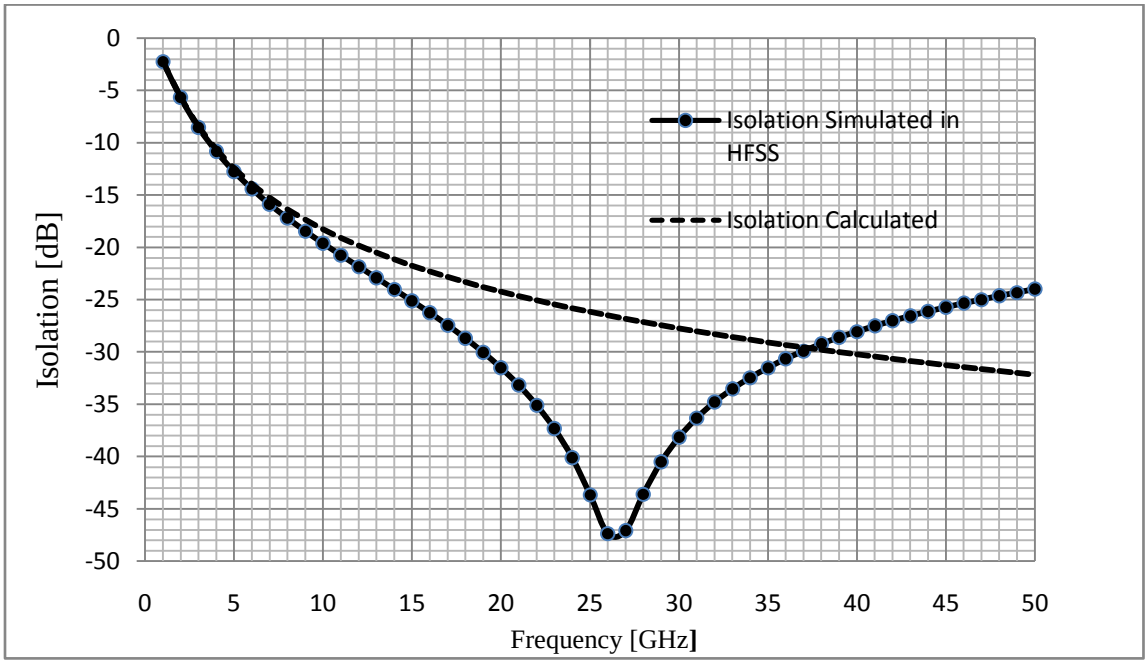

Figure 5.13: Simulated and calculated Isolation for the proposed RF-MEMS switch.

Table 5.3. **Comparison between simulated and calculated values.**

Switch Type	C_{up} **Calculated**	C_{Down} **Calculated**	C_{Down} / C_{up} **Calculated**	**Extracted Circuit Model (CLR) parameter**				C_{Down} / C_{up} **Simulated**
				C_{up}	C_{Down}	R_b	L_b	
Type A	21 fF	2.63 pF	109	27 fF	3.2 pF	0.1Ω	4.7pH	118
Type B	21 fF	2.63 pF	109	26.5 fF	1.4 pF	0.25Ω	52 pH	52

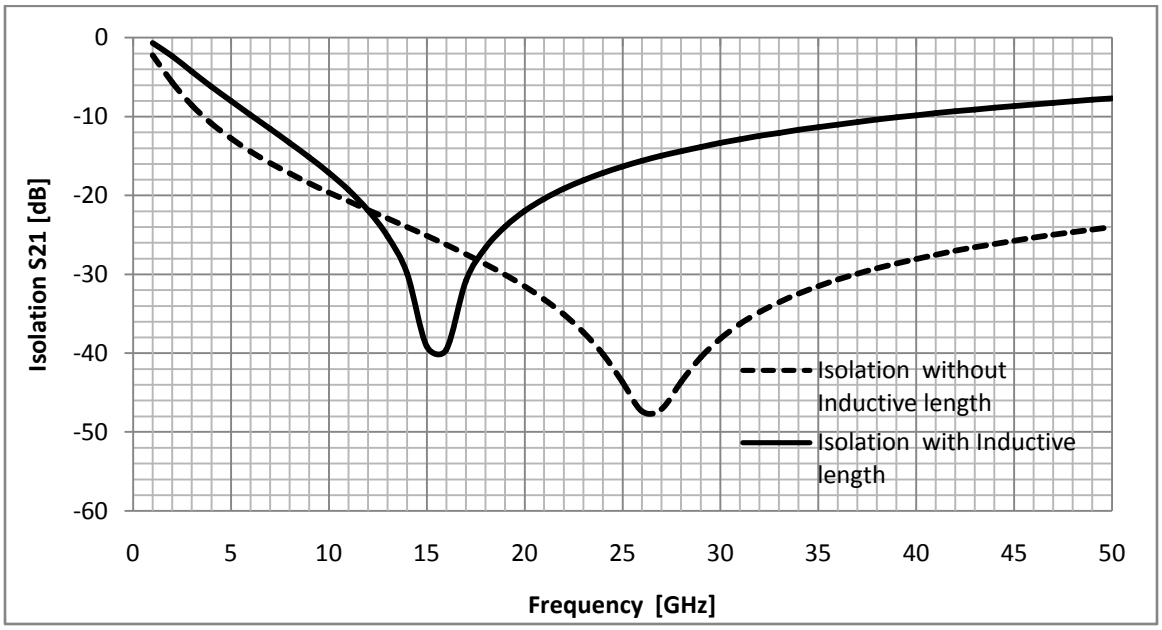

Figure 5.14: Simulated and calculated Isolation for the proposed RF-MEMS switch with and without inductive tuning.

It is observed that as we increase the inductive tuning section length and width, bridge inductance goes on increasing which in-turn reduces the down-state capacitance. This reduced down-state capacitance shifts the resonant frequency from higher to lower frequency band. This provides multiband tuning (isolation bandwidth) of RF-MEMS switch with isolation of more than 30 dB.

In order to achieve lower resonant frequency with higher isolation (>>20 dB), the bridge inductance can be increased by increasing the inductive section dimensions by adding more number of meander sections to the serpentine spring of MEMS bridge.

However it is not advisable to use more meander sections because it increases structure complexity due to space limitations. So, it is proposed that type B switch is preferable for reconfigurable antenna application because it gives adequate isolation at lower resonance frequencies.

5.7CONCLUSION

An electromagnetic modeling is used to predict the radio frequency performance in up-state and down-state of non-uniform serpentine spring based RF-MEMS switch. Good agreement between computed and simulated results confirm the validity of proposed RF-MEMS switch design. It is observed that isolation bandwidth can be achieved by introducing the inductive section with larger dimension by adding meander sections at MEMS bridge. This proposed RF-MEMS switch design (type A and type B) shows the return loss of << -20 dB up to 25 GHz and isolation of >>25 dB from 15 to 35 GHz.

CHAPTER 6

RECONFIGURABLE ANTENNA USING PROPOSED RF-MEMS SWITCH

6.1 INTRODUCTION

In wireless mobile communication system, microstrip patch antennas have attributed their attractive benefits such as low profile, light weight, and easy fabrication. These microstrip patch antennas are designed for single mode operation with linear polarization having limited bandwidth profile [126-127]. In some application such as satellite communication, the reconfigurable antenna is used to achieve switching capability between two frequency bands. This switching can be achieved by using p-i-n diode and FET switches. However various researchers have proposed the use of RF-MEMS switches for multi frequency band operation due their advantage of higher isolation with better return loss as compared to their semiconductor counterpart [127-129].

Semiconductor switches require a considerable amount of power to operate which reduces battery life time and increases the biasing issues as compared to RF-MEMS switches. Some limitations of semiconductor switches are as follows [88, 128]:

1) Semiconductor switches radiate with different frequencies as compared to RF-MEMS switches.
2) These switches increase the antenna dimensions.

3) These switches are suitable for directional patterns, however these switches are not suitable for omnidirectional receiver antenna design.
4) Semiconductor switches require separate bias line which increases the biasing circuitry, whereas the RF-MEMS switch bias line can be easily fabricated with microstrip patch design.

These main disadvantages make semiconductor switches inappropriate for portable reconfigurable microstrip patch antennas. Hence RF-MEMS switch technology is regarded as a promising technology for future reconfigurable wireless communication systems [130].

Additionally, these RF-MEMS switches can be easily controlled by using high resistive lines through actuating pads without causing any interference and degradation to the antenna radiation properties. A reconfigurable microstrip patch antenna consists of various microstrip patch elements capable of individually reconfiguring their physical structure, altering frequency and pattern properties. [18,131-133]. RF-MEMS switch have been widely utilized in antenna design with a variety of reconfigurability in terms of impedance bandwidth, radiation pattern, polarization and resonant frequency. The goal of these developed reconfigurable antennas is to reduce the system complexity for operation with diverse radiation characteristics over a wide range of frequency band. Nevertheless, reconfiguring one characteristic of the microstrip patch antenna affects the rest antenna properties, such as frequency response reconfiguration results in changed radiation pattern [18, 134]. This is an important and largest challenge in the development of reconfigurable microstrip patch antennas.

RF-MEMS switch technology is matured enough over the years and RF-MEMS switches have been successfully integrated with current communication systems having long term reliability. These wireless communication systems have a wide range of application such as radar systems, reconfigurable wireless communication and space borne satellite remote sensing [135-136]. The design diversity of reconfigurable microstrip patch antenna needs alternating / variable geometry configuration, which should be controlled precisely through high quality switches [137].

In this chapter a two circular microstrip patch antenna array with proposed RF-MEMS switches are used for WLAN frequencies (L and S band). The capacitive non-uniform serpentine spring based RF-MEMS are used in CPW configuration, so they do not require extra bias line, the bias is applied directly to the RF signal line. The lack of bias line for the RF-MEMS switches in proposed reconfigurable antenna design makes the fabrication easier, which in turn improves the radiation performance due to absence of leakage and coupling through the bias lines. This reconfigurable antenna design consists of two RF-MEMS switches, to achieve pattern and frequency reconfigurability. The proposed switch design is scaled up by a factor of 20 in order to achieve the reconfigurability in L and S band.

In this chapter section 6.2 describes the basic design of ultra wideband (UWB) circular microstrip patch antenna using single RF-MEMS switch with impedance matching. Section 6.3 describes the design and operating principal of RF-MEMS switch based reconfigurable antenna. Section 6.4 explains the simulation and analysis of the proposed design and finally section 6.5 describes the conclusion of this chapter.

6.2 ANTENNA DESIGN AND IMPEDANCE MATCHING

The base design for RF-MEMS based microstrip patch antenna consists of a CPW-fed circular disc shaped monopole having 25 mm diameter designed on 1.5 mm thick silicon (Si) substrate with 3.3 permittivity ($\tan ¢ = 0.002$). This circular patch is printed with 50Ω CPW transmission line on same side of dielectric substrate. Fig. 6.1 presents the details of the schematic design of RF-MEMS based microstrip patch antenna and its dimensions are summarized in table 6.1. The overall width and the ground plane length of the antenna are: W' = 47 mm and G_L = 10 mm, respectively. A CPW feed line with central conductor width W = 4 mm and ground signal gap S= 0.33 mm is used, resulting in a characteristic impedance (z_0) of 50 Ω [138].

The analysis of circular microstrip patch antenna impedance with and without RF-MEMS switch is done by using Ansoft HFSS™ EM simulation solver. The antenna impedance (reflection coefficient Γ) is plotted as a function of frequency on the Smith

Chart. The Smith Chart displays the complex reflection coefficient, in polar form, for arbitrary load impedance (antenna impedance) [139].

In case of simple circular microstrip patch antenna (without RF-MEMS switch), the antenna (load) impedance and return loss have been plotted in fig. 6.2 & 6.3 respectively. Fig. 6.2 depicts that the antenna impedance at point m1 corresponds to resonant frequency of 5GHz. This point m1 lies at the centre of the Smith chart Re[z] =1, which indicates that the circular microstrip patch antenna (without RF-MEMS switch) is perfectly matched with the CPW transmission line at the resonant frequency of 5GHz with adequate return loss of -37 dB as shown in fig.6.3.

When RF-MEMS switch is attached on ground plane with gap height of 0.15 mm from central conductor of CPW transmission line, as shown in fig. 6.1(b), an impedance mismatch occurs between antenna and CPW transmission line.

Table 6.1 Reconfigurable antenna design parameters

Parameter	**Value**
Substrate length (L)	47 mm
Substrate width (W')	47 mm
Circular patch radius (R)	12.5mm
Substrate Thickness (H)	1.5mm
CPW Ground thickness (T)	0.05 mm
Microstrip Patch thickness (t)	0.05 mm
CPW Ground Length (G_L)	10mm
CPW central conductor length (G_L + h)	11mm
CPW central conductor width (W)	4mm
CPW gap (S)	0.33mm
Substrate dielectric constant (ε_r)	3.3
RF-MEMS switch bridge length	12.8mm
RF-MEMS switch bridge width	2.08mm
RF-MEMS switch bridge thickness	0.1mm
Height between Switch & CPW Central conductor	0.15mm

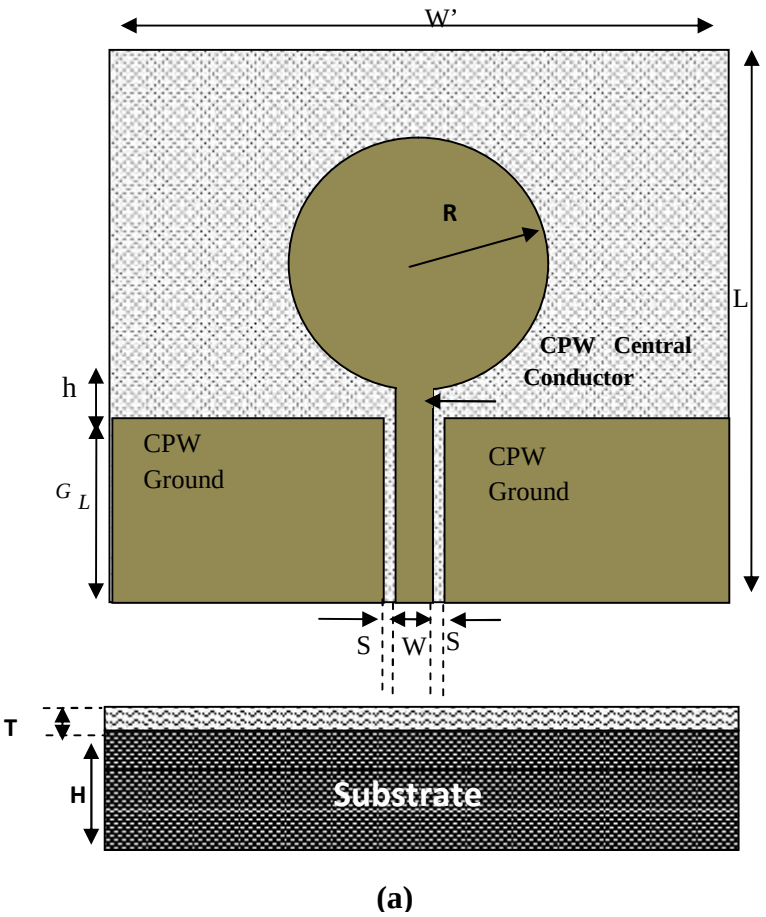

(a)

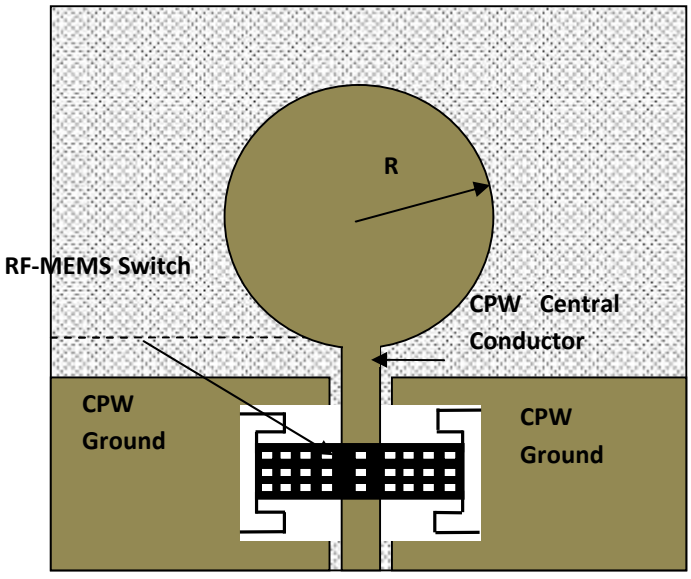

(b)

Figure 6.1: Schematic view of microstrip circular patch antenna **(a)** without RF-MEMS switch **(b)** with RF-MEMS switch

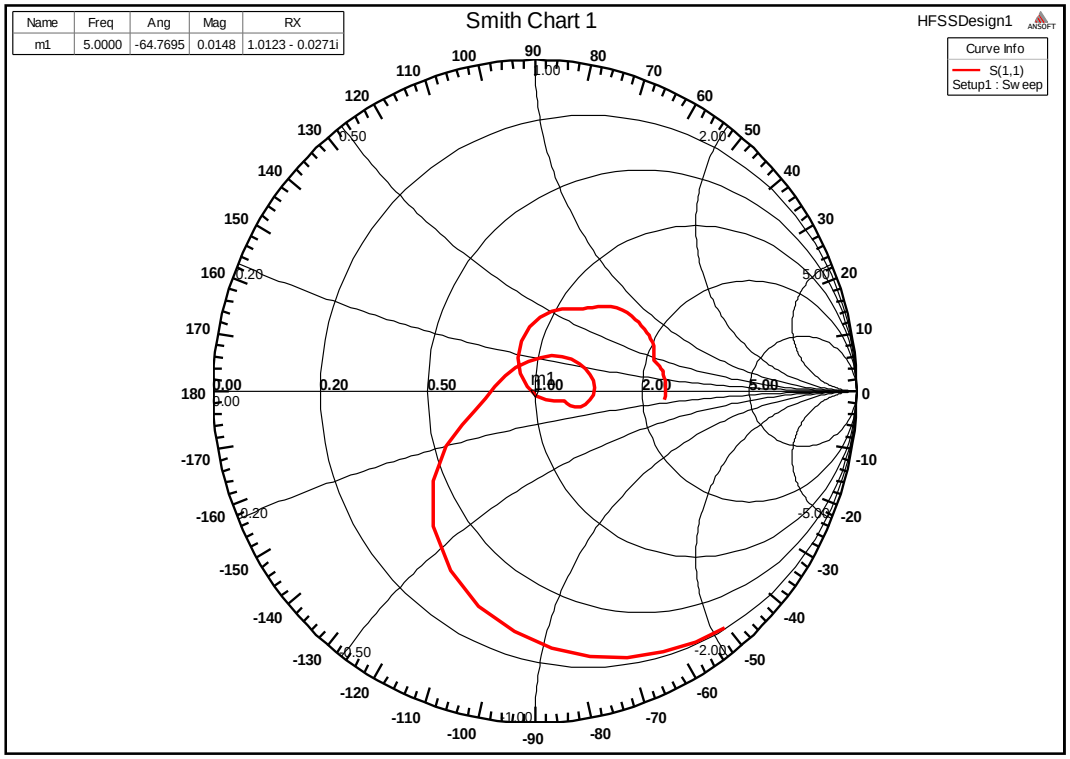

Figure 6.2: Smith Chart circular microstrip patch antenna impedance without RF-MEMS switch

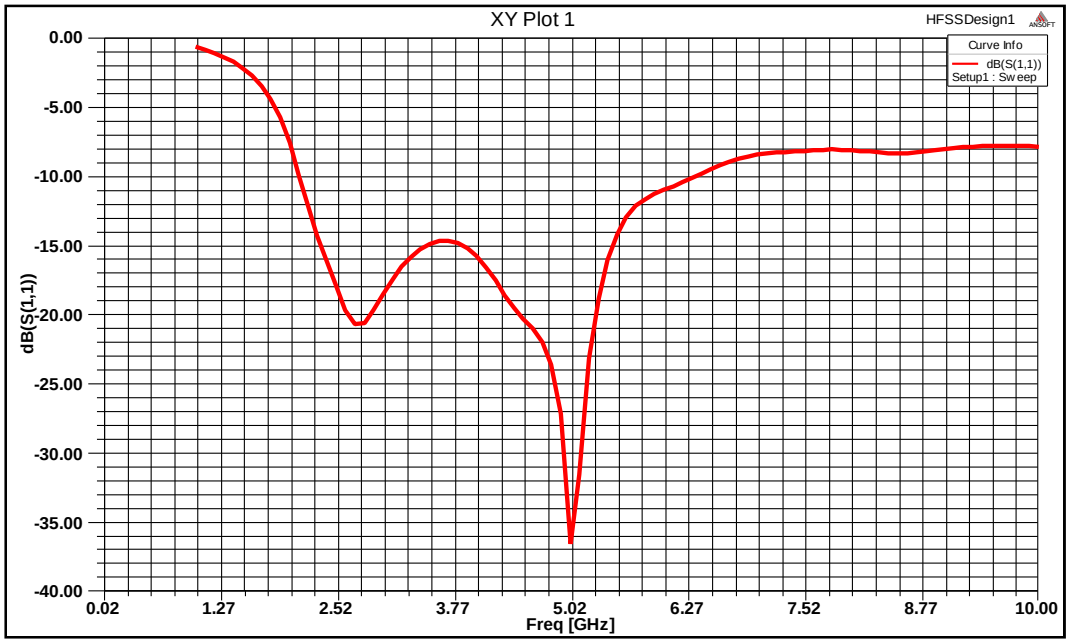

Figure 6.3: Return loss of circular microstrip patch antenna (without RF-MEMS switch).

Hence reflection losses are introduced in the transmission line with inadequate return loss of -7dB at resonant frequency 5 GHz as shown in fig. 6.4. This impedance mismatch can also be observed from Smith Chart where point m1 is moved away from Re[z] =1 circle as shown in fig. 6.5.

Impedance matching is introduced by using matching network with lumped elements (L & C), transmission line stubs, and quarter wave transformer (QWT). Various possible solutions are available for matching network circuit design, which are mainly affected by design complexity, antenna bandwidth, its implementation and adjustability [139]. The optimal design for matching network using lumped elements can be accomplished by using Smith Chart. Smith Chart allows easy calculation of a lumped element, which can be used to match the microstrip patch antenna with RF-MEMS switch perfectly. This impedance matching is a process of removing mismatch losses while introducing the RF-MEMS switch in microstrip patch antenna. So the reflection coefficient should be minimized to reduce the power reflected from the antenna, and to maximize the power delivered to the antenna. To achieve the perfect matching, the antenna impedance (Z_L) should be matched with characteristic impedance of CPW transmission line (z_0). In order to achieve the perfect matching ($Z_0 = Z_L$) by using lumped elements, the antenna impedance (Z_L) needs to move towards the center of the Smith Chart, where the reflection coefficient (τ) is zero. This antenna impedance (Z_L) can be moved towards center of the Smith Chart by using lumped element (L, C) in series or parallel configuration with CPW transmission line [140].

In order to avoid this impedance mismatch, a lumped matching network can be added between the microstrip patch antenna and CPW transmission line. This matching network can be accomplished by using Smith Chart, where the point m1 needs to move towards the centre of Re[z] =1 circle.

In case of high frequency band, the impedance matching network uses an inductor and capacitor either in series or parallel configuration with CPW transmission line [140]. This point m1 can be moved near to Re[z] =1 circle by adding an inductor of 1.62 nH in series configuration with CPW transmission line as shown in fig. 6.6.

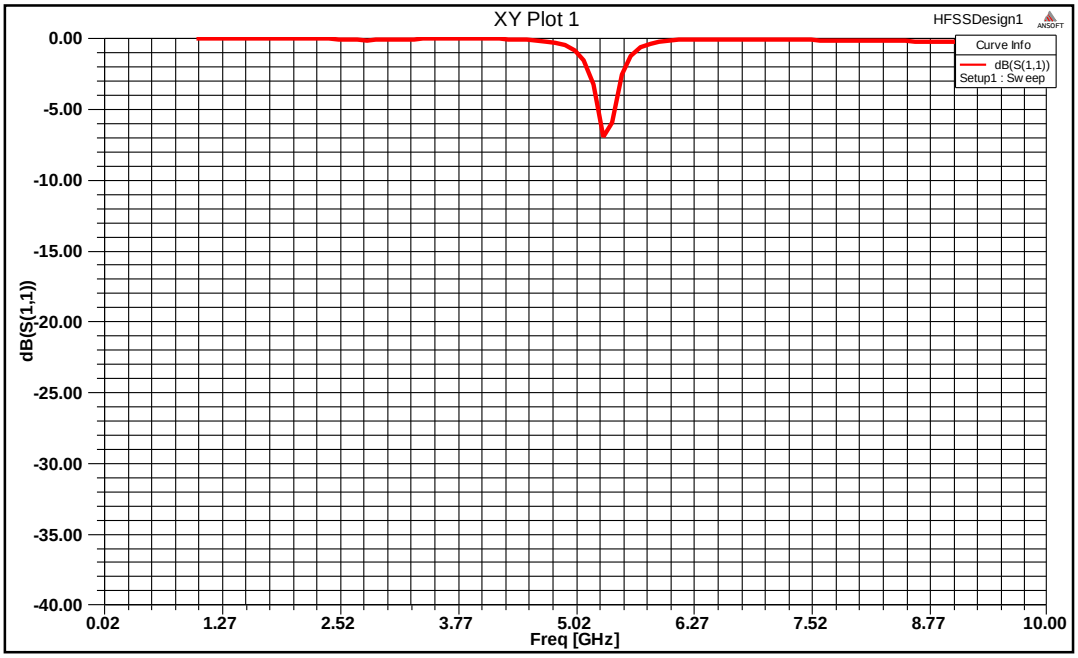

Figure 6.4: Return loss of circular microstrip patch antenna (with RF-MEMS switch).

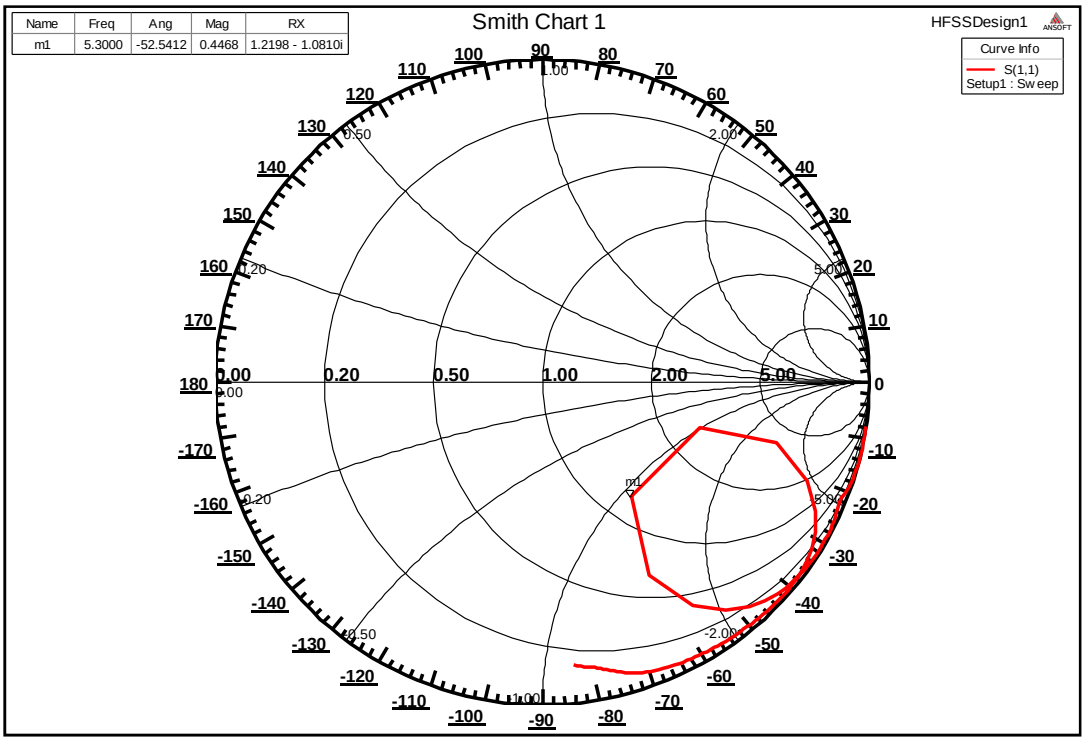

Figure 6.5: Circular microstrip patch antenna impedance with RF-MEMS switch on Smith Chart.

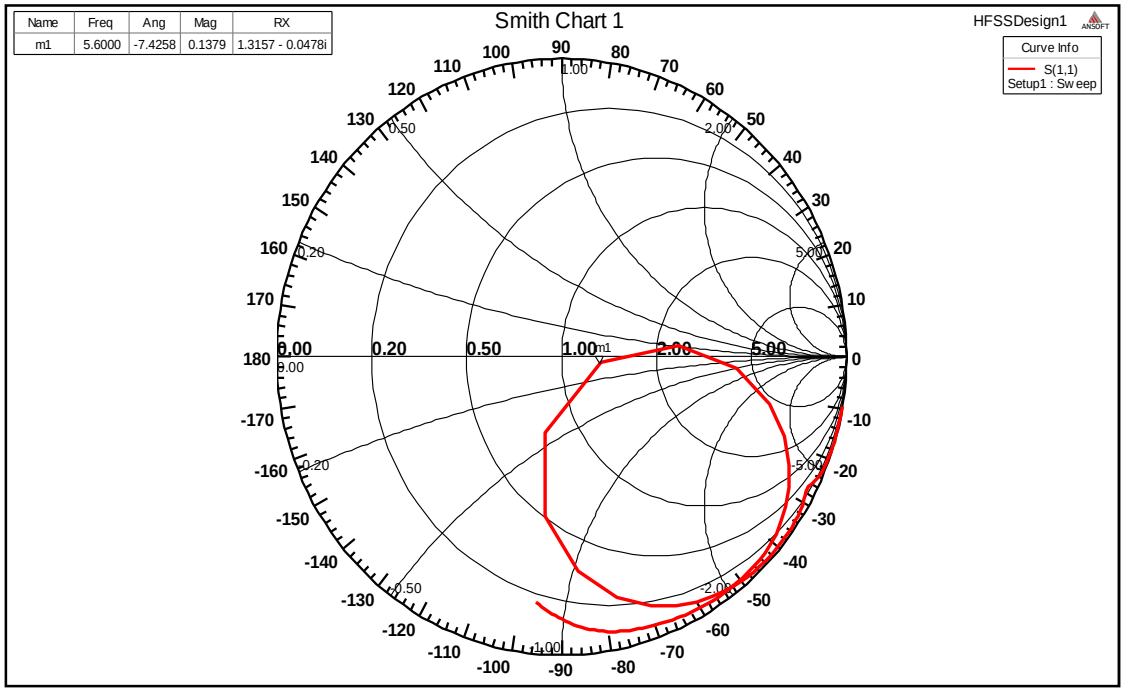

Figure 6.6: Circular microstrip patch antenna impedance with impedance matching network on Smith Chart.

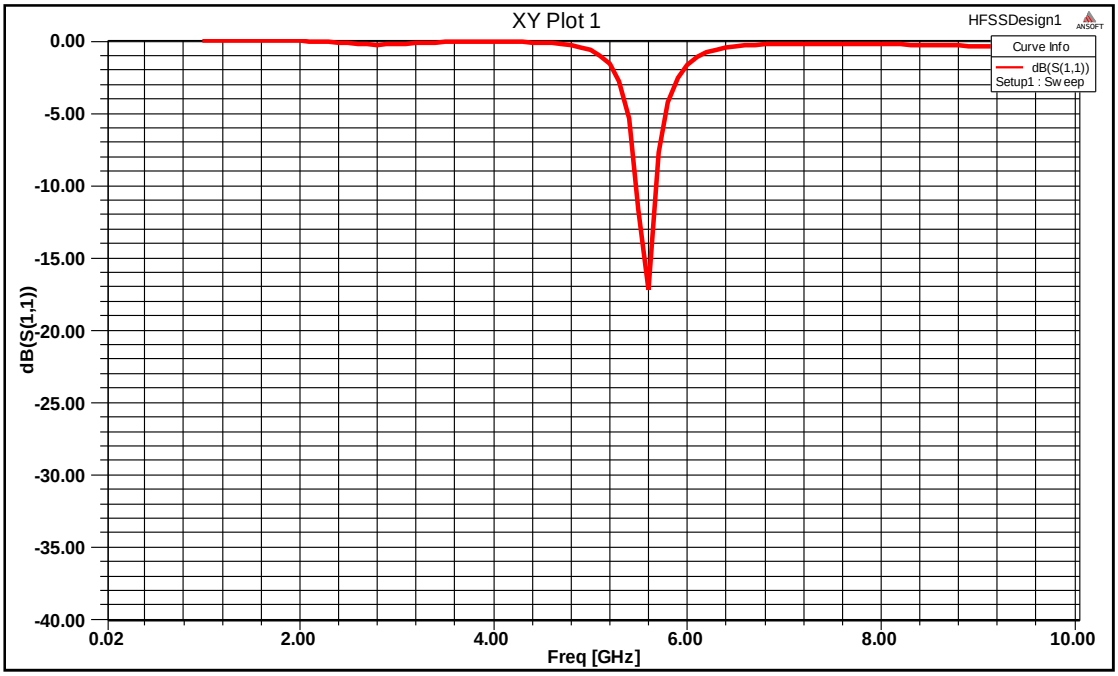

Figure 6.7: Return loss of circular microstrip patch antenna (with RF-MEMS switch) after adding inductor.

It is observed that an antenna with inductor (1.62 nH) in series configuration with CPW transmission line reduces the impedance mismatch, which reduces the return loss upto -18 dB at resonant frequency of 5.6 GHz as shown in figure 6.7. This frequency shift happens due the addition of RF-MEMS switch.

In this antenna design, the inductance effect is introduced by adjusting the gap between ground plane and central conductor plane [128]. This gap is adjusted from 0.33 to the 0.45 mm to avoid the mismatch losses between the CPW transmission line and microstrip patch.

6.3 RECONFIGURABLE ANTENNA DESIGN

Two circular patch antenna array with RF-MEMS switches are designed to achieve a reconfigurable antenna characteristics for the frequency band of 1 to 10 GHz. It consists of a pair of circular patch antenna with CPW on the same side of Si substrate. The total width (W_{tot}) and length (L_{tot}) of this antenna are 94 mm and 67 mm, respectively. Fig. 6.8 represents the schematic view of reconfigurable antenna with RF-MEMS switch, where the MEMS bridge, circular patch and ground plane dimensions are listed in table 6.1.

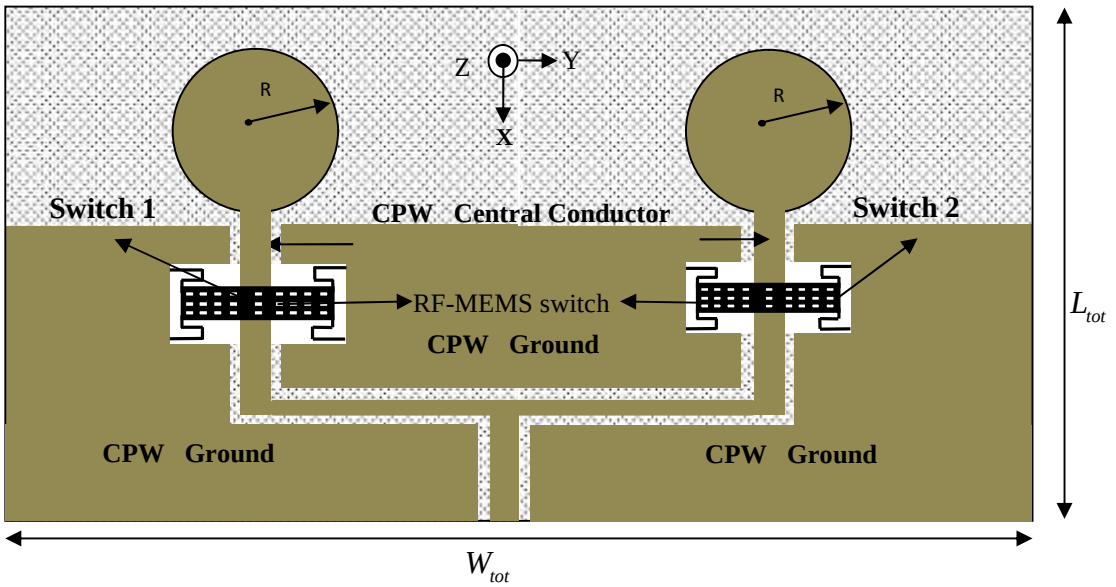

Figure 6.8: Schematic view of RF-MEMS switch based reconfigurable antenna.

A CPW feed line with central conductor width W = 4 mm and ground signal gap S= 0.45 mm is used, resulting in a characteristic impedance (Z_0) of 50 Ω as discussed in section 6.2. Two RF-MEMS switches are used to electrically connect and disconnect the two circular radiating patches. These switches are positioned at 6 mm from the circular patch along *x* axis. The bias lines are not required in CPW central conductor for MEMS switch actuation because of RF-MEMS switch topology [99].

6.3.1 RF-MEMS switch operation

RF-MEMS switches are most reliable for reconfigurable antenna design due to their excellent isolation, insertion loss and wide band response. The main issue with any switch integration in reconfigurable antenna design is with biasing the switches without altering the radiation characteristics. In order to avoid this issue, RF-MEMS switches can be used for switching operation because they do not require DC bias lines for actuation. This technique requires a DC short between the central conductor and ground plane of CPW [18].

The actuation DC voltage can be applied directly to the central conductor of CPW. When a DC bias (actuation voltage) is applied, an electrostatic force pulls down the MEMS switch and since these are capacitive contact, they create a RF and DC short between central conductor and ground plane of CPW. When no DC bias is applied, the MEMS switches are in up-state and the antenna gets the RF signal to radiate and the antenna exhibit different radiation behavior as compared to previous condition. Since there is a DC short with RF signal through MEMS switch, no extra metal lines are required to apply actuation voltage. A thin layer of silicon nitride is used to provide isolation between switch membrane and CPW central conductor and it avoid stiction failures due to dielectric charging.

In the proposed reconfigurable antenna design two RF-MEMS switches are actuated alternatively to examine the reconfigurabilty of the antenna.

6.3.2 Operational principal of Reconfigurable antenna

The reconfigurability of antenna relies on the concept of adding or removing a resonating structure. Here, the reconfigurability is achieved through the RF-MEMS switches. The RF-MEMS switch activate or deactivate the circular microstrip patches when a DC bias is applied.

For two circular microstrip patch element based antenna, the frequency band is selected or removed based on whether the RF-MEMS switches are in up-state (open), or in down-state (short) with the CPW central conductor. The proposed reconfigurable antenna is simulated for four different cases:

(i) Switch 1 in up-state (OFF) and switch 2 in up-state (OFF)

(ii) Switch 1 in down-state (ON) and switch 2 in up-state (OFF)

(iii) Switch 1 in up-state (OFF) and switch 2 in down-state (ON)

(iv) Switch 1 in down-state (ON) and switch 2 in down-state (ON)

6.4 SIMULATION AND ANALYSIS

The analysis of reconfigurable antenna using RF-MEMS switch is done using the simulation performed on Ansys HFSS electromagnetic simulator for the frequency range of 1 to 10 GHz. The reconfigurability of the antenna is analyzed for L to S band (2 to 4 GHz) in terms of return loss, VSWR, gain and radiation pattern.

6.4.1 Return loss

Fig. 6.9 shows the return loss (S_{11}) for proposed reconfigurable antenna for frequency ranging from 1 to 10 GHz. In this, both the RF-MEMS switches are taken in up-state without applying actuation voltage. So the RF power gets transmitted through the radiating patches. This plot illustrates that this antenna provide the resonance at seven resonant frequencies with >-10 dB for the frequency range of 1 to 10 GHz.

Fig. 6.10 shows the simulated return loss when an actuation voltage is applied at first switch. It shows that the antenna in this situation radiates at eight resonant frequencies. This antenna radiate with two extra resonant frequencies at 2.1 GHz and 3.4 GHz.

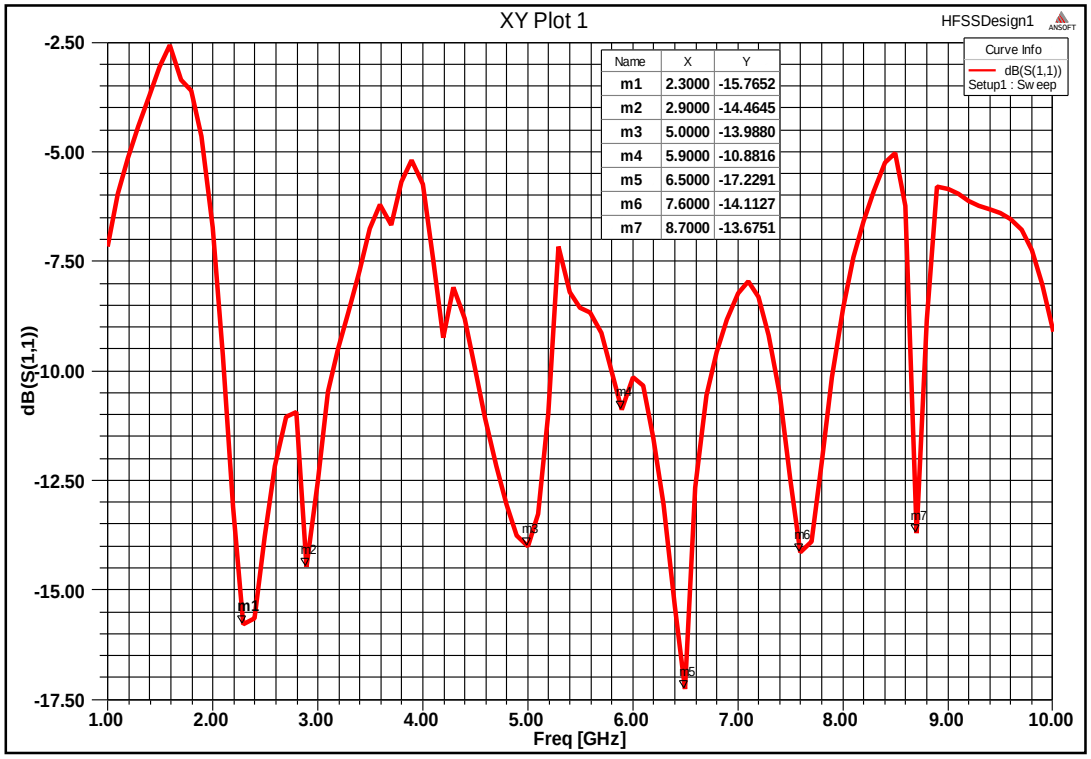

Figure 6.9: Return loss for RF-MEMS switch based two element circular microstrip patch antenna, when both switches are in up-state.

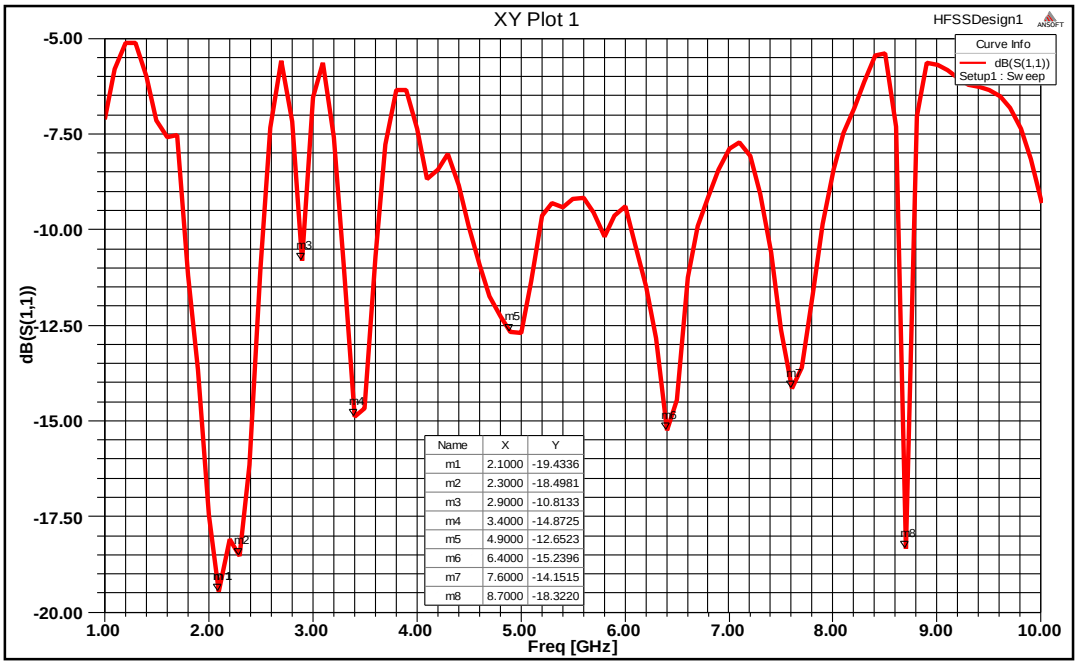

Figure 6.10: Return loss for RF-MEMS switch based two element circular microstrip patch antenna, when first switch is in down-state.

When an actuation voltage is applied at second switch, the simulated return losses are shown in fig. 6.11. It shows that this antenna radiate at seven resonant frequencies except 2.1 GHz. So from this graph it can be concluded that this antenna do not radiate at 2.1 GHz by actuating second RF-MEMS switch.

When both the switches are in down-state, the return loss is plotted in fig. 6.12. This plot illustrate that 2.1GHz to 2.9 GHz frequency band is removed by switching both the RF-MEMS switches.

6.4.2 VSWR

The simulated VSWR curve for the proposed reconfigurable antenna is shown in fig. 6.13 for four different cases. It shows that all resonant frequencies for different MEMS switch states shows a VSWR <2. It implies that this antenna is matched with CPW transmission line and these VSWR are acceptable for reconfigurable antenna design [138].

6.4.3 Gain

The gain simulation plots are taken in the directivity in *z* axis direction of the RF-MEMS switch as it is shown in fig. 6.8. These gain plots are given in fig. 6.14 to 6.17 for different switch positions. As it can be seen, that the down-state of RF-MEMS switches cause a significant degradation on the antenna gain. The antenna gain is reduced by over 2 dB at all resonating frequencies either first switch or second switch is in down-state.

When both switches are in up-state it shows the gain of 1dB to 5dB for 2 GHz to 3.8 GHz frequency band. However in down-state position of either first or second switch, antenna shows lower gain of 2.5 dB gain for 3 GHz to 3.8 GHz frequency band. It is observed that antenna is reconfigurable for 2 GHz to 3.8 GHz band at 2.3 & 2.9 GHz when switches are in up-state and 3 GHz to 3.8 GHz band at 3.4 GHz when either first or second switch is in down-state position as shown in fig. 6.14 to 6.16.

When both the switches are in down-state it shows that the gain of 2.5 dB to frequency band 3.2 to 3.6 GHz, as compared when both switches are in up-state as shown in fig. 6.20.

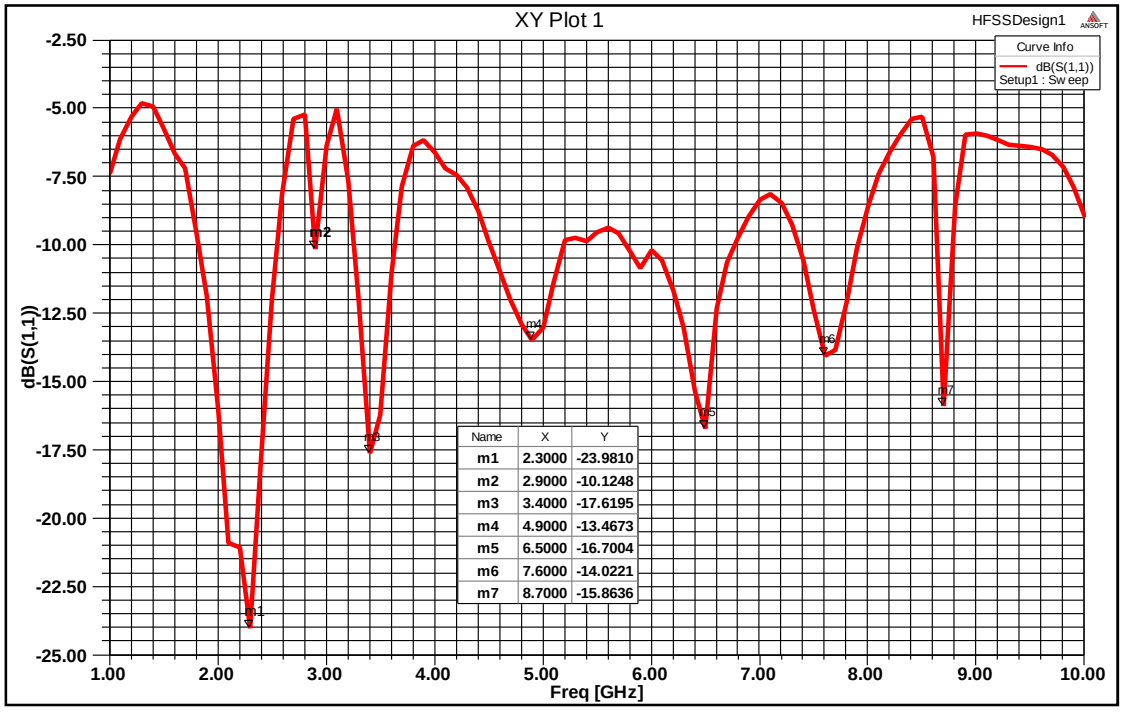

Figure 6.11: Return loss for RF-MEMS switch based two element circular microstrip patch antenna, when second switch is in down-state.

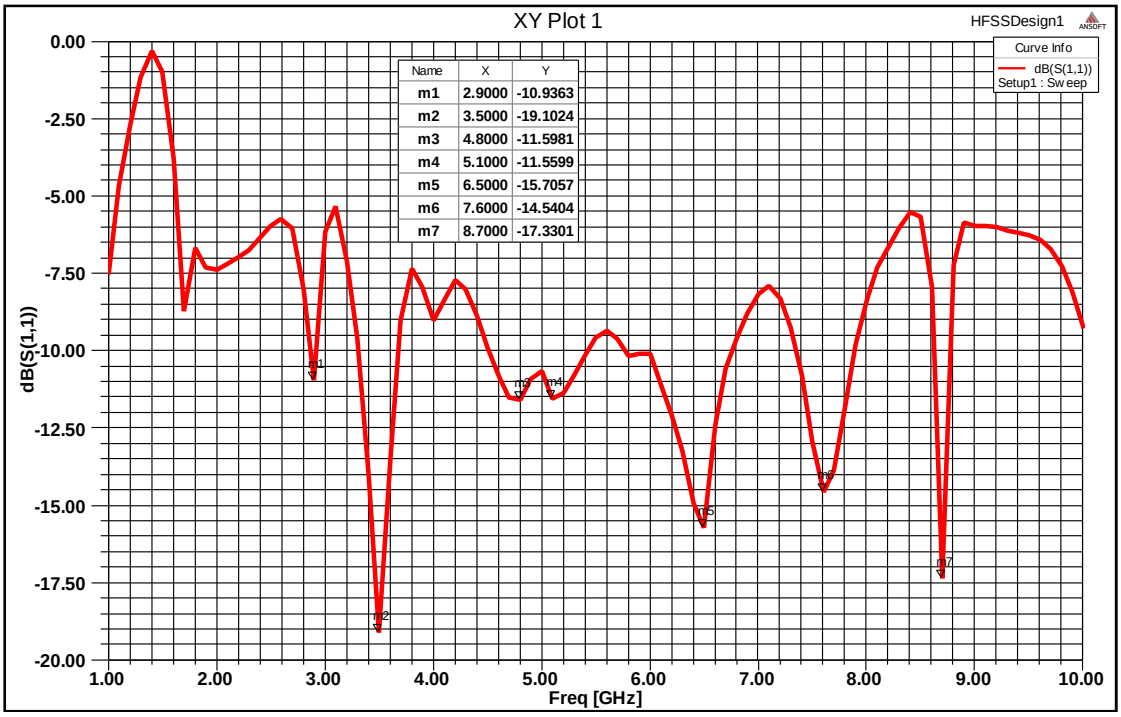

Figure 6.12: Return loss for RF-MEMS switch based two element circular microstrip patch antenna, when both the switch are in down-state.

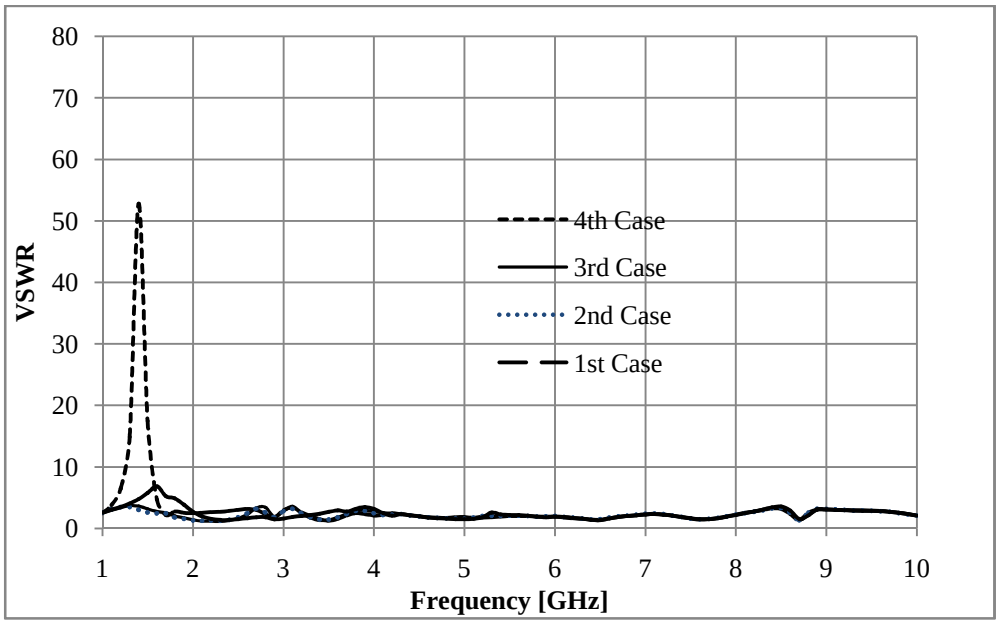

Figure 6.13: VSWR for RF-MEMS switch based two element circular microstrip patch antenna for four different cases.

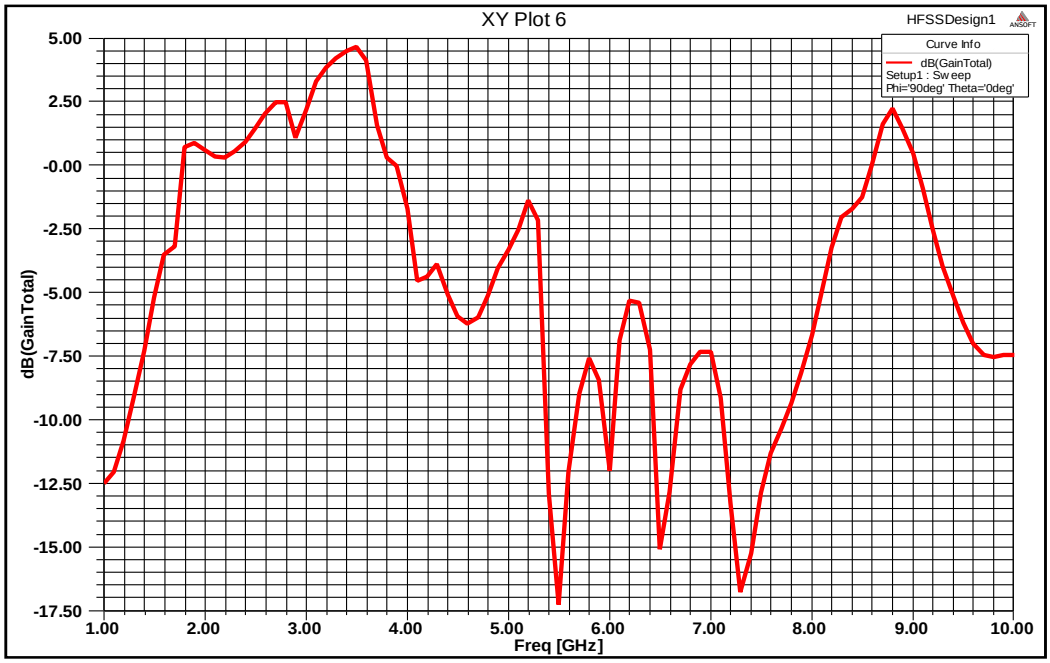

Figure 6.14: Gain plot for RF-MEMS switch based two element circular microstrip patch antenna, when both switches are in up-state.

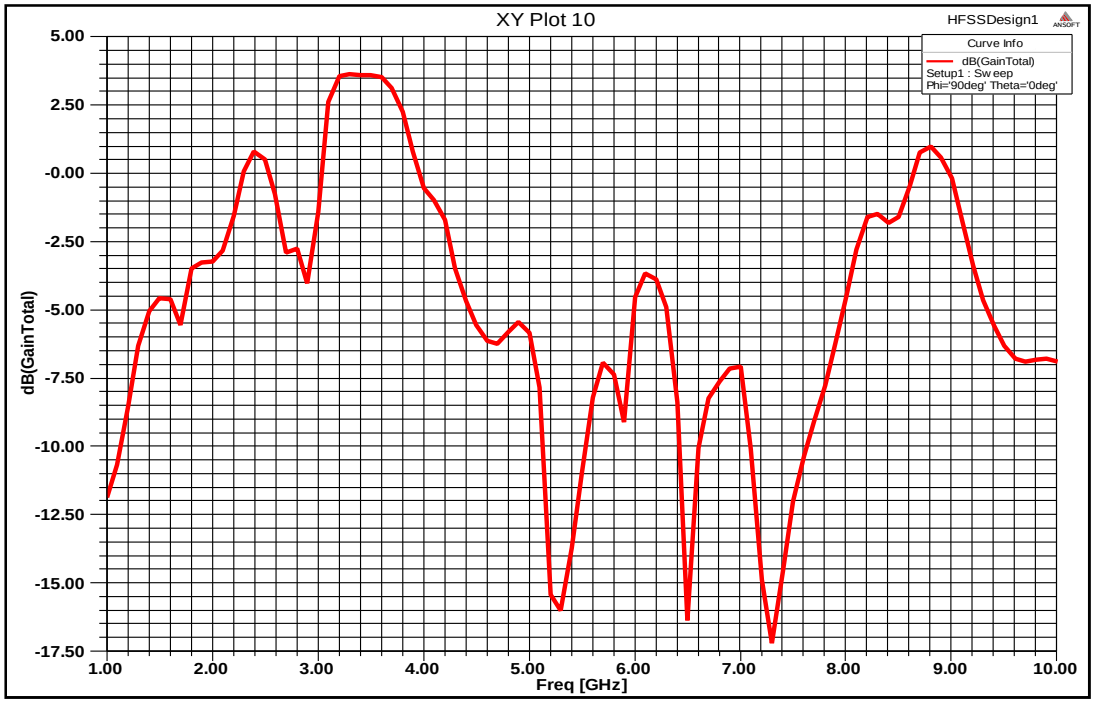

Figure 6.15: Gain plot for RF-MEMS switch based two element circular microstrip patch antenna, when first switch is actuated.

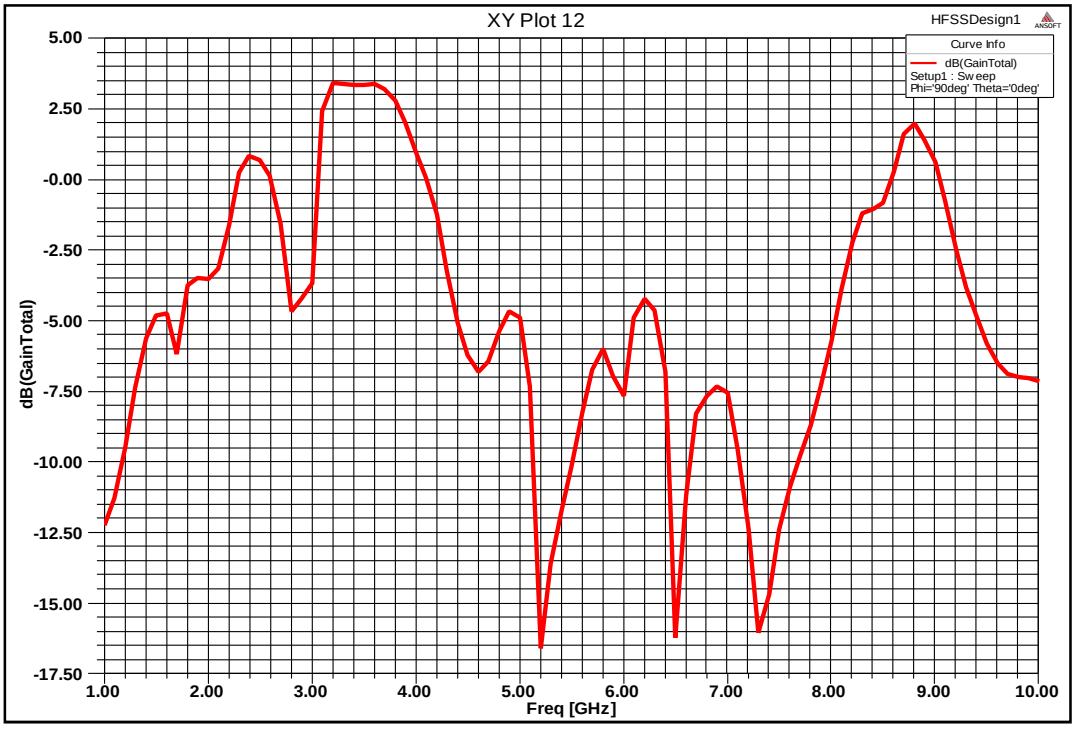

Figure 6.16: Gain plot for RF-MEMS switch based two element circular microstrip patch antenna,when second switch is actuated.

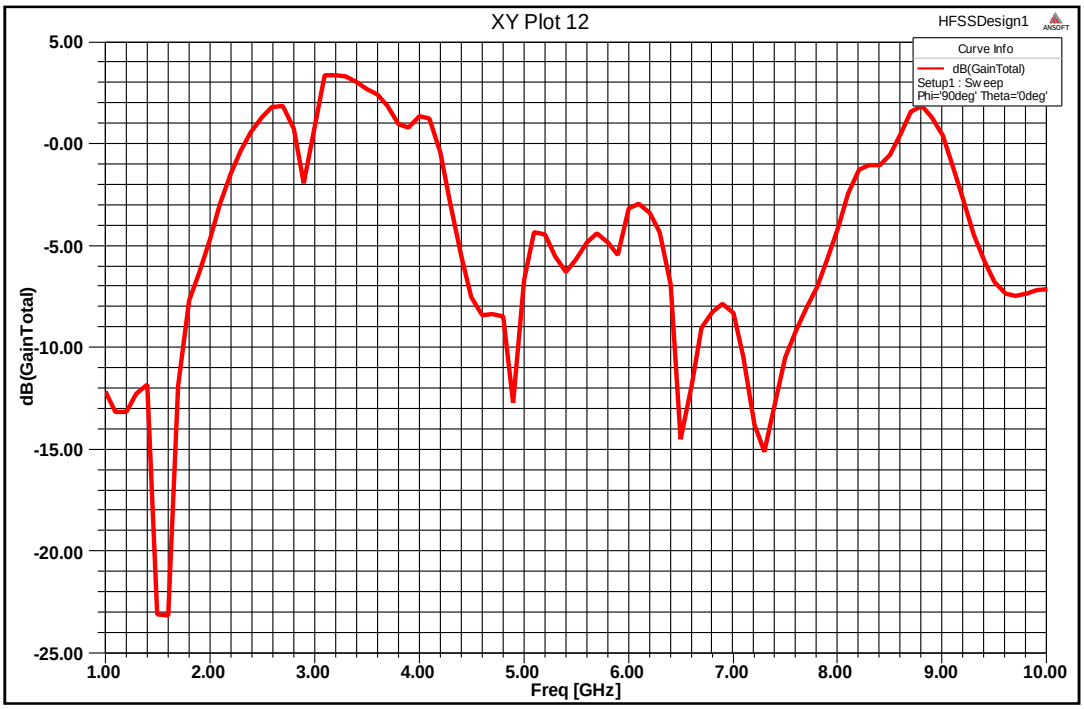

Figure 6.17: Gain plot for RF-MEMS switch based two element circular microstrip patch antenna, when both the switches are actuated.

From this figure it can be concluded that this antenna can be made reconfigurable from 3.2 to 3.6 GHz band at 3.4 GHz when both switches are in down-state.

From these gain plots it is observed that this antenna is frequency reconfigurable at 2.3 GHz, 2.9 GHz and 3.4 GHz.

6.4.4 Radiation Pattern

The E-plane (*x*-*y*) radiation patterns are simulated (φ=90) for different switch positions and are shown in fig. 6.18 to 6.24. Fig. 6.18 and 6.19 shows the radiation pattern at 2.3 GHz and 2.9 GHz.

When first switch is actuated, this antenna shows a different radiation pattern at 2.3 GHz as shown in fig. 6.20. It shows that radiation pattern can be reconfigured slightly to the left side by switching the first RF-MEMS switch.

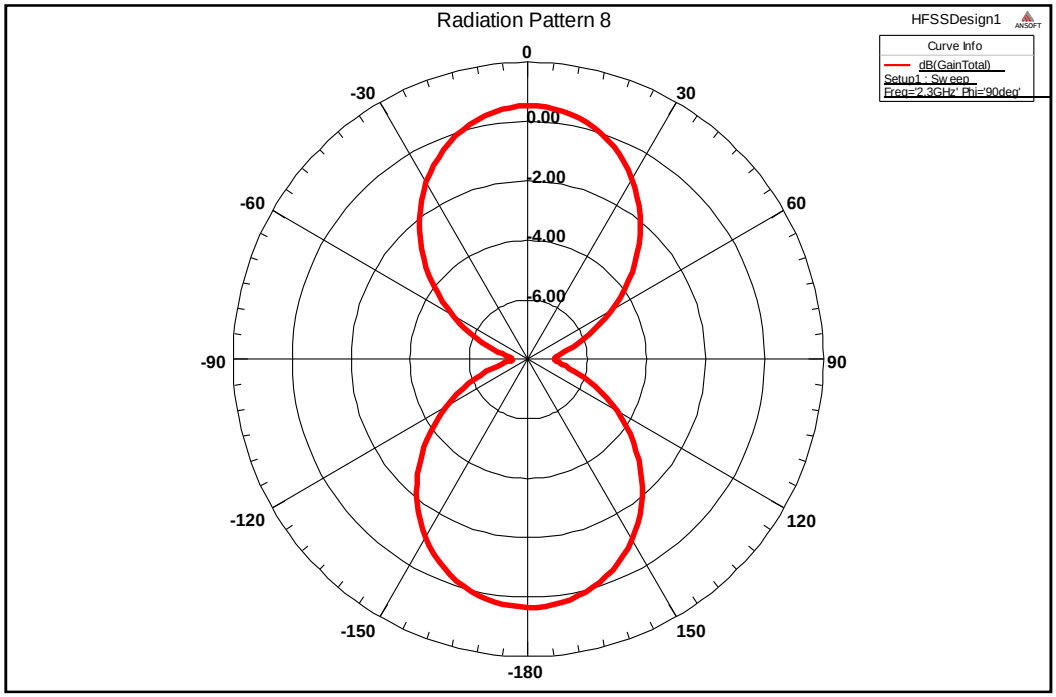

Figure 6.18: 2-D E-plane radiation pattern at 2.3 GHz of RF-MEMS switch based two element circular microstrip patch antenna, when both switches are in up-state.

When second switch is actuated the radiation pattern shifts towards the right hand side at 2.3 GHz as shown in fig. 6.21. It is observed that left and right pattern reconfigurability can be obtained at 2.3 GHz by actuating either first or second switch.

Fig. 6.22 shows the antenna radiation pattern at 3.4 GHz when first switch is actuated. This radiation pattern gets changed at 3.4 GHz when second switch is in down-state as shown in fig. 6.23. Fig. 6.24 shows that when both the switches are in down-state, this antenna radiates with different radiation pattern at 3.4 GHz as compared to fig. 6.23.

From these plots it is observed that the radiation pattern at 2.3 GHz get significantly changed in left side or in right side after actuating the first or second switch. On the other hand it shows the pattern reconfigurability at 3.4 GHz when first switch or second switch are actuated.

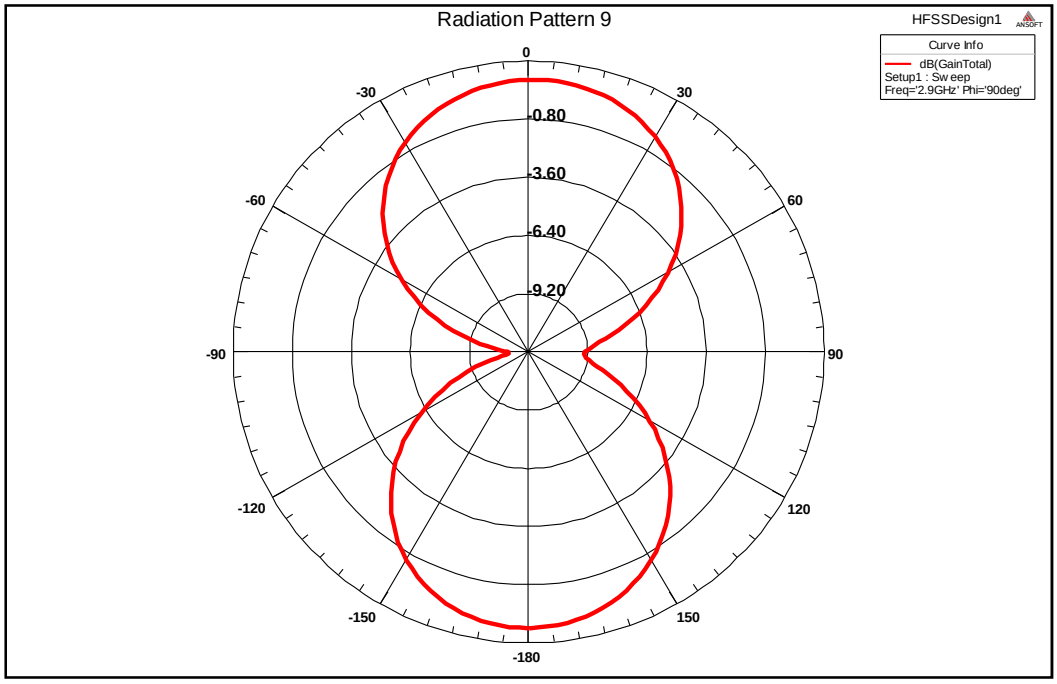

Figure 6.19: 2-D E-plane radiation pattern at 2.9 GHz of RF-MEMS switch based two element circular microstrip patch antenna, when both switches are in up-state.

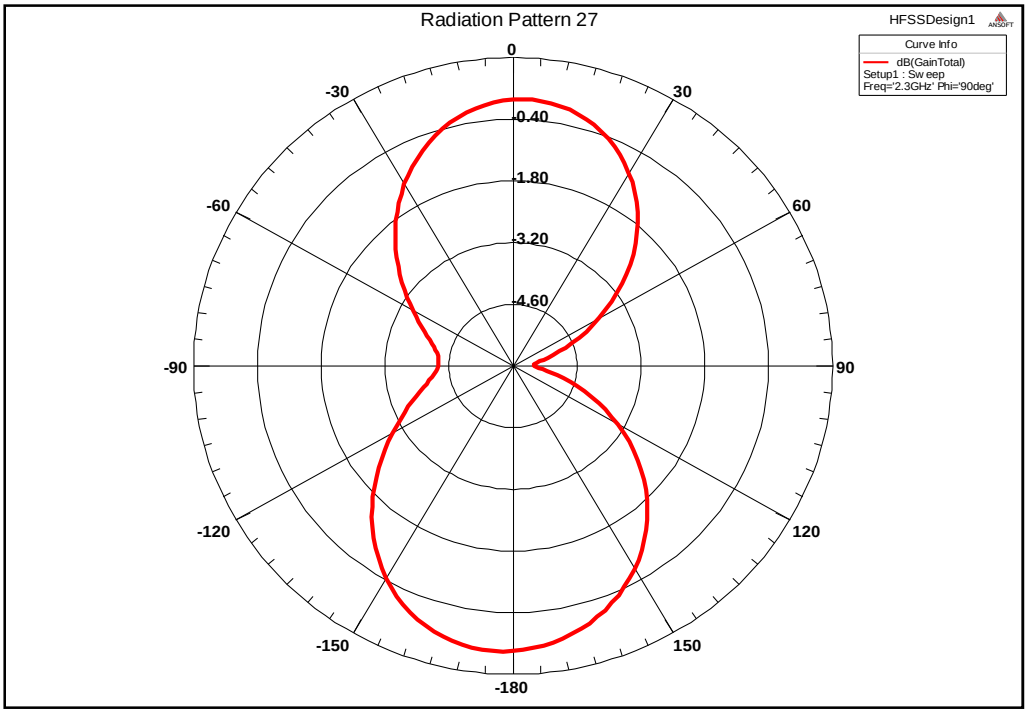

Figure 6.20: 2-D E-Plane radiation plot at 2.3 GHz for RF-MEMS switch based two element circular microstrip patch antenna, when first switch is actuated.

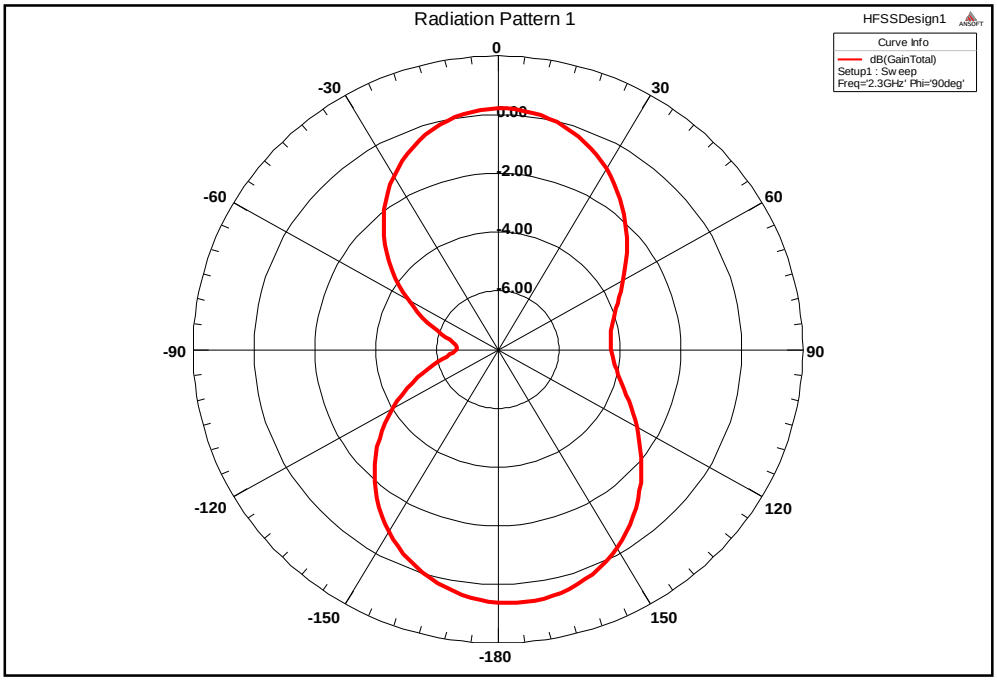

Figure 6.21: 2-D E-Plane radiation plot at 2.3 GHz for RF-MEMS switch based two element circular microstrip patch antenna, when second switch is actuated.

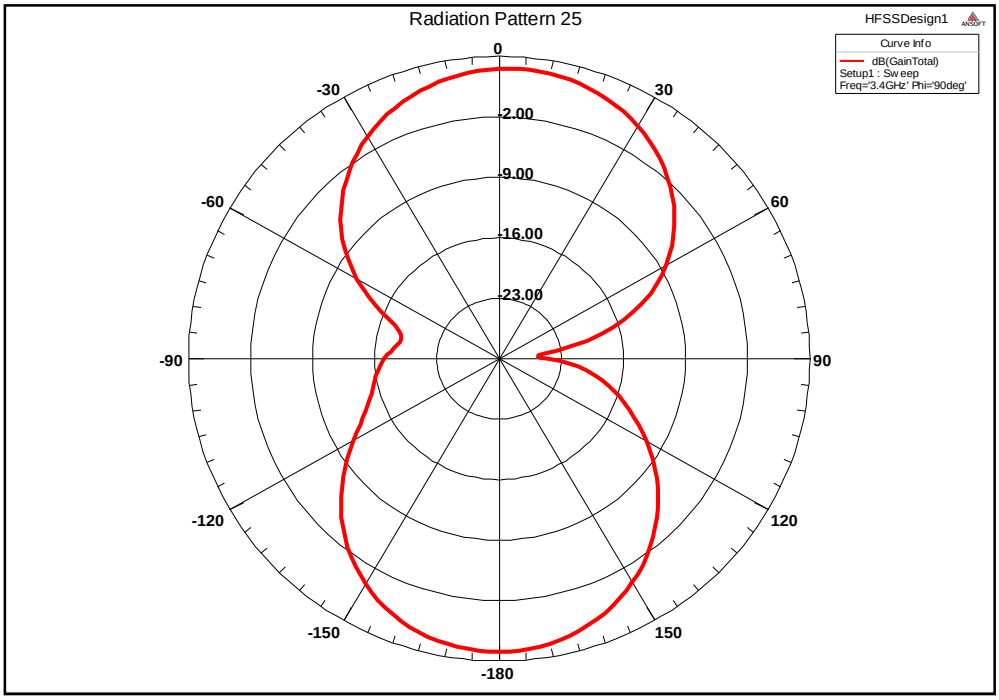

Figure 6.22: 2-D E-Plane radiation plot at 3.4 GHz for RF-MEMS switch based two element circular microstrip patch antenna, when first switch is actuated.

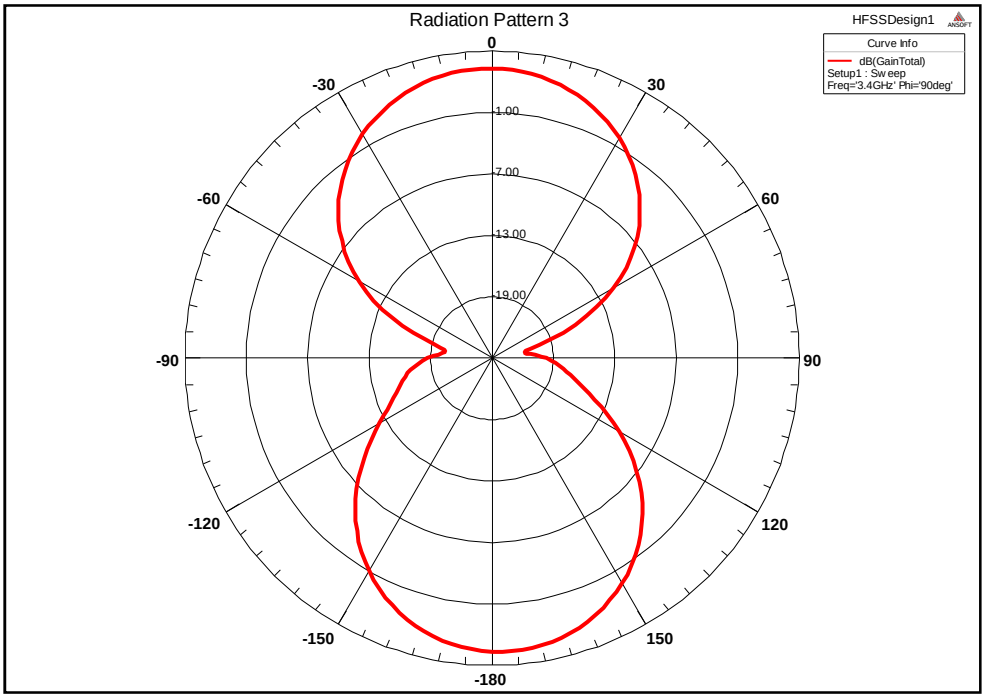

Figure 6.23: 2-D E-Plane radiation plot at 3.4 GHz for RF-MEMS switch based two element circular microstrip patch antenna, when second switch is actuated.

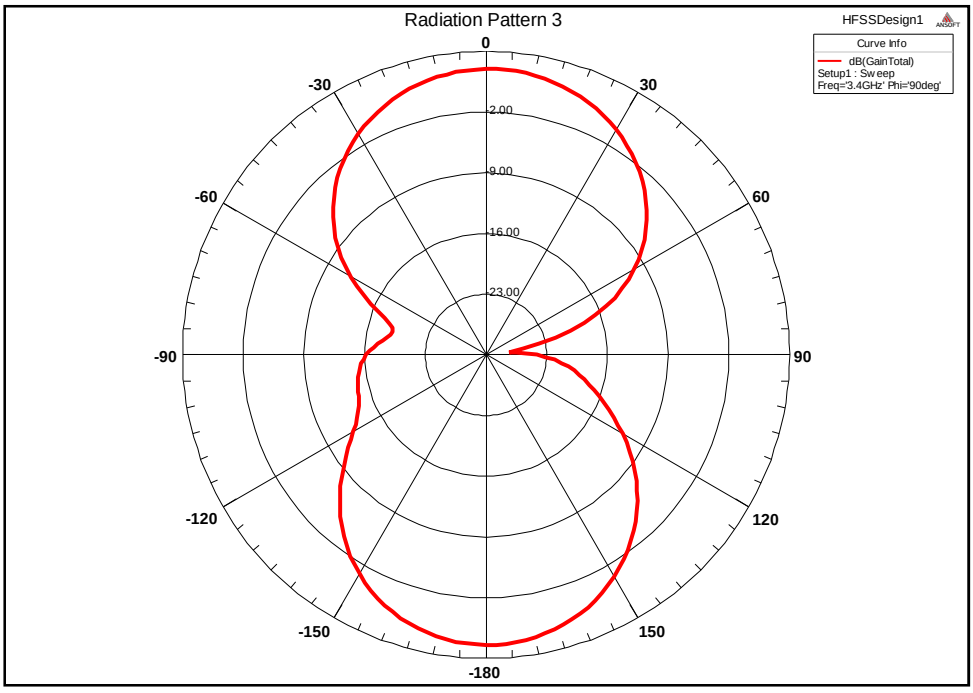

Figure 6.24: 2-D E-Plane radiation plot at 3.4 GHz for RF-MEMS switch based two element circular microstrip patch antenna, when both switches are actuated.

6.5 CONCLUSION

The use of circular microstrip resonating elements integrated with RF-MEMS switches were implemented for reconfigurable microstrip antenna for the frequency band ranging from 1 to 10 GHz. It is observed that a series inductor can be used as lumped matching network to minimize impedance mismatch between microstrip circular patch antenna and CPW transmission line. This reconfigurable antenna shows pattern reconfigurability at 2.3 GHz and 3.4 GHz, when both the switches are actuated and when either first or second switch is actuated. It shows a frequency reconfigurabilty at 2.3 GHz, 2.9 GHz and 3.4 GHz when either first or second switch is actuated.

CONCLUSION

In the demanding world of modern communication systems reconfigurable antenna plays an important role for higher frequency applications. Pattern and frequency reconfigurable antennas are most complex electromagnetic structures and their radiation characteristics depend on the relationship between their structure size and the operating frequency. Thus, in order to increase the design flexibility and broaden the antenna application areas, RF-MEMS switches are the highly demanding switching element. They offer superior RF performance (isolation and insertion loss) hence they can be integrated within the antenna structure. Additionally, capacitive RF-MEMS switches can be controlled without using high resistance bias lines, which imply that RF-MEMS switches can be used extensively in reconfigurable antenna design without interfering and degrading the antenna radiation properties.

The RF-MEMS switches also consume less actuation voltage and this is an important requirement for large antenna arrays especially for mobile or satellite implementations. Their small size and their ability to get integrated monolithically with the antennas elements on substrate, make the RF-MEMS switches the best solution for millimeter to microwave reconfigurable antennas structures. However on the other hand RF-MEMS switches suffer from high actuation voltage requirements, low RF power handling capability and low RF characteristics.

Thus the main goal of the present work, has been to explore the design feasibility of low actuation RF-MEMS switches with better RF power handling capabilities and RF characteristics. In most of the cases RF-MEMS switches have been designed with higher

actuation voltage because of its low switching time, which results in higher switching speed. However, in many wireless communication applications, high performance - low power consumption switching systems are preferred, with better RF power handling capabilities, where switching time of 0.5-10 milliseconds is adequate.

In the view of above, present work is focused on RF-MEMS switch design by optimizing material choice for the switch beam material and the spring constant of serpentine flexure structure to achieve low actuation voltage and better RF power handling capability with adequate switching speed.

In addition, material selection for RF-MEMS capacitive shunt switch with the help of Ashby's approach has been discussed in this thesis. Three performance indices based on different material indices to enhance the performance of the MEMS Bridge were optimized. Based on material selection charts, it is observed that gold and aluminum are the appropriate materials to be used as bridge material in RF-MEMS switch to obtain the desire properties to give the best performance of the switch in reconfigurable antenna. As gold is very expensive material as compared to aluminum, so if we have to go for mass production of switch, we propose aluminum as the best material to be used as bridge material for RF-MEMS switch.

In order to achieve low actuation voltage, a low spring constant based flexure support has been investigated. Therefore a non-uniform serpentine meander based flexure design has been proposed in this thesis. An analytical expression of spring constant for non-uniform serpentine flexure is calculated through electromechanical modeling. This analytically calculated spring constant is verified by finite element method (FEM) simulation tool COMSOL Multiphysics. It is observed that the proposed flexure design achieved a spring constant of 0.6–0.04 N/m with span beam length of 100 μm to180μm for single meander based flexure design. This analytically calculated spring constant is 10–30 % higher than the simulated values. This spring constant analysis is used to achieve low actuation voltage of 15-3 V with better RF power handling capabilities of 4.29 to 0.2 W for span beam length varying from 100 to 280μm. In this the proposed RF-MEMS switch is designed with single meander section using a non-uniform

serpentine flexure with 180 μm span beam length, offers an actuation voltage of 6.3 V, RF power handling capability of 0.6 W with adequate switching time of 3.5 millisecond.

The electromagnetic behavior of this switch has been discussed in terms of electrical (CLR) model. The non-uniform serpentine flexure based RF-MEMS switch is implemented in CPW configuration through ANSYS HFSS electromagnetic simulator. The detailed discussion of the electrical model parameters (CLR) extraction through S-parameter measurement provides the RF performance of the proposed switch design. The proposed switch designs shows with better RF response in terms of return loss of << -20 dB up to 25 GHz and isolation of >>25 dB from 15 to 35 GHz.

This proposed switch design is used to implement a pattern and frequency reconfigurable microstrip patch antenna as a case study of RF-MEMS switch application. This reconfigurable antenna design shows the pattern reconfigurability at 2.3 GHz and 3.4 GHz with frequency reconfigurability for 2.3 GHz, 2.9 GHz and at 3.4 GHz.

FUTURE SCOPE OF WORK

The proposed non-uniform serpentine flexure based RF-MEMS switch design needs further study in terms of switch lifetime and temperature sensitivity. Non-uniform serpentine flexure spring constant needs further optimization to balance the switching time in order to improve the switching speed for RF applications. The integration of RF-MEMS switches with microstrip patch antenna needs further investigation of DC isolation circuits to avoid the DC to the patch antenna. The proposed reconfigurable antenna design demands more improvements for pattern and frequency reconfigurability. This switch design needs to be fabricated with microstrip patch antenna design to analyze the exact performance of the reconfigurable antenna. This can be accomplished in two ways, first by integrating the RF-MEMS switches on PCB substrate, second by monolithically fabricating RF-MEMS switch with the antenna patches in single manufacturing process.

With current technology it is possible to fabricate the RF-MEMS switch with antenna patches monolithically. The topics of future work related to the designing to the reconfigurable antenna are listed below.

1. The study of DC isolation circuits for reconfigurable antennas.
2. Reconfigurable antenna design optimization for better performance.
3. Fabrication of the reconfigurable antenna.
4. Measurements of electromechanical properties of RF-MEMS switch such as actuation voltage, RF power handling capability and switching time.

5. Measurements of electromagnetic properties of RF-MEMS switch.
6. Measurements of reconfigurable antenna properties such as radiation pattern, gain, return loss and VSWR.

REFERENCES

[1]. G. M. Rebeiz. "RF MEMS: Theory, Design, and Technology", 3rd ed. John Wiley & Sons, Inc., Hoboken, New Jersey 2003, 2-10.

[2]. L. E. Larson, R. H. Hackett, M. A. Melendes, R. F. Lohr. " Micromachined microwave actuator (MIMAC) technology - a new tuning approach for microwave integrated circuits" in Microwave and Millimeter-Wave Monolithic Circuits Symposium Digest, Boston, MA. June 1991, pp. 27-30.

[3]. J. J. Yao, M. F. Chang. "A surface micromachined miniature switch for telecommunications applications with signal frequencies from DC to 4 GHz" in International Conference on Solid State Sensors and Actuators Digest, Stockholm, Sweden. June, 1995, pp. 384-387.

[4]. J. Bouchaud, B. Knoblich. "RF MEMS Switches Deliver on Early Promise" *Sensors & Transducers Journal*. vol. 86, 2007, pp.1802-1808l.

[5]. G. M. Rebeiz, K. Entesari , I. Reines, S. J. Park, M. Eltanani, A. Grichener, A. Brown. "Tuning in to RF MEMS" *IEEE microwave magazine*. 2009, vol.10, pp.55-72.

[6]. L. Dussopt G. M. Rebeiz. "Intermodulation distortion and power handling in RF MEMS switches, varactors and tunable filters" *IEEE Transaction on Microwave Theory and Techniques*. vol. 51, 2003, pp.1247-1256.

[7]. K. V. Caekenberghe. "RF MEMS on the radar" *IEEE Microwave magazine*, vol. 10, 2009, pp.99-116.

[8]. J.J. Yao. "Topical review - RF MEMS from a device perspective, *Journal of Micromechanics and Microengineering*", vol. 10, 2000, pp. 9-38.

[9]. C. Goldsmith, T. H. Lin, B. Powers, W. R. Wu, B. Norvell. "Micromechanical membrane switches for microwave applications", IEEE Microwave Theory and Techniques Symposium, vol.1, 1995, pp.91-94.

[10]. C. Goldsmith, J. Randall, S. Eshelman, T. H. Lin, D. Denniston, S. Clhen, B. Norvell. "Characteristics of micromachined switches at microwave Frequencies", IEEE Microwave Theory and Techniques Symposium, vol. 2, 1996, pp. 1141-1144.

[11]. C. Goldsmith, Z. Yao, S. Eshelman, D. Denniston. "Performance of low-loss RF MEMS capacitive switches", *IEEE Microwave Guided Wave Letters*, vol. 8, 1998, pp. 269-271.

[12]. G. L. Tan, G.M. Rebeiz. "DC-26 GHz MEMS series-shunt absorptive switches," IEEE Microwave Theory and Techniques Symposium, vol. 1, 2001, pp.325-328.

[13]. E. R. Brown. "RF-MEMS switches for reconfigurable integrated circuits" *IEEE Transaction on Microwave Theory and Techniques*. vol. 46, 1998, pp.1868–1880.

[14]. D. Peroulis, K. Sarabandi, L.P.B. Katchi. "Design of reconfigurable slot antenna", *IEEE Transaction on Antennas and Propagation*. vol.53, 2005, pp. 645-654.

[15]. B. A. Cetiner, H. Jafarkhani, J. Y. Qian, H. J. Yoo, A. Grau, F. D. Flaviis. "Multifunctional reconfigurable MEMS integrated antennas for adaptive MIMO systems" *IEEE Communications Magazine*. vol. 42, 2004, pp. 62-70.

[16]. A. Grau, H. Jafarkhani, F. D. Flaviis. "A reconfigurable multiple-Input multiple-output communication system", *IEEE Transaction on Wireless Communication*,vol. 7, 2007, pp.1719- 1733.

[17]. C.W. Jung, M. J. Lee, F. D. Flaviis. "Reconfigurable dual-band antenna with high frequency ratio (1.6:1) using MEMS switches", *Electronics Letter*, vol.44, 2008, pp.76-77.

[18]. D. E. Anagnostou, G. Chryssomallis, M. T. Zheng, J. C. Lyke, G. E. Ponchak, J. Papapolymerou, C. G. Christodoulou. "Design, fabrication, and measurements of an RF-MEMS based self-similar reconfigurable antenna", *IEEE Transaction on Antennas and Propagation*, vol. 54, 2006, pp.422-432.

[19]. K. J. Vinoy, H. Yoon, J. Taeksoo, V. K. Varadan. "RF MEMS and Reconfigurable Antennas for Communication Systems, MEMS Components and Applications for Industry", Automobiles, Aerospace, and Communication II, Proceedings of SPIE, vol. 4981, 2003, pp.164-175.

[20]. M. A. Saed. "Reconfigurable Broadband Microstrip Antenna Fed by a Coplanar Waveguide", *Progress in Electromagnetics Research, (PIER)*. vol. 55, 2005, pp. 227-239.

[21]. B. A. Cetiner, J. Y. Qian, S. Liu, L. Joffre, G. P. Li, F. D. Flaviis, "A compact wideband MEMS switched diversity antenna for indoor mobile channels", IEEE Microwave Theory and Techniques Symposium, vol. 3, 2003, pp.1711-1714.

[22]. B. Elamaran, I. M. Chio, L. Y. Chen, J. C. Chiao. "A Beam steerer using reconfigurable PBG ground plane", IEEE Microwave Theory and Techniques Symposium, vol. 2, 2000, pp. 835-838.

[23]. N. Hassan, N. Kumar, S. C. Gupta, V. Sharma. "Design of a Dual-Band Reconfigurable Antenna", *Global Journal of Computer Science and Technology*. vol. 9, 2010, pp.21-24.

[24]. Y. Tawk, A. R. Albrecht, S. Hemmady, G. Balakrishnan, C. G. Christodoulou. "Optically Pumped Frequency Reconfigurable Antenna Design", *IEEE Antennas and Wireless Propagation Letters*, vol. 9, 2010, pp. 280-287.

[25]. H. Salti, E. Fourn, R. Gillard, H. Legay. "Minimization of MEMS breakdowns effects on the radiation of a MEMS based reconfigurable reflectarray", *IEEE Transaction on Antennas and Propagation*, vol. 58, 2010, pp. 2281-2287.

[26]. H. Rajagopalan, Y. R. Samii, W. A. Imbriale. "RF MEMS actuated reconfigurable reflectarray patch-slot element", *IEEE Transaction on Antennas and Propagation*. vol. 56, 2008, pp. 3689-3699.

[27]. A. Grau, J. Romeu, M. Lee, S. Blanch, L. Jofre, F. D. Flaviis. "A dual-linearly polarized MEMS-reconfigurable antenna for narrowband MIMO communication systems", IEEE Transaction on Antennas and Propagation, vol. 58, 2010, pp. 4-17.

[28]. Q. Luo, J.R. Pereira, H.M. Salgado. "Reconfigurable dual-band C-shaped monopole antenna array with high isolation", *Electronics Letter*, vol. 46, 2010, pp. 888 - 889.

[29]. T. H. Lin, S. Paul, S. Lu, H. Lu. "A study on the performance and reliability of magnetostatic actuated RF MEMS switches", *Microelectronics Reliability, Elsevier*, vol. 49, 2008, pp. 59-65.

[30]. P. Ekkels, X. Rottenberg, R. Puers, H. A. C. Tilmans. “Evaluation of platinum as a structural thin film material for RF-MEMS devices”, *Journal of Micromechanics and Microengineering*, vol. 19, 2009, pp. 1-8.

[31]. S. K. Lahiri, H. Saha, A. Kundu. “RF MEMS SWITCH: An overview at a glance”, International Conference on Computers and Devices for Communication, 2009.

[32]. B. Lacroix, A. Pothier, A. Crunteanu, P. Blondy. “Phase Shifter Design Based on Fast RF MEMS Switched Capacitors”, Proceedings of the 38th European Microwave Conference, Amsterdam, 2008, January 19, 1505-1508.

[33]. R. Yamase, T. Maeda, I. Khmyrova, E. Shestakova, E. Polushkin, A. Kovalchuk, S. Shapoval. “Study of fringing effects in multi-cantilever HEMT-based resonant MEMS”, *International Journal of Applied Electromagnetics and Mechanics*, vol.38, Issue 2-3, 2012, pp. 93-100.

[34]. W. Wang, Y. Zhao, Q. Lin, G. Yuan. “A three-axial micro-force sensor based on MEMS technology”, *International Journal of Applied Electromagnetics and Mechanics*, vol. 33, Issue 3-4, 2012, pp. 991-999.

[35]. V. Puyal, D. Dragomirescu, C. Villeneuve, J. Ruan, P. Pons, R. Plana. “Frequency scalable model for MEMS capacitive shunt switches at millimeter-wave frequencies”, *IEEE Transaction on Microwave Theory and Techniques*, vol.57, no.11, 2009, pp. 2824-2833.

[36]. J.Y. Park, G.H. Kim, K.W. Chung, J.U. Bu. “Monolithically integrated micromachined RF MEMS capacitive switches”, *Sensors & Actuators*,vol.89, 2001, pp.88-94.

[37]. K.E. Petersen. “Micromechanical membrane switches on silicon”, *IBM Journal of Research and Development*, vol. 23, 1979, pp.376–385.

[38]. S. P. Pacheco, C.-T. Nguyen, L.P.B. Katehi. “Micromechanical electrostatic K-band switches”, IEEE Microwave Theory and Techniques Symposium, vol. 3, 1998, pp. 1569-1572.

[39] S. P. Pacheco, C. T. Nguyen, L.P.B. Katehi. “Design of low actuation voltage RF MEMS switch”, IEEE Microwave Theory and Techniques Symposium, vol. 1, 2000, pp.165-168.

[40]. D. Balaraman, S.K. Bhattacharya, F. Ayazi, J. Papapolymerou. “Low-Cost low actuation voltage copper RF MEMS Switches”, IEEE Microwave Theory and Techniques Symposium, vol. 2, 2002, pp. 1225-1228.

[41]. S. D. Lee, B. C. Jun, S. D. Kim, H. C. Park, J. K. Rhee, K. Mizuno. “An RF-MEMS switch with low-actuation voltage and high reliability”, *Journal of Microelectromechanical systems*, vol. 15, 2006, pp. 1605 - 1611.

[42]. J. Kim, S. Kwon, H. Jeong, Y. Hong, S. Lee, .I Song, B. Ju. “A stiff and flat membrane operated dc contact type RF MEMS switch with low actuation voltage”, *Sensors and Actuators*, vol. 153, 2009, pp. 114–119.

[43]. A. Kundu, S. Sethi, N.C. Mondal, B. Gupta, S.K. Lahiri, H. Saha. “Analysis and optimization of two movable plates RF MEMS switch for simultaneous improvement in actuation voltage and switching time”, *Microelectronics Journal*, vol. 41, 2010, pp.257-265.

[44]. R.G. Polcawich, J.S. Pulskamp, D. Judy, P. Ranade, S. T. McKinstry, M. Dubey. “Surface micromachined microelectromechancial ohmic series switch using thin-film

piezoelectric actuators", *IEEE Transaction on Microwave Theory and Techniques*, vol. 55, 2007, pp. 2642-2654.

[45]. H. C. Lee, J. C. Park, Y. H. Park. "Development of shunt type ohmic RF MEMS switches actuated by piezoelectric cantilever", *Sensors and Actuators*, vol 136, 2007, pp. 282–290.

[46]. J.B. Muldavin, G.M. Rebeiz. "30 GHz tuned MEMS switches", IEEE Microwave Theory and Techniques Symposium,1999, pp.1511-1514.

[47]. J.B. Rizk, J.B. Muldavin, G. L. Tan, G.M. Rebeiz. "Design of X-Band MEMS Microstrip Shunt Switches", 30th European Microwave Conference 2000, 1-4.

[48]. J.B. Muldavin, G.M. Rebeiz. "High-isolation inductively-tuned x-band MEMS shunt switches", IEEE Microwave Theory and Techniques Symposium, vol. 1, 2000, pp.169-172.

[49]. G. L. Tan, G.M. Rebeiz. "A DC-contact MEMS shunt switch", *IEEE Microwave Guided Wave Letters*, vol.12, 2002, pp. 212-214.

[50]. J.B. Rizk, G.M. Rebeiz. "W-band cpw RF MEMS circuits on quartz substrates," *IEEE Transaction on Microwave Theory and Techniques*, vol. 51, 2003, pp. 1857-1862.

[51]. B. Ghodsian, P. Bogdanoff, D. Hyman. "Wideband DC-contact MEMS series switch," *Journal of Micro & Nano Letters*, vol. 3, 2008, pp. 66-69.

[52]. Y.-H. Jang, Y.-S. Lee, Y.-K. Kim, J.-M. Kim. "High isolation RF MEMS contact switch in V-band and W-band using two dimensional motions", *Electronics Letters*, vol. 46, 2010, pp. 153-155.

[53]. D. Yamane, W. Sun, H. Seita, S. Kawasaki, H. Fujita, H. Toshiyoshi. "Ku-band dual-SPDT RF-MEMS switch by double-side SOI bulk micromachining", *Journal of Microelectromechanical systems*, vol. 20, 2011, pp. 1211 - 1221.

[54]. X. Yuan, J.C.M. Hwang, D. Forehand, C.L. Goldsmith. "Modeling and characterization of dielectric-charging effects in RF MEMS capacitive switches", IEEE Microwave Theory and Techniques Symposium, 2005, pp. 753-756.

[55]. J. R. Reid, R. T. Webster. "Measurements of charging in capacitive microelectromechanical switches", *Electronics letters*, vol. 38, 2002, pp. 1544-1545.

[56]. C. Goldsmith, J. Ehmke, A. Malczewski, B. Pillans, S. Eshelman, Z. Yao, J. Brank, M. Eberly. "Lifetime characterization of capacitive RF MEMS switches", IEEE Microwave Theory and Techniques Symposium, vol.1, 2001, pp. 227-230.

[57]. P. Czarnecki, X. Rottenberg, P. Soussan, P. Ekkels, P. Muller, P. Nolmans, W. De Raedt, H.A.C. Tilmans, R. Puers, L. Marchand, I. De Wolf. "Influence of the substrate on the lifetime of capacitive RF MEMS switches", IEEE 21st International conference on Micrco electrical Mechanical systems, 2008, pp.172 – 175.

[58]. W.S.H. Wong, C.H. Lai. "Longer MEMS switch lifetime using novel Dual-pulse actuation voltage", *IEEE Transaction on Devices and Material Reliability*, vol. 9, 2009, pp. 569-575.

[59]. X. Rottenberg, I.D. Wolf, B.K.J.C. Nauwelaers, W. De Raedt, H.A.C. Tilmans. "Analytical model of the DC actuation of electrostatic MEMS devices with distributed dielectric charging and nonplanar electrodes", *Journal of MEMS*, vol. 16, 2007, pp. 1243-1253.

[60]. B. Pillans, J. Kleber, C. Goldsmitht, M. Eberly. “RF power handling of capacitive RF MEMS devices”, IEEE Microwave Theory and Techniques Symposium, vol. 1, 2002, pp. 329-332.

[61]. B. D. Jensen, Z. Wan, L. Chow, K. Saitou , K. Kurabayashi, J. L. Volakis. “Integrated electrothermal modeling of RF MEMS switches for Improved power handling capability”, IEEE Topical Conference on Wireless Communication Technology, 2003, pp.10-11.

[62]. D. Peroulis, S.P. Pacheco, L.P.B. Katehi. “RF MEMS switches with enhanced Power-handling capabilities”, IEEE Microwave Theory and Techniques Symposium, vol. 52, 2004, pp. 59-68.

[63]. K. Grenier, D. Dubuc, E. Ducnrouge, V. Conedera, D. Bourrier, E. Ongareau, P. Derderian, R. Plana. “High power handling RF MEMS design and technology”, IEEE 21st International conference on Micrco electrical Mechanical systems, MEMS, 2005, pp. 155-158.

[64]. R. Mahameed, G.M. Rebeiz. “Power handling of temperature-stable thin-RF MEMS capacitive switches”, 40th European Microwave conference, 2010, pp. 97-100.

[65]. A. Stehle, C. Siegel, V. Ziegler, B. Schonlinner, U. Prechtel, H. Seidel, U. Schmid. “High-power handling capability of low complexity RF-MEMS switch in Ku-band”, *Electronics letters*, vol. 43, 2007, pp. 1367 - 1368.

[66]. C. Palego, J. Deng, Z. Peng, S. Halder, J.C.M. Hwang, D.I. Forehand, D. Scarbrough, C.L. Goldsmith, I. Johnston, S.K. Sampath, A. Datta. “Robustness of RF MEMS capacitive switches with molybdenum membranes”, *IEEE Transaction on Microwave and Theory Techniques*, vol. 57, 2009, pp. 3262-3269.

[67]. R. Mahameed, G.M. Rebeiz. “A high-power temperature-stable electrostatic RF MEMS capacitive switch based on a thermal buckle-beam design”, *Journal of Microelectromechanical systems*, vol. 19, 2010, pp. 816 - 826.

[68]. R. Mahameed, G. M. Rebeiz. “Electrostatic RF MEMS tunable capacitors with analog tunability and low temperature sensitivity”, IEEE Microwave Theory and Techniques Symposium, 2010, pp. 1254-1257.

[69]. J. Muldavin, C.O. Bozler, S. Rabe, P.W. Wyatt, C.L. Keast. “Wafer-scale packaged RF microelectromechanical switches”. *IEEE Transaction on Microwave and Theory Techniques*, vol. 56, 2008, pp. 522-529.

[70]. R. Mahameed, G.M. Rebeiz. “RF MEMS Capacitive Switches for Wide Temperature Range Applications Using a Standard Thin-Film Process”, *IEEE Transaction on Microwave and Theory Techniques*, vol. 59, 2011, pp. 1746-1752.

[71]. V.K. Varadan, K.J. Vinoy, K.A. Jose. “RF MEMS and their applications”, John Wiley & Sons Ltd, England, 2003.

[72]. Park J, Shim ES, Choi W, Kim Y, Kwon Y, Cho D-i. “A non-contact-type Rf-MEMS switch for 24-GHz radar applications”, *Journal of Microelectromechanical systems*, vol. 18, 2009, pp.163 - 173.

[73]. M. Hoffmann, H. Kuppers, T. Schneller, U. Bottger, U. Schnakenberg, W. Mokwa, R. Waser. “Theoretical calculations and performance results of a PZT thin film actuator”, *IEEE Transactions on Ultrasonics, Ferroelectrics, and Frequency Control*, vol. 50, 2003, pp. 1440-1446.

[74]. H.A.C. Tilmans, E. Fullin, H. Ziad, M.D.K.J. Van de Peer, J. Kesters, E. Van Geffen, J. Bergqvist, M. Pantus, E. Beyne, K. Baert, F. Naso. “A fully-packaged

electromagnetic microrelay", International conference on Micrco electrical Mechanical systems, 1999, pp. 25-30.

[75]. Y. Wang, Z. Li, D.T. McCormick, C.N. Tien. "A low-voltage lateral MEMS switch with high RF performance", *Journal of MEMS*, vol. 13, 2004, pp. 902-911.

[76]. D. E. Anagnostou, M.T. Chryssomallis, B. D. Braaten, J. L. Ebel, N. Sepúlveda. "Reconfigurable UWB Antenna With RF-MEMS for On-Demand WLAN Rejection", *IEEE Transactions on Antennas and Propagation*, vol. 62, no. 2, 2014, 602-608.

[77]. J. Taye, K. Guha, S. Baishya. "Design and Analysis of RF MEMS Shunt Capacitive Switch for Low Actuation Voltage and High Capacitance Ratio," *Physics of Semiconductor devices, Springer*, vol.5, 2014, 445-448.

[78]. M. B. Fathi, H. Veladi, S. Golmohammadi. "A new electrostatically actuated low voltage RF MEMS switch," *European Scientific Journal*, vol.9, No.33, 2013, pp.400-412.

[79]. D. Bansal, A. Kumar, A. Sharma, P. Kumar, K. J. Rangra. "Design of novel compact anti-stiction and low insertion loss RF MEMS switch," *Microsystems Technologies*, vol. 20, 2014, pp. 337-340.

[80]. T. M. Vu, G. Prigent, J. Ruan, and R. Plana. "Design and fabrication of rf-mems switch for v-band reconfigurable application", *Progress In Electromagnetics Research B*, vol. 39, 2012, pp. 301-318.

[81]. A. Pourziad, S. Nikmehr, H. Veladi. "A Novel Multistate integrated RF MEMS switch for reconfigurable antenna application", *Progress in Electromagnetics Research*, vol. 139, 2013, pp. 389-406.

[82]. X. Meng. “Small-size eight-band frequency reconfigurable antenna loading a MEMS switch for mobile handset applications,” *International Journal of Antennas and Propagation*, vol . 6, 2014, pp. 1-6.

[83]. C. J. A. Armenta, S. Porter, A. Marvin. “Reconfigurable phased array antennas with RF-MEMS on a PCB substrate”, Loughborough Antennas & Propagation Conference 2012, pp. 1-5.

[84]. S. Lucyszyn, S. Pranonsatit. “RF MEMS for antenna applications”, 7th European Conference on Antennas and Propagation (EUCAP 2013), Gothenburg, 2013, pp. 1988 - 1992.

[85]. B. A. Cetiner, G. R. Crusats, L. Jofre, N. Bıyıklı. “RF MEMS integrated frequency reconfigurable annular slot antenna”, *IEEE Transactions on Antennas and Propagation*, vol.58, no.3, 2010, pp.626-632.

[86]. S. Cheng, P. Rantakari, R. Malmqvist, C. Samuelsson, T. Vaha-Heikkila, A. Rydberg, J. Varis. “Switched beam antenna based on RF MEMS SPDT switch on Quartz substrate”, *IEEE Antennas Wireless Propagation Letters*, vol.8, 2009, pp. 383-386.

[87]. C. C. Cheng, B. Lakshminarayanan, A. Abbaspour-Tamijani. “A programmable lens-array antenna with monolithically integrated MEMS switches”, *IEEE Transaction on Microwave Theory Techniques*, vol.57, no.8, 2009, pp. 1874-1884.

[88]. C. W. Jung, M. J. Lee. “Reconfigurable scan-beam single-arm spiral antenna integrated with RF-MEMS switches”, *IEEE Transaction on Antenna and Propagation*, vol.54, no.2, 2006, pp. 455-463.

[89]. V. T. Srikar, S. M. Spearing. “Material selection for microfabricated electrostatic actuators”, *Sensors and Actuators A*, vol. 102, 2003, pp. 279-285.

[90]. R. V. Rao. “A Material selection model using graph theory and matrix approach”, *Materials Science and Engineering: A*, vol.431, 2006, pp. 248-255.

[91]. R. Roth, F. Field, J. Clark. “Multi-attribute utility analysis”, *Journal of Computer-Aided Materials Design*, vol.1, no.3, 1994, pp. 325-342.

[92]. G. Guisbiers, E. Herth, B. Legrand, N. Rolland, T. Lasri, L. Buchaillot. “Materials selection procedure for RF-MEMS”, *Microelectronic Engineering*, vol.87, 2010, pp. 1792-1795.

[93]. M. F. Ashby. “Materials selection in mechanical design”, 2nd ed. Oxford (UK): Butterworth-Heinemann; 1999.

[94]. V. Puyal, D. Dragomirescu, C. Villeneuve, J. Ruan, P. Pons, R. Plana. “Frequency scalable model for MEMS capacitive shunt switches at millimeter-wave frequencies”, *IEEE Transaction on Microwave Theory Techniques*, vol.57, no.11, 2009, pp. 2824-2833

[95]. P. Ekkels, X. Rottenberg, R. Puers, H. A. C. Tilmans. “Evaluation of platinum as a structural thin film material for RF-MEMS devices”, *Journal of Micromechanics and Microengineering*, vol.19, 2009, pp. 065010-065018

[96]. A. H. M. Z. Alam, M. R. Islam, S. Khan, N. B. Mohd Sahar, N. B. Zamani. “Effects of MEMS material on designing a multi-band reconfigurable antenna”, *Iranian Journal Of Electrical and Computer Engineering*, vol. 8, no.2, 2009, pp. 112-118.

[97]. G. P. Reddy, N. Gupta. “Material selection for microelectronic heat sinks: an application of the Ashby approach”, *Materials and Design*, vol. 31, 2010, pp. 113-117.

[98]. W. D. Callister. “Material science and engineering: An introduction”. 7th ed. New York: John Wiley & Sons Inc; 2007.

[99]. N. Kingsley, D. E. Anagnostou, M. Tentzeris, J. Papapolymerou. “RF MEMS sequentially reconfigurable sierpinski antenna on a flexible organic substrate with novel dc-biasing technique”, *Journal of Microelectromechanical Systems,* vol.16, no.5, 2007, pp. 1185-1192.

[100]. I. Reines, B. Pillans, G.M. Rebeiz. “Thin-film aluminum RF MEMS switched capacitors with stress tolerance and temperature stability”, *Journal of Microelectromechanical Systems*, vol. 20, no.1, 2011,pp. 193-202.

[101]. C. L. Dai, J.-H. Chen. “Low voltage actuated RF micromechanical switches fabricated using CMOS-MEMS technique”, *Microsystem Technologies,* vol.12,2006, pp. 1143-1151.

[102]. L. Meirovitch. “Analytical Methods in Vibrations”, Macmillan Publishing Co., Inc., New York, 1967.

[103]. G. K. Fedder. “Simulation of microelectromechanical systems," Ph.D. dissertation, Electrical Engineering and Computer Science, University of California at Berkeley,USA, 1994.

[104]. G. Delapierre. “Micro-machining a survey of the most commonly used processes,” *Sensors and actuators*, 1989, pp. 123-138.

[105]. C.-J. Kim, A. P. Pisano, R. S. Muller M. G. Lim. “Polysilicon microgripper,” IEEE Solid State Sensor and Actuator Workshop, Technical Digest, June 1990, pp.48-51.

[106]. W. Yun, R. T. Howe, P. R. Gray. “Surface micromachined, digitally force-balanced accelerometer with integrated CMOS detection circuitry”, IEEE Solid State Sensor and Actuator Workshop,Technical Digest, June 1992, pp. 21-25.

[107]. W. C. Tang, T. C. H. Nguyen, R. T. Howe. “Laterally driven polysilicon resonant microstructures", IEEE Micro Electro Mechanical Systems Workshop Proceedings, February 1989, pp. 53-59.

[108]. L. S. Fan, Y. C. Tai, R. S. Muller. “Integrated movable micromechanical structures for sensors and actuators," *IEEE Transaction on Electronic Devices*, vol. 35 no.6, June 1988, pp. 724-730.

[109]. A. P. Pisano, Y. H. Cho. “Mechanical design issues in laterally-driven microstructures," 5th Inter. Conf. on Solid-State Sensors and Actuators Technical Digest, Switzerland, June 1989, pp. 1060-1064.

[110]. Y. H. Cho, A. P. Pisano. “Optimum structural design of micromechanical crab-leg exures with microfabrication constraints," ASME Winter Annual Meeting Proceedings, Texas, November 1990.

[111]. W. C. Tang. “Electrostatic comb drive for resonant sensor and actuator applications,” PhD thesis, University of California November 1990.

[112]. S. P. Timoshenko, J. M. Gere. “Mechanics of Materials,” Van Nostrand Reinhold Company Ltd. 1971.

[113]. V. P. Jaecklin, C. Linder, N. F. de Rooij. “Optical microshutters and torsional micromirrors for light modulator arrays," IEEE Micro Electro Mechanical Systems Workshop Proceedings, Florida, February 1993, pp. 124-127.

[114]. Z. L. Zhang, N. MacDonald. “An rie process for submicron, silicon electromechanical structures," In Technical Digest, 6th Inter. Conf. on Solid-State Sensors and Actuators, 1991, pp. 520-523.

[115]. S. P. Timoshenko, J. N. Goodier. “Theory of Elasticity,” McGraw-Hill, New York, New York, 3rd ed., 1970.

[116] . Comsol Multiphysics 4.2 US.

[117]. A. K. Sharma, N. Gupta. “Material selection of RF-MEMS switch used for reconfigurable antenna using ashby's methodology”, *Progress in Electromagnetics Research Letters*, vol. 31, 2012, pp.147-157.

[118]. M. Zahn. “Electromagnetic Field Theory: A Problem Solving Approach”, John Wiley & Sons, New York, 1979.

[119]. R. P. Feynman, R. B. Leighton, M. Sands. “The Feynman Lectures on Physics”, vol. 2, 1964.

[120]. D. Peroulis. “RF MEMS devices for multifunctional Integrated circuits and antennas,” Ph.d thesis, The University of Michigan, 2003.

[121]. N. S. Barker. “Distributed MEMS Transmission Lines”, Ph.D. thesis, University of Michigan, Ann Arbor, 1999.

[122]. J. B. Muldavin, G.M. Rebeiz. “High-Isolation CPW MEMS switches: part 1: modeling”, *IEEE Transaction on Microwave Theory and Techniques*, vol. 48, 2011, pp. 1045-1052.

[123]. J. B. Muldavin, G.M. Rebeiz. “High-isolation CPW MEMS switches: part 2: design”, *IEEE Transaction on Microwave Theory and Techniques*.vol. 48, 2000, pp. 1053-1056.

[124]. K. Topalli, M. Unlu, H.I. Atasoy, S. Demir, O.A. Civi, T. Akin. “Empirical formulation of bridge inductance in inductively tuned RF MEMS shunt switches”, *Progress in electromagnetic research, PIER,* 97, 2009, pp. 343-356.

[125]. C.H. Wong, M.J. Tan, K.M. Liew. “Electrical Characterisation of RF capacitive microswitch”, *Sensors and Actuators A*, vol. 102, 2003, pp. 296-310.

[126]. O. Bayraktar, O. A. Civi, T. Akin. “Beam Switching Reflectarray Monolithically Integrated With RF MEMS Switches”, *IEEE Transactions on Antennas and Propagation*, vol. 60, no. 2, 2012, pp. 854-862.

[127]. E. Erdil, K. Topalli, M. Unlu, O. A. Civi, T. Akin. “Frequency tunable microstrip patch antenna using RF MEMS technology,” *IEEE Transactions on Antennas and Propagation*, vol. 55, Apr. 2007, pp. 1193-1196.

[128]. S. Nikolaou, N. D. Kingsley, G. E. Ponchak, J. Papapolymerou, and M. M. Tentzeris. “UWB elliptical monopoles with a reconfigurable band notch using MEMS switches actuated without bias lines,” *IEEE Transactions on Antennas and Propagation*, vol. 57, 2009, pp. 2242-2251.

[129]. S. Genovesi, A. Monorchio, M. Borgese, S. Pisu, F. M. Valeri. “Frequency-Reconfigurable Microstrip Antenna With Biasing Network Driven by a PIC Microcontroller”, *IEEE Antennas and Wireless Propagation Letters*, vol. 11, 2012, pp. 156-159.

[130]. Y.J. Sung. “Frequency and polarisation reconfigurability from an open-loop square ring antenna”, *IET Microwave Antennas Propagation*, vol. 6, 2012, pp. 505-509.

[131]. Y. Dong, H. Toyao, T. Itoh. “Design and Characterization of Miniaturized Patch Antennas Loaded With Complementary Split-Ring Resonators”, *IEEE Transactions on Antennas and Propagation*, vol. 60, 2012, pp. 772-785.

[132]. Z. Q. Liu, Z. Qian, Z. P. Han, S. W. Zhou. “Design and Implementation of a New Multipolarization Antenna”, *IEEE Antennas and Wireless Propagation Letters*, vol. 11, 2012, pp. 6-9.

[133]. D. Sánchez-Escuderos, M. Ferrando-Bataller, M. Baquero-Escudero, J. I. Herranz. *“*Reconfigurable Slot-Array Antenna With RF-MEMS*”, IEEE Antennas and wireless propagation letters*, vol. 10, 2011, pp. 721-725.

[134]. F. C. Comm., “First report and order, revision of part 15 of the commission’s rule regarding ultra wideband transmission systems,”FCC, Apr. 22, 2002, pp. 02-48.

[135]. K. Chung, J. Kim, J. Choi. “Wideband microstrip-fed monopole antenna having frequency band-notch function,” *IEEE Microwave and Wireless Component Letters*, vol. 15, 2005, pp. 766-768.

[136]. J. C. Chiao, Y. Fu, I. M. Chio, M. DeLisio L.Y. Lin. “MEMS reconfigurable vee antenna,” IEEE MTT-S International Microwave Symposium Digest, Anaheim, CA, 1999, vol. 4, pp. 1515-1518.

[137]. A. C. K. Mak, C. R. Rowell, R. D. Murch, C. L. Mak. “Reconfigurable multiband antenna designs for wireless communication devices,” *IEEE Transactions on Antennas and Propagation.*, vol. 55, no. 7, 2007, pp. 1919-1928.

[138] J. Liang, L. Guo, C.C. Chiau, X. Chen, C.G. Parini. “Study of CPW-fed circular disc monopole antenna for ultrawide band antenna”, *IEE Procceding on Microwave and Antennas Propagation*, vol. 152, no. 6, December 2005, pp. 520-526.

[139] D.M. Pozar. “Microwave Engineering”, 3rd ed. wiley & sons (Asia) Pte. Ltd., Singapore, pp.222-265.

[140] R. Garg, P. Bhartia, I. bhal, A. Ittipiboon. “Microstrip anenna design handbook ,” Artech House INC., Boston, June 2001.

[141] Z. Zhang. “ An alternative technique for solving impedance matching problems on the smith chart ,” *IEEE potentials*, vol. 32, no.2, 2013, pp. 27-31.

LIST OF PUBLICATION

Publication in Peer Reviewed Journals:

1. Ashish K. Sharma and Navneet Gupta,"Material Selection of RF-MEMS switch used for reconfigurable antenna using Ashby's Methodology" *Progress in Electromagnetics Research Letters (PIER-L),* pp. 147-157, vol. 31 (2012). [Impact factor- 3.74]

2. Ashish K. Sharma and Navneet Gupta," Microelectromechanical System (MEMS) Switches for Radio Frequency Applications-A Review," *Sensors & Transducers*, pp. 11-21, vol. 148 (2013). [Impact factor- 0.705]

3. Ashish K. Sharma and Navneet Gupta, "Analytical Modeling for Spring Constant of Non-Uniform Serpentine Radio Frequency – Micro Electro Mechanical Systems Switch" *Advanced Science, Engineering and Medicine,* American Scientific Publishers**,** pp. 1322-1325, vol. 5, No.12 (2013)**.** [Impact factor- 0.428]

4. Ashish K. Sharma and Navneet Gupta, "Investigation of Actuation Voltage for Non-Uniform serpentine Flexure design of RF-MEMS switch", *Microsystem Technologies:* Springer, pp. 413-418, vol. (20) 2014. [Impact factor- 0.952]

5. Ashish K. Sharma and Navneet Gupta, "Electromagnetic Modeling and Parameter Extraction of RF-MEMS Switch" *Microsystem Technologies:* Springer-Verlag Berlin. (In press). Doi: 10.1007/s00542-013-1952-3.[Impact factor 0.952]

6. Ashish K. Sharma and Navneet Gupta, "An Improved Design of MEMS Switch for Radio Frequency Applications", *International Journal of Applied Electromagnetics and Mechanics,* IOS Press, Japan. (In press). [Impact factor- 0.737]

Publication in Peer Reviewed Conferences:

1. Ashish K. Sharma and Navneet Gupta, " Micro-electro-mechanical-system (MEMS) Switches for radio frequency (RF) applications-An Overview", *National Conference on "Recent Advancement in Communication System & Image Processing RACSIP* -2012, BKBIET, Pilani, April 2-3, 2012.

2. Ashish K. Sharma and Navneet Gupta, " Material Selection Approach for Dielectric Layer in RF-MEMS Switch", *International Conference on Emerging Technologies - Micro to Nano; ETMN*-2013, BITS, Pilani - KK Birla Goa Campus, India, February 23-24, 2013.

3. Ashish K. Sharma and Navneet Gupta, " Switching time analysis for non-uniform serpentine flexure based RF-MEMS switches" *IEEE Students Conference Engineering and Systems (SCES),* MNNIT Allahabad, April 12-14, 2013 (**Best Paper Award).**

4. Ashish K. Sharma and Navneet Gupta, "Electromagnetic Modeling of Non-Uniform serpentine flexure based RF-MEMS switch" *IEEE International Conference on Advance Electronic Systems (ICAES),* CSIR-CEERI Pilani, India, Sep 21-23, 2013.

5. Ashish K. Sharma and Navneet Gupta, "Impedance Matching for RF-MEMS Based Microstrip Patch Antenna" *ECTI-CON*-2014, Suranaree Univ. of Tech., Nakhon Ratchasima, Thailand, May 14-17, 2014. (**Travel Grant Award from the Organizers**).

BRIEF BIOGRAPHY OF THE CANDIDATE

Ashish Kumar Sharma obtained B.Tech (Electronics and Communication) in 2006 from Dr. Ram Manohar Lohia University, Faizabad (U.P.). He received M.Tech in Communication Syatems from Visvesvaraya Technological University, Belgaum, Karnataka, in 2008. He started his carrier as Engineer in Mind Tree Wireless Pvt. Ltd. (formally Kyocera Wireless India) Bangalore.

Later he joined Birla Institute of Technology and Science (BITS), Pilani as Research scholar in 2010. His research interests include RF-MEMS, antenna design and material selection strategies. He has over 6 research publications in reputed peer reviewed international journals with good impact factors, and 5 in conference proceedings. He has published one book chapter in the area of MEMS Technologies and its Applications. He received Senior Research Fellowship (SRF) Award from Council of Scientific and Industrial Research (CSIR), New Delhi, INDIA.

BRIEF BIOGRAPHY OF THE SUPERVISOR

Dr. Navneet Gupta obtained M.Sc (Physics-Electronics) in 1995 from H.N.B Garhwal Central University (HNBGU), Srinagar with first rank in the University. He received M.Tech in 1998 from Indian Institute of Technology (IIT-BHU) (formerly IT-BHU). He did his Ph.D in 2005 from HNBGU.

He joined Birla Institute of Technology and Science (BITS), Pilani, Rajasthan in 2005. Presently, he is Assistant Professor and Convener-Departmental Research Committee (DRC) in Electrical and Electronics Engineering Department, BITS, Pilani, Rajasthan. During May to July 2014, he was Visiting Professor at National Taiwan University of Science and Technology (NTUST), Taipei, Taiwan.

He guided one PhD student and currently guiding four Ph.D candidates. He is on doctoral advisory committee (DAC) for 6 PhD students. He completed two research and sponsored projects from UGC and DST. His research interests include Device modeling (Semiconductor and MEMS), computation material science and applied electromagnetics. He is senior member of various professional bodies.

He has over 65 research publications (of which 30 are in reputed peer reviewed international and national journals, and 35 are in conference proceedings.). He received *certificate of appreciation* from NTUST, Taiwan in 2014, *Bharat Jyoti Award* in 2011 by IIFS, New Delhi, *DST Young Scientist Award* (Fast track Scheme) in Physical Sciences in 2007 and *Gold Medal* in M.Sc., from HNGBU, Srinagar in 1995. His biography is included in *Marquis Who's Who in World* and *Marquis Who's Who in Science and Engineering*. He **v**isited National University of Singapore, Singapore, and Malaysia for presenting research papers.

He is expert reviewer of five International Journals. He reviewed five books of Oxford University Press, Pearson Education and McGraw Hill publishers.